UNIVERSITÀ DEGLI STUDI DELL'INSUBRIA

FACOLTÀ DI SCIENZE MM. FF. NN.

Dottorato di ricerca XXIV ciclo in
"Biologia Cellulare e Molecolare"

Scuola di Dottorato in
"Scienze Mediche e Biologiche"

Laboratorio di Fisiologia cellulare e molecolare

STRUCTURE – FUNCTION RELATIONSHIPS
IN THE OLIGOPEPTIDE TRANSPORTER
PepT1

Docente guida:
Prof. Antonio Peres

Coordinatore:
Prof.ssa Magda de Eguileor

Dottoranda:
Dott.ssa Maria Daniela Renna

2008 - 2011

A chi da lontano mi è stato vicino.

Learn from yesterday,
live for today,
hope for tomorrow.
The important thing is
not stop questioning.

Albert Einstein

Summary

The proton-dependent di- and tripeptide transporter PepT1 represents the major route of dietary amino acid intake in the intestine of many species. This transporter belongs to the solute carrier family SLC15 and because of its electrogenic properties it may be studied both through electrophysiological and radiotracer uptake experiments.

In this work some functional and structural aspects of PepT1 have been investigated at the molecular level. In addition to the physiological relevance, understanding of the details of its mechanisms of operation is important since PepT1 appears to be involved in the absorption of many important, orally administered, drugs such as antibiotics, angiotensin-converting inhibitors, and antiviral agents.

The electrophisyiological and biophysical properties of PepT1 expressed in *Xenopus* oocytes were investigated with two-electrode voltage-clamp.

Most of the above functional observations were derived from uptake data, in absence of control of the membrane voltage, or from electrophysiological measurement of steady transport currents, in the presence of a dipeptide substrate. Important additional informations regarding the transport mechanism may arise from measurement of presteady-state currents, the electrophysiological signals that can be observed in absence of organic substrate, and that represent the first steps in the transport cycle. A unified kinetic model for PepT1 has been devised that can describe the different characteristics of the

isoforms of different species, with respect to both presteady-state and transport-associated currents.

Mutational studies have provided significant evidence for the functional role of some residues in PepT1. Particularly Arg282 and Asp341, in the transmembrane domain 7 and 8 of the transporter, have been reported to form a charge pair that may break and reform during the transport cycle. The attention has been focused on these two oppositely charged aminoacids to better understand their functional role in the absorption pathway.

Finally, the functional and structural basis of reverse operation of wild-type and mutated forms of PepT1 have been studied. Mutants in the putative charge pair residues Arg282 and Asp341 of rabbit PepT1 have been shown exhibit properties useful to better understand the possibility of reverse transport. This reversed mode of operation may be either the effect or the cause of abnormal or pathological conditions.

Contents

Chapter 1.   Introduction

1.1   Protein digestion and absorption

Proteins are essential components for nutritional homeostasis in humans. Normally, a western diet provides between 70 and 100 g of protein/day and, in addition, 50-60 g/day of endogenous proteins are secreted along the oro-gastrointestinal tract. These proteins undergo a complex series of degradative processes by the hydrolytic enzymes secreted from stomach and pancreas or bound to the brush border membrane of enterocytes. The result of this proteolytic activity is a mixture of amino acids and small peptides that are rapidly and efficiently absorbed by the small intestinal enterocytes (Erickson and Kim, 1990;Daniel, 2004).

Transport across the enterocyte involves uptake from the gut across the brush-border membrane, diffusion through the cytoplasm, and exit to the portal blood across the basolateral membrane. The brush borders contain unique transport properties, while the basolateral membranes are very similar to plasma membranes of nonepithelial cells (Stevens *et al.*, 1984). Distinct carrier mechanisms exist in the brush border membrane for the transport of free amino acids and peptides. In fact, not only the free amino acids, but also di- and tripeptides are taken up by intestinal epithelial cells in intact form by an oligopeptide transporter named PepT1 (Fig.1.1). Following apical influx, di- and tripeptides are sequentially hydrolyzed by multiple cytosolic hydrolases followed by basolateral efflux of the amino acids via different amino acid transporting systems. Peptides

not undergoing hydrolysis can exit the cell by a basolateral peptide-transporting system not yet identified on a molecular basis (Daniel, 2004).
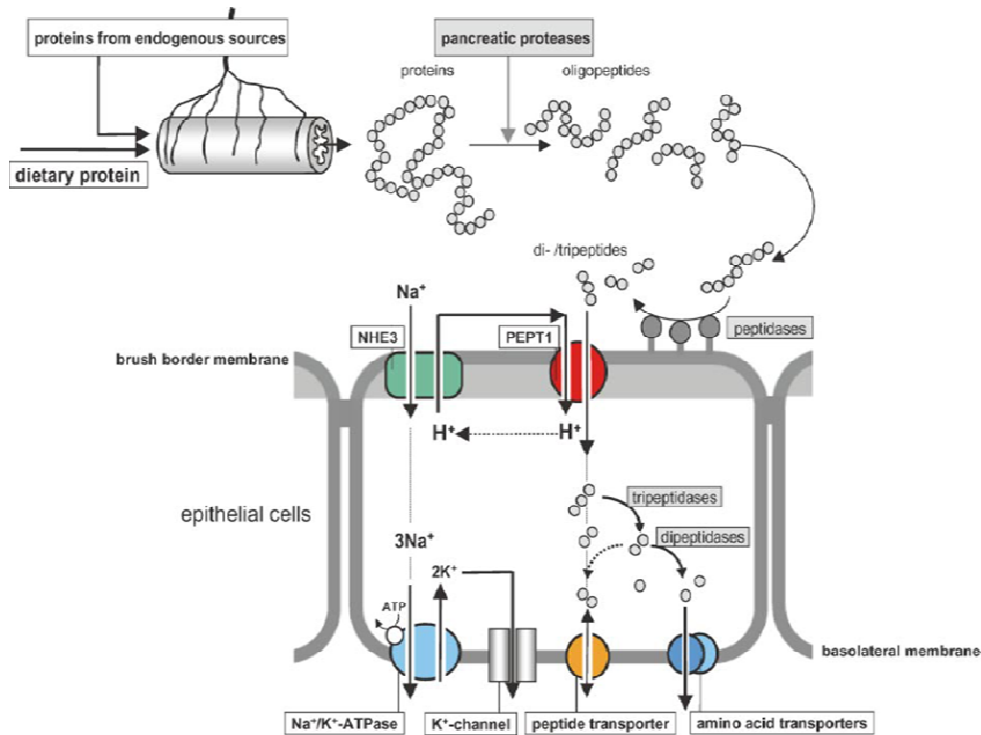
Fig.1.1 *Generation and uptake of di- and tripeptides (Daniel, 2004).*

1.2   PepT1 overview

1.2.1 PepT1 discovery… a bit of history

PepT1 is an electrogenic H^+-coupled transporter of oligopeptides and peptide-derived drugs identified by expression cloning from a rabbit intestinal cDNA library and functional characterization in *Xenopus* oocytes in 1994. It presents the unique feature of utilizing an inwardly directed proton gradient to allow

peptides to enter the cell even against the concentration gradient; indeed, the electrogenic PepT1-mediated uptake is independent of extracellular Na^+, K^+ and Cl^-, and of membrane potential (Fei *et al.*, 1994). The H^+-peptide cotransport process across apical membranes of enterocytes was dimostred in 1980s in earlier studies employing brush border membrane vescicles (Ganapathy *et al.*, 1984;Ganapathy *et al.*, 1985). The acid-loading activity of PepT1 requires the apical Na^+/H^+ antiporter activity which exports protons entering the cell via PepT1 in exchange for extracellular Na^+ ions (Ganapathy and Leibach, 1985;Kennedy *et al.*, 2002).

The controversial discussion about the active transport of short chain peptides in the mammalian gut epithelium started in 1960 with the discovery of intracellular hydrolysis of dipeptides during intestinal absorption (NEWEY and SMYTH, 1960). That oligopeptides were able to cross apical membranes was demonstrated by measuring hydrolytic activity of peptidases in homogenates of the mucosa and in isolated brush border membranes. The almost total activity of peptidases with specificity for di- and tripeptides was originated from the soluble cytosolic fraction: this suggested that oligopeptides, but not tetrapeptides and more longer ones are absorbed in intact form (Sterchi and Woodley, 1980;Daniel, 2004).

After the cloning of the PepT1 cDNA, an important demonstration of its relevance in the transfer of intact oligopeptides from the gut lumen into blood circulation came from pharmacokinetics and cystinuria studies. In this disease the transport of amino acids such as arginine and lysine is not sufficient, but patients suffering from cystinuria do not develop a lysine deficiency

when they provide this essential amino acid as a lysil-dipeptide and not in free form (Hellier *et al.*, 1971;de Sanctis *et al.*, 2001). Finally, drugs resistant to hydrolysis, such as aminocephalosporins or ACE-inhibitors, that utilize PepT1 for intestinal absorption rapidly appear in circulation (Fig.1.2). However, the molecular nature of the basolateral transport is not known (Daniel, 2004).

Apical   **Basolateral**
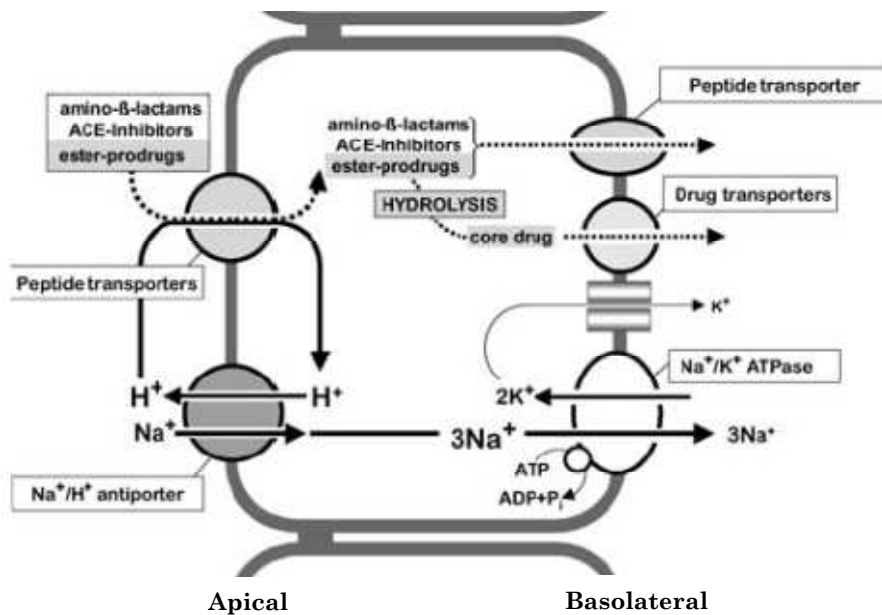
Fig.1.2 *Transport of peptidomimetics (Daniel and Kottra, 2004).*

1.2.2 SLC15 family

All the SoLute Carrier (SLC) genes have been classified by the Human Genome Organisation (HUGO) in a list of transporter families that currently includes almost 50 families and more than 300 transporter genes. The SLC series includes genes encoding passive transporters, ion-coupled transporters and exchangers. The remaining transporter-related genes encoding ATP-driven transporters, channels, ionotropic receptors, aquaporins, transporter and channels subunits,

auxiliary/regulatory transport proteins don't belong to SLC series (Hediger *et al.*, 2004).

PepT1 is the prototype member of the proton oligopeptide cotransporter family SLC15 (Fig.1.3). Transporters of the SLC15 family are electrogenic and utilize the proton-motive force for uphill transport of short chain peptides and peptido-mimetics into a variety of cells. Four transporters belong to the SLC15 family: the oligopeptide transporters, PepT1 and PepT2, and the peptide/histidine transporters PHT1 e PHT2. The first two have been identified into intestinal and renal epithelial cells and more recently into bile duct epithelium (PepT1), glia cells and epithelia of the choroid plexus, lung and mammary gland (PepT2). Whereas, it is not yet clear if PHT1 and PHT2 are located on the plasma membrane or represent lysosomal transporters for the proton-dependent export of histidine and dipeptides from lysosomal protein degradation into the cytosol (Daniel and Kottra, 2004).

Human Gene Name	Protein Name	Aliases	Predominant substrates	Coupling ions	Tissue distribution and cellular expression	Human gene locus	Sequnece Accession ID
SLC15A1	PepT1	Oligopeptide transporter 1, H^+/peptide transporter 1	Di- and tripeptides protons	H^+	Intestine, kidney apical, lysosomal membrane	13q33-q34	NM_005073
SLC15A2	PepT2	Oligopeptide transporter 2, H^+/peptide transporter 2	Di-, and tripeptides protons	H^+	Kidney, lung, brain, mammary gland, bronchial epithelium	3q13.3-q21	NM_021082
SLC15A3	PHT2 hPTR3	Peptide/histidine transporter 2, human peptide transporter 3	Histidine, di- and tripeptides protons	H^+	Lung, spleen, thymus (faintly in brain, liver, adrenal gland, heart)	11q12.1	NM_016582
SLC15A4	PHT1 PTR4	Peptide/histidine transporter 1, human peptide transporter 4	Histidine, di- and tripeptides protons	H^+	Brain, retina, placenta	12q24.32	NM_145648

Tab.1.1 *SLC15 family (Daniel and Kottra, 2004).*

SLC15 transporters present from 450 to more than 750 aminoacidic residues (the procaryotic variants are smaller than the

eukaryotic ones) and contain 12 transmembrane domains (TMD) with the N- and C-termini facing the cytosol. Conserved residues are found in all family members (Steiner *et al.*, 1995). There is a protein stretch located in the end region of the TMD2, the following intracellular loop and reaching into TMD3. The second more conserved signature motif is found in the central part of TMD5 and comprises a stretch of 11 amino acid residues (Hauser *et al.*, 2005). Moreover, in the mammalian species there is a histidyl residue obligatory for the catalytic activity of PepT1 and PepT2 (Fei *et al.*, 1997).

PepT1 and PepT2 are able to transport all 400 different dipeptides and 8000 different tripeptides derived from the 20 proteinogenic L-α-amino acids; PepT1 represent the low-affinity/high-capacity variant, and PepT2 the highaffinity/low-capacity variant. PHT1 and PHT2 accept also free histidine as a substrate, but it is not known if they can transport the same spectrum of di- and tripeptides of PepT1 and PepT2. The peptide/histidine transporters appear to be phylogenetically similar to proton oligopeptide transporters found in plants, which mediate the transport of histidine, nitrates, di- and tripeptides. The mammalian SLC15 members can only transport di- and tripeptides, whereas in bacteria, yeast and plants there are proton oligopeptide cotransporter with the capability of transporting peptides containing more than three amino acid residues. (Daniel and Kottra, 2004).

1.2.3 PepT1 gene

In 1994, the complementary DNA coding for rabbit PepT1 was cloned screening an intestinal cDNA library by uptake of glycyl-sarcosine ^{14}C-labelled in *Xenopus laevis* oocytes (Fei *et al.*, 1994). Subsequently, PepT1 was isolated by expression and genomic cloning from other species such as human (Liang *et al.*, 1995), rat (Saito *et al.*, 1995), *Caenorhabditis elegans* (Fei *et al.*, 1998), mouse (Fei *et al.*, 2000), sheep, cow, pig, chicken (Chen *et al.*, 1999;Chen *et al.*, 2002), zebrafish (Verri *et al.*, 2003) and macaco (Zhang *et al.*, 2004).

The gene encoding hPepT1 maps to human chromosome 13q33–34 (Liang *et al.*, 1995) and consists of 23 exons. The open reading frame encodes 708 amino acids and the sequence presents 50% identity and 70% similarity to PepT2. In general, mammalian *PepT1* genes present a high degree of similarity in both clustering and coding sequences. In particular, it is thought that *PepT1* orthologues genes evolved by exon shuffling and rearrangements of functional modules, because the genomic structures of human and mouse *PepT1* genes are modular, with each transmembrane segment and loop unit encoded by a different exon (Fig.1.3). The putative promoter region of *hPepT1* contains TATA boxes and GC-rich regions. TATA boxes are located in unusual positions (511 bp and 517 bp upstream from the transcription start site), while GC boxes are located near the start site (at -29 bp and several others within 300 bp). This kind of structure suggests that the GC box is a more important promoter in the regulation of *hPepT1* than is the TATA box. However, there may also be more than one transcription start site. There is also a potential insulin responsive element located upstream from the transcription

start site: this suggests that insulin might be involved in the regulation of *hPepT1* transcriptional activity (Urtti *et al.*, 2001).
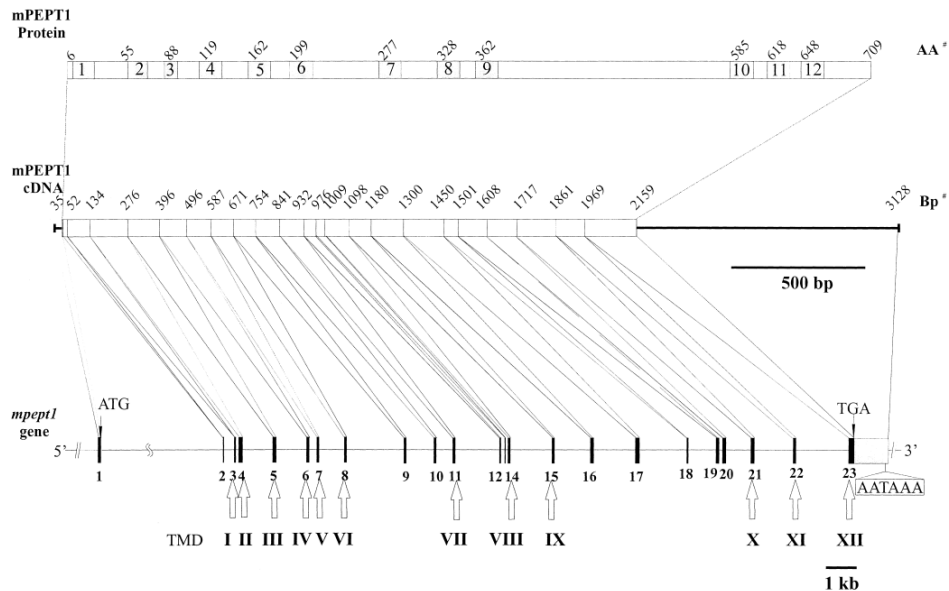
Fig.1.3 *Gene and cDNA organization of mouse PepT1 (Fei et al., 2000).*

1.2.4 PepT1 structure: from the prediction to the crystal

Rabbit PepT1 is a protein of 707 amino acids organized into 12 membrane-spanning regions and a big loop between TMD9 and TMD10 with the N- an C-termini facing the cytosol (Fig.1.4). The molecular weight is 71 kD of which at least 11 kD are due to N-linked glycosylation: the putative N-glycosylation sites are Asn 50, 439, 498 and 513. There are also a protein kinase C site (PKC, Ser 357) and a cAMP dependent phosphorylation site (PKA, Thr 362) (Fei *et al.*, 1994).

8
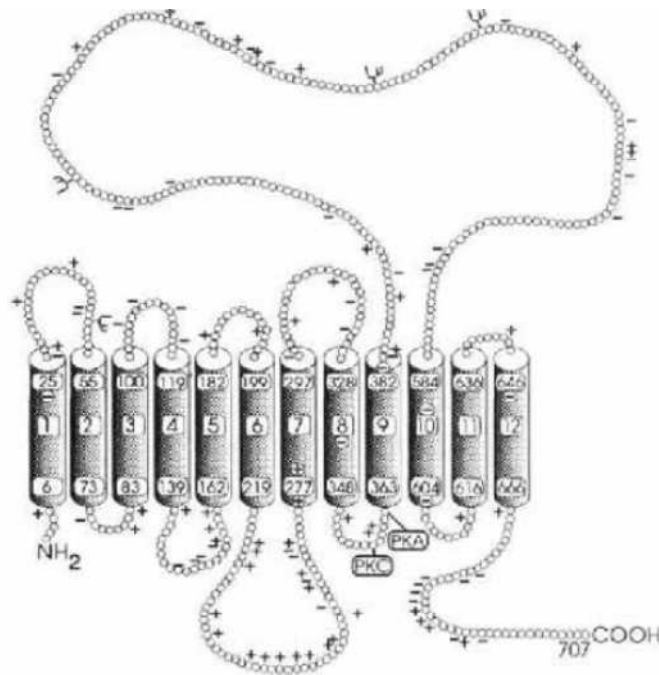
Fig.1.4 *Membrane topology of rabbit PepT1 (Fei et al., 1994).*

The membrane topology of PepT1 has been proposed from the first cloning from rabbit small intestine: the classical hydropathy plot suggested that rbPepT1 has 12 TMD (Fei *et al.*, 1994). This model was tested and confirmed in hPepT1 (81% identity with rbPepT1) by inserting epitope tags into predicted intra- or extracellular loops, and determining their accessibility to an anti-epitope antibody (Covitz *et al.*, 1998). More recently, other information about the mode in which the TMDs might be arranged in the membrane are derived from site-directed mutagenesis of individual residues (Meredith, 2004), cysteine scanning of TMDs (Kulkarni *et al.*, 2003a;Kulkarni *et al.*, 2003b) and from indirect computer-based approaches. The original 12 TMDs model has been refined by using the program MEMSAT (MEMbrane protein Structure and Topology) which predicted, with 78% accuracy,

the exact residues forming TMDs 1 and 2 (McGuffin *et al.*, 2000) and the program Cn3D correlating the rbPepT1 sequence with those of the previously crystallized bacterial transporters LacY (*E.coli* proton-coupled lactose permease, (Abramson *et al.*, 2003) and GlpT (glycerol-3-phosphate/inorganic phosphate antiporter, (Huang *et al.*, 2003;Meredith and Price, 2006). Moreover, there are evidences that PepT1 acts as a multimer: according to the suggested modeling PepT1 could be a tetramer, with a minimum requirement of two functional subunits in each protein complex (Panitsas *et al.*, 2006).

Finally, in the end of 2010, the crystal structure of a peptide transporter from the bacterium *Shewanella oneidensis*, PepT$_{So}$, has been reported by Newstead and coworkers (Newstead *et al.*, 2011). This bacterial homologue shows 30% identity within the TM regions to the mammalian PepT1 and PepT2 proteins and kinetic properties very similar to those reported for hPepT1. All previously identified residues proposed to be functionally important in the mammalian transporters are conserved (Newstead *et al.*, 2011). The overall fold adopted by TM helices is the same observed for the 12 TMDs in LacY, GlpT and EmrD (*E.coli* multidrug transporter) (Abramson *et al.*, 2003;Huang *et al.*, 2003;Yin *et al.*, 2006). But PepT$_{So}$ contains 14 TMD: helices H1–H6 and H7–H12 form six-helix bundles that come together to form a 'V'-shaped transporter, related by a pseudo two-fold symmetry axis running perpendicular to the membrane plane. The two additional TM helices, HA and HB, are inserted into the cytoplasmic loop forming a hairpinlike structure to connect the N- and C-terminal bundles (Fig.1.5 A). They do not contribute to any

conserved transport mechanism because are absent in all other species (Newstead *et al.*, 2011).
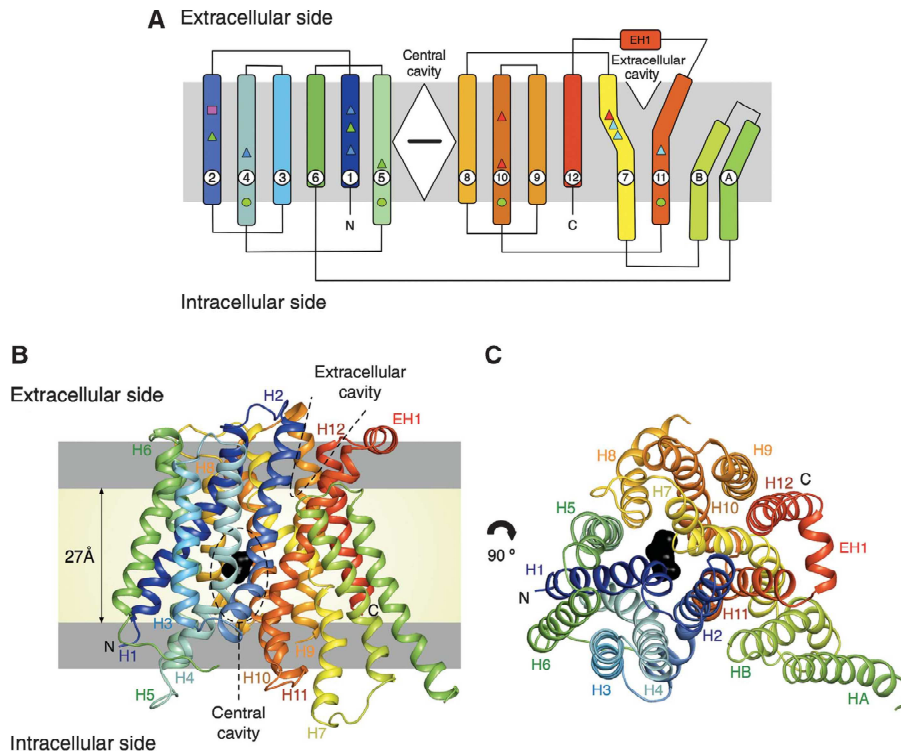
Fig.1.5 *Structure of PepT$_{So}$. A: PepT$_{So}$ topology. B: View in the plane of the membrane. C: View from the extracellular side of the membrane (Newstead et al., 2011).*

In the crystal structure there are two hydrophilic cavities, one central and one smaller extracellular (Fig.1.5 B). The central cavity is in the centre of the membrane closed to the extracellular space by a gate formed by helices H1, H2, H7 and H8. Access to the cytoplasm from this cavity is restricted by an intracellular gate formed by side-chain interactions between two-helix hairpins, helices H4 and H5 on the N-terminal side, and H10 and H11 on the opposing C-terminal side (Fig.1.5 C) (Newstead *et al.*, 2011). The interaction between these helices occurs through residues that are conserved across the

11

vertebrate peptide transporters; the most prominent of these interactions involves part of the highly conserved PTR2 (Peptide Transport family) motif (FYxxINxG) in which point mutations inactivate or greatly impair the transport (Hauser *et al.*, 2005).

The smaller extracellular cavity is also located at the interface between the N- and C-terminal domains. It is cone shaped, with the apex at the bottom near the central cavity, opening outward and its overall dimensions are ~16 x 8 x 8 Å. This cavity can represent the vestiges of entrance for peptides because is similar to the one representing the exit pathway for substrate in EmrD (Newstead *et al.*, 2011).

1.2.5 The oligopeptide-binding site

Waiting for the crystal structure, different groups using computer modeling methods predicted an arrangement of the 12 TMDs to form a transmembrane channel (Bolger *et al.*, 1998; Yeung *et al.*, 1998). This model of hPepT1, based on the amphipathicity of the helices and on minimizing interactions of the faces of TMDs in pairwise fashion, was refined by Lee and coworkers. The transmembrane channel is described like a "bubble", a vestibule large enough to accommodate a dipeptide (Lee *et al.*, 1999). Some years later, Meredith by modeling rat PepT1 on the LacY crystal structure reviewed the position of the TMDs (Fig.1.6 A). This model corrected Lee's group assumptions that TMDs adjacent in the sequence are also physically adjacent in the membrane and that the helices cross the lipid bilayer perpendicular to the surface. The helical wheels were arranged in order to keep in the central channel the residues that were

predicted to have a role in the substrate binding (Fig.1.6 B) (Meredith and Price, 2006).
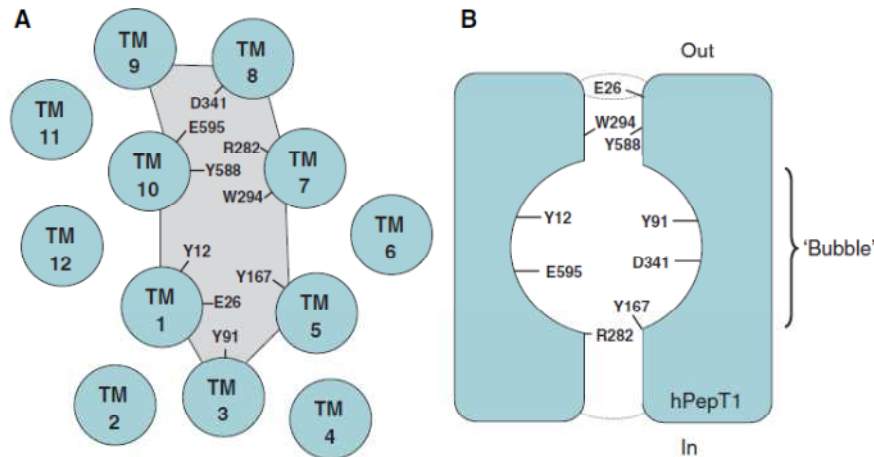
Fig.1.6 *A: 12-TM model for hPepT1. B: Schematic representation of the transmembrane channel with vestibule ('bubble') (Meredith and Price, 2006).*

After the crystallization of PepT$_{So}$ (Newstead *et al.*, 2011), it is believed that the central hydrophilic cavity observed in crystal could represent the oligopeptide-binding site because its dimensions, ~ 13 x 12 x 11 Å, are sufficient to accommodate both di- and tri-peptides. Moreover, these dimensions are sterically restrictive for larger tetra-peptide ligands and can also explain the lack of affinity for single amino acids that cannot interact sufficiently with both the N- and C-terminal domains of the transporter.

The binding site (Fig.1.7) is formed by residues from helices H1, H2, H4 and H5 from the N-terminal six-helix bundle and from helices H7, H8, H10 and H11 from the C-terminal bundle. On the N-terminal side there is a positively charged cluster of three conserved residues, Arg25(27), Arg32(34) and Lys127(140) (numbers in brackets correspond to the equivalent residues in human PepT1). And also two

13

conserved tyrosine residues, Tyr29(31) and Tyr68(64), are positioned close to this. On the C-terminal side, at a distance of ~ 13 Å from Lys127(140), are two further strictly conserved residues, Glu419(595) and Ser423(599), located in close proximity to Tyr154(167). The presence of a negatively charged residue at this position is important because the arrangement of opposite charges within the binding site could be a role in the recognition and orientation of peptides through the creation of a dipole moment. The presence of several possible hydrogen-bond donors and acceptors, as the tyrosine residues, could be advantageous in adapting to peptides of various lengths, sequences and charges (Newstead *et al.*, 2011).
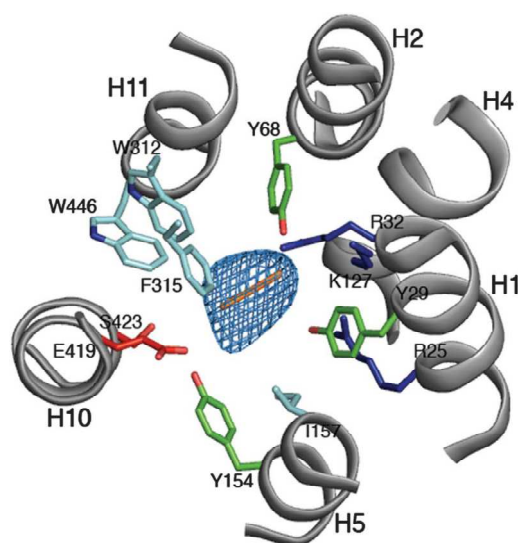
Fig.1.7 *The Peptide-binding site of PepT$_{So}$ (Newstead et al., 2011).*

Water also plays a key role in the docking process indeed both the two cavities observed in the crystallized PepT$_{So}$ are fully solvated. Water acts as a versatile space filling buffer between the substrate and the carrier-binding site and both charged and polar, as well as large apolar substrates can be accommodated at the same site (Tame *et al.*,

1996). But most of the conserved residues in the binding site are hydrophobic residues, including Ile157(170), Trp312(294), Phe315(297) and Trp446(622). These hydrophobic pockets, predicted also by biochemical studies, are likely to provide a suitable environment for peptide side chains generally (Bailey *et al.*, 2000) more hydrophobic than the peptide backbone. In fact, mutation of Trp312(294) of PepT1 to alanine reduces substrate uptake in HEK293 cells (Bolger *et al.*, 1998). Interestingly, some conserved residues are not located in the peptide-binding site but close to the central cavity and may have an important role in positioning residues involved in the substrate-binding (Newstead *et al.*, 2011).

Detailed structural information about the substrate binding site are important not only to understand the mode of transport by which PepT1 binds and transports its substrates that it's of great interest to researchers, but also to make PepT1 a good drug delivery system.

1.2.6 Substrate specificity

All information about the substrate specificity of PepT1 derive from detailed studies in which an enormous number of di- and tripeptides, amino acid derivatives and inhibitors have been tested by electrophysiological techniques, competition assays and also computational modeling. This large analysis has provided a good prediction of the substrate-binding template before than the binding site features were published with the crystal structure of a prokaryotic homologue of PepT1 (Newstead *et al.*, 2011).

PepT1 can transport thousands of di- and tripeptides that differ in structure, molecular size, polarity, net charge, stereochemistry, and

even the mesomeric structure of the peptide bond. It's hard to imagine that a single carrier protein would be able to transport these quite different substrates. For example, the molecular mass can vary between 132 Da for a di-glycine and 577 Da for a tri-tryptophane, and the net charge can range (at pH 7) from neutral to trivalently anionic, as for a triglutamate, or trivalently cationic, as for a tri-lysine. But evidences of multiple peptide transporters for the different substrate groups, initially postulated in the brush border membrane of intestinal epithelial cells, have not yet provided (Daniel, 2004).

The most simple substrate structures transported by PEPT1 are omega-amino fatty acids. This demonstrates that minimal molecular determinants of substrates for recognition by the transporter are two oppositely charged head groups (i.e., amino and carboxy groups) separated by at least four methylene groups (Fig.1.8). The distance of 5.5 to 6.3 Å between the centers of the head groups explains why neither free amino acids nor tetrapeptides can be bound or transported (Doring *et al.*, 1998b).

All additional structural features in a compound either modulate substrate affinity or even prevent substrate binding, indeed the peptide bond is not a prerequisite for substrate recognition. When an additional carbonyl group is incorporated into the backbone, as realized in delta-aminolevulinic acid (ALA), substrate affinity of the amino fatty acid increases. The carbonyl oxygen in the peptide bond is the relevant functional component because it can form additional hydrogen bonds with the substrate-binding domain. Whereas, if the peptide bond is replaced by an isosteric thioxo bond or if the peptide-bond nitrogen is methylated there is a reduction in substrate affinity

(Doring *et al.*, 1998a). Moreover, the α-amino group of the peptide transporter substrates and its spatial location play a crucial role in binding affinity and translocation. This group may form a salt bridge with either an acidic residue or a histidine residue located in the substrate binding pocket. In fact, peptides containing proline residues are critical substrates not only with respect to the conformation of the peptide bond but also with respect to other structural constraints. When provided in an aminoterminal position in peptides, the α-amino group is embedded into the pyrrolidine ring system: the peptide bond has a rigid, planar double-bond structure and the carbonyl-oxygen that generally increases the affinity of substrates, becomes negatively charged impairing interaction with the transporter. The consequence is a marked reduction in substrate affinity (Brandsch *et al.*, 1998). However, there are substrates in which the α-amino group is not present, such as in some ß-lactams and ACE-inhibitors that are transported by PepT1. Therefore, other groups in these compounds could interact with different residues in the binding domain (Daniel, 2004). The transporter can accommodate such a large number of different structures because water shields electric charges of amino acid side chains in the carrier's substrate-binding domain weakening unfavorable interactions between charged substrate groups and the protein (Tame *et al.*, 1996). Moreover, the substrate binding site of PepT1 is strongly stereoselective and oligopeptides containing solely D-enantiomers of amino acids are not transported. However, PepT1 is able to transport peptides containing both L- and D-amino acid residues: in this case the affinity depends from the D-enantiomers location in the oligopeptide. D-enantiomers are fairly well accepted in

the amino-terminal location, whereas when located in the carboxy-terminal position of a peptide, affinity is markedly reduced (Daniel, 2004).
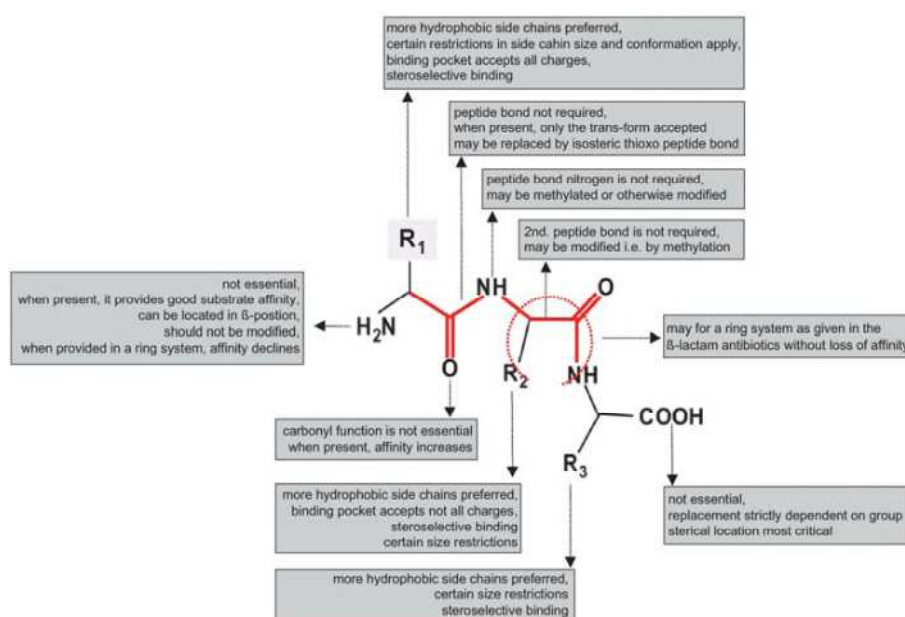
Fig.1.8 *Molecular determinants of PepT1 substrates*
(Daniel and Kottra, 2004).

1.2.7 Critical residues in PepT1

Significant evidences about the critical role of some residues in PepT1 derive from mutational studies. Histidine 57 (H57) in the second transmembrane domain (TM2) is essential for PepT1 function (Fei *et al.*, 1997;Chen *et al.*, 2000;Uchiyama *et al.*, 2003) and the protonation of this residue is a necessary step in the transport cycle (Steel *et al.*, 1997). In fact, when protonated, H57 has been proposed to bind the carboxy terminus of the peptide substrate (Terada *et al.*, 1996;Bailey *et al.*, 2000). The neighboring tyrosine, Y56, has also been shown to stabilize proton binding and, together with Y91 and

Y167, to play important roles in determining the affinity and transport rate of rabbit PepT1 forming hydrogen bonds and providing a hydrophobic environment for side chains (Uchiyama *et al.*, 2003;Pieri *et al.*, 2009). In addition, histidine 121 (H121) in TM4 has a functional role in the central cavity of PepT1 (Terada *et al.*, 1996) and also three residues of TM7, F293, L296 and F297, subjected to cysteine-scanning mutation analysis, are structurally important for PepT1, because of their hydrophobic packing interaction (Kulkarni *et al.*, 2003b). Again a structural role was proposed for tryptofane 294 (W294), because some PepT1 mutants in this residue don't have any detectable transport activity, even if W294 was tolerant of cysteine replacement in human PepT1 (Bolger *et al.*, 1998;Panitsas *et al.*, 2006). Various mutants of glutamate 595 (E595) in PepT1 have been reported to drastically reduce transport activity, except where mutation was to an aspartic acid (Xu *et al.*, 2009), indicating the importance of a negatively charged residue at this position. In fact, E595 could bind the amino termini of PepT1 substrates, since together with H57 forms a dipole moment important in the recognition and in the arrangement of peptides (Bailey *et al.*, 2000). Other residues have been found to affect PepT1 activity in interesting ways: particularly Arg282 (R282) and Asp 341 (D341) have been reported to form a charge pair that may break and reform during the transport cycle (Kulkarni *et al.*, 2007;Pieri *et al.*, 2008;Meredith, 2009). Interestingly mutation R282E appeared to convert the cotransporter in a substrate-gated, rater unspecific channel (Meredith, 2004;Pieri *et al.*, 2008).

1.3 Electrophysiological properties of PepT1

Overexpression of ion-coupled cotransporters in heterologous systems, especially *Xenopus laevis* oocytes, allows precise electrophysiological measurements which reveal detailed features in the kinetic mechanism.

PepT1 as well as most cotransporters displays two main kinds of electrical activity: in the absence of organic substrate, transient presteady-state currents (I_{pre}) are generated by charge relocation during voltage steps; in the presence of substrate, transport-associated currents (I_{tr}) are recorded.

1.3.1 Presteady-state currents and transport-associated currents

I_{pre} has the characteristics of an intramembrane charge movement, as it is transient, saturable and symmetric (Mager *et al.*, 1993;Bossi *et al.*, 1999;Forlani *et al.*, 2001). Conversely, I_{tr} is true transmembrane current, as the actual charge carriers physically move from the extracellular to the cytosolic compartment or vice versa. I_{pre} and I_{tr} are reminiscent of two distinct currents in voltage-dependent ionic channels: the gating current and ionic current through the channel itself, respectively (Armstrong and Bezanilla, 1974;Hille, 2001). In ionic channels clearly distinct functions have been assigned to the two currents. The gating currents are believed to signal the conformational changes that accompany opening (or closing) of the permeation pathway (Catterall, 1993). The current through the channel can only occur when the gates are open, and therefore a simple relation, based on Ohm's law, exists between the probability of the

channel being open and the current flux. Whereas the ionic current obviously depends on the presence and on the equilibrium potential of the permeating ion and this parameter does not affect the gating currents (Fesce *et al.*, 2002).

In cotransporters the situation is certainly less clear, in fact, the charges responsible for I_{pre} cannot be clearly distinguished from those giving rise to the transmembrane current flux. I_{pre} of cotransporter may also be explained as due to rearrangement of a charged portion of the protein in the membrane field (Mager *et al.*, 1996;Loo *et al.*, 1998); however, the charge relocation might be due to the motion of ions that move back and forth between the external solution and an open vestibule in the transporter facing the extracellular side (Mager *et al.*, 1996;Lester *et al.*, 1996). Whatever the actual mechanism, it is generally agreed that presteady-state currents represent a partial step in the transport cycle. The time integral of this kind of current represents the amount of charges that moves in the membrane electrical field in response to the voltage change. It is possible to note that the same amount of charges moves during the "on" (from the holding potential, V_h, to a given potential) and the "off" (when the voltage is returned back to V_h) of the voltage pulse (Fig.1.9 B). Such behavior is reproduced by a simple electrical circuit constituted by a resistor and a capacitor in series (Fig.1.9 A): here a voltage step ΔV generates a current given by:

$$I = \frac{\Delta V}{R} \exp\left(-\frac{t}{RC}\right),$$
[eq.1.1]

which declines to zero with a time constant given by $\tau = RC$ and displaces an amount of charge $Q = C\Delta V$ onto the capacitor plates (Fig.1.9 B) (Peres *et al.*, 2004).

21
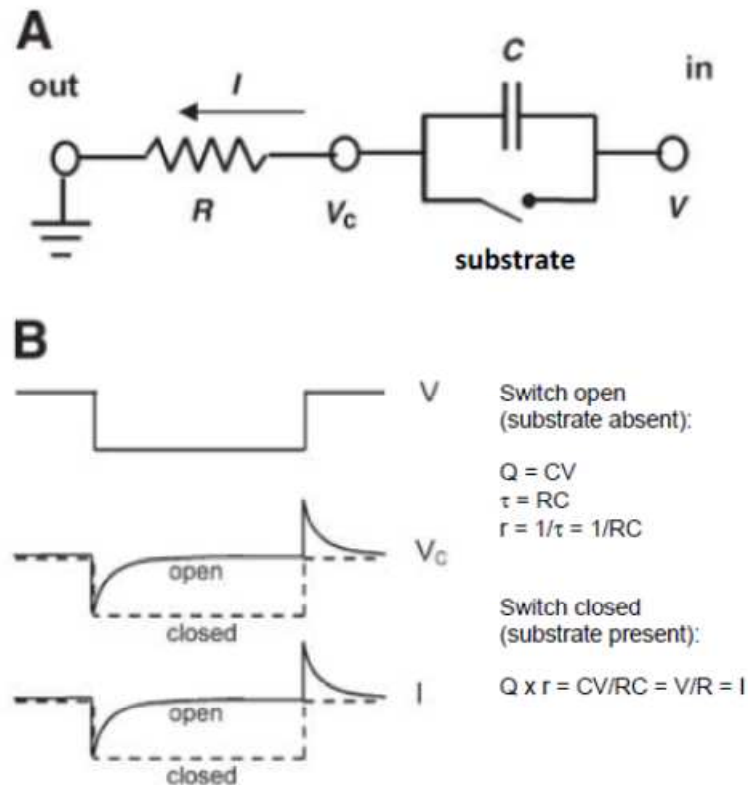
Fig.1.9 *A: Electrical circuit simulating intramembrane charge movement. B: time course of the relevant electrical quantities in response to step voltage changes across the membrane (Peres et al., 2004).*

1.3.2 Intramembrane charge movement

The empirical relations explaining electrophysiological observations represent the starting point for the development of kinetic schemes of heterologously espressed transporters. In the simplest formalization a two-state system is assumed: in state A the electrical charge associated with the transporter is located near the internal limit of the membrane electrical field, while in state B the charge is displaced toward the outer membrane margin (Fig.1.10). Clearly, the relative occupation of the two states will depend on the

membrane potential: assuming a positive mobile charge, state A in Fig.1.10 will be populated at negative internal potentials, while at positive potentials the most populated state will be B. This description may be translated in terms of reaction kinetics described in the figure:
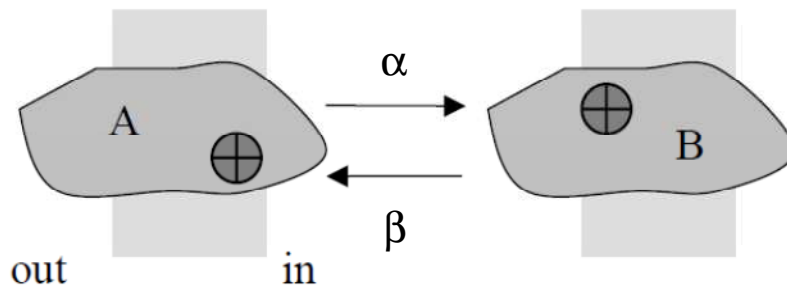
Fig.1.10 *Elementary representation of a two-state system explaining intramembrane charge movement.*

in which α and β are the voltage-dependent unidirectional rate constants (dimensions s^{-1}) for the outward and inward charge movement, respectively.

Consistent with the laws of electrodiffusion, α and β will depend on the membrane voltage according to the following general kind of expressions:

$$\alpha = k_\alpha \exp(q\delta V / 2kT)$$

[eqs 1.2]

$$\beta = k_\beta \exp(-q\delta V / 2kT)$$

where q is the elementary charge, δ is the fraction of electrical field over which the charge movement occurs, k is Boltzmann's constant, T the absolute temperature and k_α and k_β are the zero voltage rate constants. Clearly, α will increase as the membrane potential is made more positive and β will increase as the membrane potential is made more negative.

Considering a given population of molecules that can undergo reaction in Fig.1.10, $A + B = $ constant, and defining the relative amounts of A and B as:

$$A^* = \frac{A}{A+B} \quad \text{and} \quad B^* = \frac{B}{A+B} \qquad \text{[eqs 1.3]}$$

we have:

$$\frac{dA^*}{dt} = -\alpha A^* + \beta B^*$$

$$\frac{dB}{dt} = \alpha A^* - \beta B^* \qquad \text{[eqs 1.4]}$$

it is easy to verify that at equilibrium, B* is given by:

$$B^* = \alpha/(\alpha + \beta) \qquad \text{[eq.1.5]}$$

and therefore, replacing eqs 1.2 in eq.1.5:

$$B^* = \frac{1}{1+\frac{k_\beta}{k_\alpha}\exp{(-Vq\delta/kT)}} \qquad \text{[eq.1.6]}$$

which is a Boltzmann relation with slope $s = q\delta/kT$, and in which the molecules are equidistributed in the two states at voltage $V_{1/2} = \ln{(k_\beta/k_\alpha)}/$s.

From eqs 1.4 it is also easy to derive the differential equation that describes the approach to equilibrium following a voltage jump:

$$\frac{dB^*}{dt} = \alpha - (\alpha + \beta)B^* \qquad \text{[eq.1.7]}$$

which may be solved to give:

$$B^* = B_0^* + (B_\infty^* - B_0^*)\,(1\text{-}exp[\text{-}t/\tau]) \qquad \text{[eq.1.8]}$$

where the subscript 0 and ∞ respectively refer to the value before and after the voltage jump, so that B_0^* and B_∞^* are the fractions of molecules in state B before and after the voltage change respectively; they may be obtained from eq.1.5 by using the corresponding values of α and β:

$$B_0^* = \frac{\alpha_0}{\alpha_0 + \beta_0}$$

[eqs 1.9]

$$B_\infty^* = \frac{\alpha_\infty}{\alpha_\infty + \beta_\infty}$$

The time constant of the exponential is:

$$\tau = 1/(\alpha_\infty + \beta_\infty)$$ [eq.1.10]

Calling Q_{max} the total amount of electrical charge involved in the process, the time course of the transient current elicited by voltage changes can be obtained by differentiating eq.1.8 and multiplying the result by Q_{max}, which gives:

$$I = \frac{Q_{max}(B_\infty^* - B_0^*)}{\tau} \exp\left(-t/\tau\right)$$ [eq.1.11]

This expression constitutes the basis for the analysis of the presteady-state currents observed in transporters. Fitting eq.1.11 to the experimental traces of transient current yields the time constant of decay, τ, while the time integral gives:

$$\int_0^\infty I = Q_{max}(B_\infty^* - B_0^*)$$ [eq.1.12]

which represents the amount of charge moved by the voltage jump.

In particular, at any membrane voltage the quantity of charge displaced towards the inner side is given by $Q_{in}(V) = Q_{max}A^* = Q_{max}\frac{\beta}{\alpha+\beta}$. If, in agreement with standard notation, a minus sign is assigned to inward charge movement, this may be rewritten as: $Q(V) = -Q_{max}\frac{\beta}{\alpha+\beta}$.

The analysis of presteady-state currents is performed by first of all isolating these currents from the endogenous components of the oocytes and from other contributions to the total current; this may be

achieved by subtracting the traces recorded in conditions in which the presteady-state currents have been eliminated, by the use, for instance, of saturant concentration of substrate (Fig.1.11B), from the corresponding traces recorded in control conditions (Fig.1.11A) (Bossi *et al.*, 1999). A correction of the baseline may consequently be necessary before performing the integration of the transients (Fig.1.11C). The graph of the integrated charge against voltage shows the typical sigmoidal shape (Fig.1.11E) expected from eq.1.6. For each voltage step the "on" and "off" integrals coincide, as expected in a process in which the fraction of charge in the two positions at equilibrium conditions is determined only by voltage.

The relaxation time constant τ may be obtained by fitting single or multiple exponentials to the current records at each potential; a representative τ vs. V plot is shown in Fig.1.11D. The τ vs. V plot is bell-shaped, confirming the expectations of equations 1.2 and 1.10. Furthermore, the theory outlined above predicts that the maximum value of τ should occur at the voltage where 50% of the charge is in one position and 50% in the other and τ should depend only on the voltage after the jump.
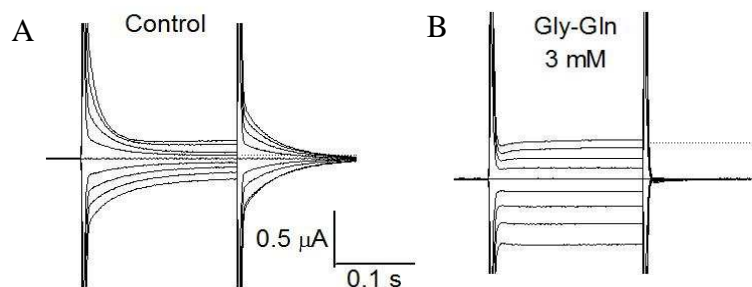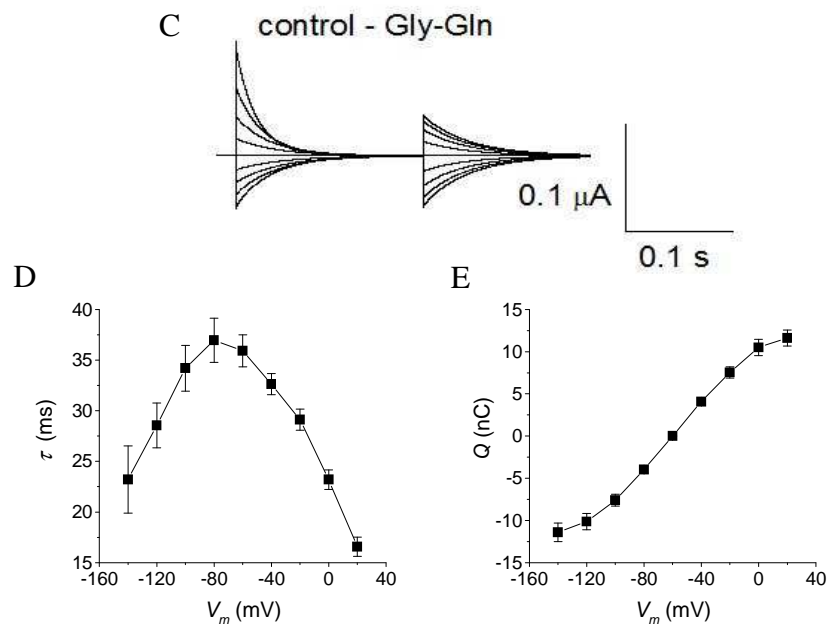
Fig.1.11 *Analysis of presteady-state currents for the oligopeptide transporter rbPepT1. A: traces recorded in physiogical solution, containing 98 mM Na$^+$ among other ions; B: traces from the same oocyte after adding 3 mM Gly-Gln; C: isolated presteady-state currents resulting by the subtraction of the traces in B from those in A. D: relaxation time constant of the transient currents in C as function of voltage; E: charge vs. V plot from the integration of the transient currents.*

1.3.3 Transport mechanism of PepT1

In 1996, Wright and coworkers have investigated the transport mechanism of human intestinal PepT1 with regard to voltage dependence, steady-state kinetics and transient charge movements using two microelectrode voltage clamp in *Xenopus* oocytes expressing the transporter. They found that H$^+$/Gly-Sar cotransport obey Michaelis-Menten-type kinetics. The apparent affinity constant for Gly-Sar is ~ 0.7 mM at V_m -50 mV (in the pH range 5.0–6.0). At each V_m, Hill coefficients are ~1 for H$^+$ activation of the Gly-Sar-evoked current, suggesting 1 H$^+$:1 Gly-Sar transport stoichiometry. In

27

the presence of H^+, but in the absence of Gly-Sar, they observed voltage-dependent presteady-state currents. According to their model (Fig.1.12), these transient currents are due to binding/dissociation of H^+ to/from the cotransporter and a conformational change of the unloaded carrier between the external and internal membrane interfaces. Presteady-state data indicate that H^+ can bind to the empty carrier in the absence of oligopeptide. The steady-state data indicate that H^+ and oligopeptide are translocated simultaneously in the same reaction step, because, at least at V_m more positive than -70 mV, the affinity of the carrier for substrate (Gly-Sar) deteriorates at diminishing $[H^+]_o$. Moreover, the transporter prefers to bind H^+ and substrate in an orderly fashion, H^+ first. In fact, the apparent maximal transport rate is significantly attenuated only once $[H^+]_o$ was reduced 100-fold, and even then the reduction in I_{max} is less than for a system in which activator and substrate binding was random (Mackenzie *et al.*, 1996).
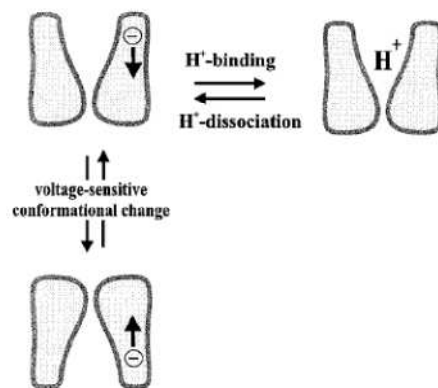
Fig.1.12 *Model of charge movement proposed by Wright and coworkers for hPepT1 (Nussberger et al., 1997).*

One year after, a more detailed transport mechanism considering the affect of intracellular pH on the pre-steady-state kinetics of rabbit PepT1 was purposed (Nussberger *et al.*, 1997).
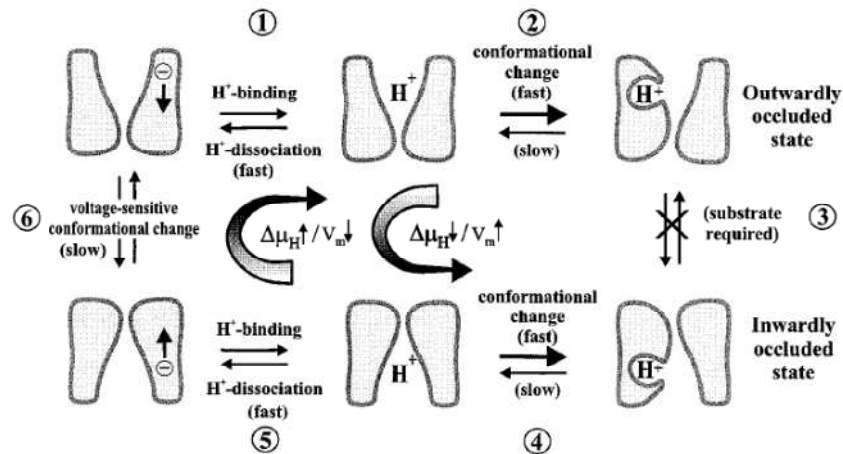
Fig.1.13 *Model of charge movement proposed by Hediger and coworkers for rabbit PepT1 (Nussberger et al., 1997).*

According to this revised model (Fig.1.13) the empty carrier has a single H^+-binding site that is symmetrically accessible from both sides of the membrane. H^+ binding to the extra- or intracellular surface is followed by a conformational change resulting in the formation of outwardly or inwardly facing occluded states, respectively, and that these protonated states cannot cycle between the inside or outside in the absence of peptide. The pre-steady-state currents in response to voltage jumps are due to binding or dissociation of H^+ within the membrane electric field near the extra- or intracellular transporter surface (steps 2/1 and 4/5) and to reorientation of the empty carrier during the voltage sensitive conformational change (step 6). Increasing the H^+ chemical gradient and/or decreasing V_m (hyperpolariza- tion) shift the carrier toward the outwardly occluded

state. In other words, acidic pH increases the number of PepT1 molecules in the outwardly facing state that has an increased affinity for peptides. Similarly, decreasing the H^+ chemical gradient and/or increasing V_m (depolarization) shift the carrier toward the inwardly occluded state.

Thus, the model predicts that the magnitude and polarity of the transient charge movements depend on the H^+ electrochemical gradient. According to the authors, from a physiological perspective, this concept makes sense because the pH near the intestinal brush border membrane is acidic (pH 5.5–6.0), which favors the outwardly occluded state and promotes efficient peptide absorption (Nussberger *et al.*, 1997).

New implications for proton-driven peptide symport derive from crystal structure of PepT1.
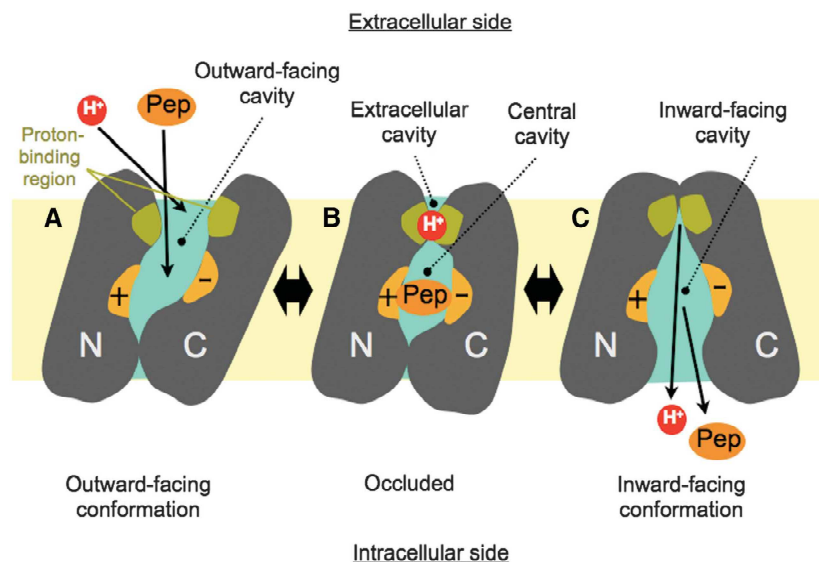
Fig.1.14 *Mechanism for peptide–proton symport proposed for PepT$_{So}$ (Newstead et al., 2011).*

The PepT$_{So}$ structure presents a ligand-bound occluded conformation with a clearly identified substrate-binding site. Both ends of the central cavity containing residues involved in peptide binding are closed. For uptake of peptide, the central cavity needs to be connected to the extracellular space, potentially through the extracellular cavity (Fig.1.14). The central and extracellular cavities are separated by a putative extracellular gate, which is made of helix H7. Opening of the intracellular gate seems to be controlled by the movement of helix hairpin H10–H11 in the C-terminal helix bundle. This hairpin, forming a restriction for exit of bound peptide to the intracellular side, would move together with the subbundle C1, composed of helices H7, H11 and H12. From this structural model employed to explain PepT1 transport, the N-terminal helix bundle seems less dynamic, whereas the C-terminal helix bundle contains the mobile gates, quite possibly driven by the proton electrochemical gradient. To understand the mechanism in full however, it will be essential to determine the PepT$_{So}$ structure in different conformational states and determine the sites of protonation and peptide binding (Newstead *et al.*, 2011).

1.3.4 Mode of transport

How does PepT1 successfully link the transport of such diverse compounds to the cotransport of protons? In 1997, Hediger and coworkers published a study in which they examine the stoichiometry of neutral and charged dipeptides transported by rabbit PepT1 expressed in *Xenopus* oocytes and the pH dependence of the transporter (Steel *et al.*, 1997). First of all, the independence of PepT1

uptake of extracellular Na^+, K^+ and Cl^- is confirmed (Fei *et al.*, 1994) and, moreover, it was demonstrated that peptide-evoked fluxes are entirely due to H^+ movement since the transporter doesn't display substrate-gated anion conductances. Using a set of substrates, kinetic parameters and transport efficiency are determinated for various classes of dipeptides. Neutral, acidic as well as basic dipeptides induce intracellular acidification. Maximal transport of Gly-Leu, Gly-Glu, Gly-Lys and Ala-Lys occur at pH 5.5, 5.2, 6.2 and 5.8, respectively. The I_{max} values are relatively pH independent but the apparent affinity (K_m) values for these peptides are highly pH dependent. In other words, at physiological pH (pH 5.5-6.0) PepT1 prefers neutral and acidic peptides.

The rate of intracellular acidification (measured using a pH-sensitive microelectrode), the initial rates of the uptake of radiolabelled peptides and the associated charge fluxes gave proton-substrate coupling ratios of 1:1, 2:1 and 1:1 for neutral, acidic and basic dipeptides, respectively. In particular, according to the purposed model for the coupled transport (Fig.1.15), negatively charged dipeptides are cotransported with two protons, one of which is involved in H^+ coupling while the other is predicted to neutralize the charge on the substrate creating a zwitterionic species. On the other hand, a single proton is cotransported with positively charged dipeptides and the transport optima is shifted towards more basic pH values. To account for this, a histidine residue located near the peptide site is predicted to be deprotonated at or above pH 6.0 to allow binding and translocation of positively charged dipeptides (Steel *et al.*, 1997).
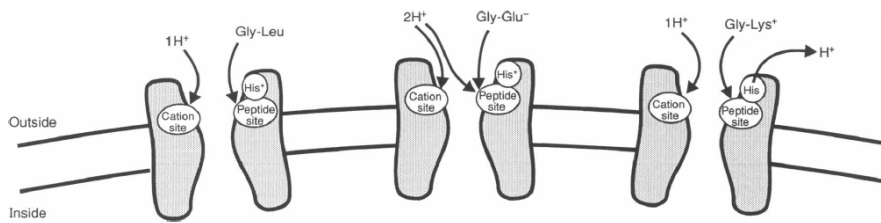
Fig.1.15 *Model for coupled transport of neutral and charged dipeptides by PepT1 (Steel et al., 1997).*

1.4 Regulation, pathological implications and pharmacology of PepT1

1.4.1 Regulation of PepT1 transport activity

PepT1 activity is modulated by regulation factors acting on the gene expression or influencing the targeting of the transporter on the membrane.

Intracellular signaling pathways induce acute changes in the transport activity. An activation of PKC stimulates endocitotic mechanisms causing a rapid decline in apical peptide uptake based on a decreased V_{max} without changes in substrate affinity.

Prolonged exposure to substrates also causes PepT1 retrieval from the membrane via endocytosis without to involve PKC pathways (Mertl *et al.*, 2008). In contrast with these observations, conducted on rabbit PepT1 expressed in *Xenopus* oocytes, long-term incubation of human intestinal Caco-2 cells in a dipeptide-containing culture medium increases the V_{max} of hPepT1 with no change in K_m (Thamotharan *et al.*, 1998).

These apparently opposite findings can be explained by the presence in Caco-2 cell model of a compensation mechanism to

increase *de novo* synthesis of new carrier proteins; since the oocyte does not express endogenously oligopeptide transporters, and it cannot respond like a mammalian cell with alterations in gene transcription, the type of adaptation observed in Caco-2 cells cannot be expected in oocytes (Mertl *et al.*, 2008).

Other regulation pathways involve cAMP; increasing intracellular cAMP levels by cholera toxin or forskolin treatment inhibits peptide transport (Muller *et al.*, 1996), whereas a decrease in the cAMP-level, for example, by the adrenoreceptor agonist clonidine, stimulates transport as shown in Caco2–3B cells and in the rat jejunum (Berlioz *et al.*, 1999;Berlioz *et al.*, 2000).

An acute effect on the transport activity of PepT1 is observed by alterations in intracellular free calcium concentration. An increase in free calcium rapidly decreases activity, whereas a decrease in free calcium causes an increased V_{max} of PepT1 (Wenzel *et al.*, 2002).

PepT1 transport activity also depends on the transmembrane proton gradient, which is mainly generated by the apical Na^+/H^+ exchanger and any alterations of pH gradients and membrane potential secondarily affect PepT1 activity (Thwaites *et al.*, 2002).

Indeed, a pH-sensing regulatory factor of *hPepT1* (*hPepT1*-RF) was cloned and characterized; its amino acids sequence is more shorter but almost the same than PepT1: residues 18–195 in *hPepT1*-RF are identical to residues 8–185 in hPepT1, whereas residues 1–17 and 196–208 are unique. When expressed in *Xenopus* oocytes, *hPepT1*-RF alone does not induce any peptide transport activity, but when it is coexpressed with hPepT1, Gly-Sar uptake is more strongly

inactivated at lower pH than in presence of PepT1 alone (Saito *et al.*, 1997).

A regulation of PepT1 abundance and activity in epithelial cells can be observed by hormones such as insulin, leptin, growth hormone, and thyroid hormone (Thamotharan *et al.*, 1999b;Buyse *et al.*, 2001;Ashida *et al.*, 2002). Insulin stimulates dipeptide uptake into Caco-2 cells increasing the V_{max} without changes in K_m (Thamotharan *et al.*, 1999b). Similarly, leptin was shown to enhance dipeptide uptake into Caco-2 cells and in the rat intestine (Buyse *et al.*, 2001). Whereas both hormones appear to increase the PepT1 protein density in the apical membrane by recruitment of preformed transporters, without changes at the transcriptional level, treatment of Caco-2 cells with 3,5,3'-triiodothyronine (T3) reduces the V_{max} for dipeptide influx significantly with a concomitant reduction in the PepT1 mRNA to 30% of control level (Ashida *et al.*, 2002). Recombinant human growth hormone has recently been shown to increase peptide transport activity in Caco-2 cells (Sun *et al.*, 2003) and in combination with epidermal growth factor also increased PepT1 expression in the rabbit small intestine after midgut resection (Avissar *et al.*, 2001).

Several studies have demonstrated that the expression level of PepT1 and its function is altered by dietary treatments. In rats, a brief fast (Thamotharan *et al.*, 1999a), as well as sustained starvation and malnourishment (Ihara *et al.*, 2000), is associated with a high expression level of PepT1. This is important also with respect to protein assimilation in states of impaired jejunal structure and function, suggesting that the high resistance of the intestinal oligopeptide transport activity to tissue damage is based on an

increased protein synthesis rate (Tanaka *et al.*, 1998). Moreover, free amino acids and dipeptide, especially Phe and Gly-Phe, increase PepT1 expression by a mechanism involving transcription factors associated with gene regulation under essential amino acids deprivation (Pohjanpelto and Holtta, 1990;Guerrini *et al.*, 1993).

Recently, a microRNA-mediated regulation of PepT1 expression was observed during the differentiation of intestinal epithelial Caco-2 cells. It was demonstrated that microRNA-92b (miR-92b) suppresses PepT1 expression, by directly targeting the PepT1 3'-untranslated region, at both mRNA and protein levels, with subsequent reduced PepT1 transport activity. In addition, miR-92b suppresses bacterial peptide-induced proinflammatory responses in intestinal epithelial cells by inhibiting PepT1 expression (Dalmasso *et al.*, 2011).

PepT1 activity shows also a circadian rhythm: substrate transport and mRNA expression of intestinal rat PepT1 are greater in the dark phase than the light phase. In contrast, renal isoform of the transporter shows little diurnal rhythmicity in protein and mRNA expression. These findings indicate that PepT1 regulation could affect the intestinal absorption of dietary protein (Pan *et al.*, 2002).

1.4.2 PepT1 implications in pathological states

Several studies have demonstrated PepT1 implications in pathological states that alter the expression level and the function of the transporter.

Diabetes, for example, induces an increased protein expression level of PepT1 in the small intestine, in fact, in rats made diabetic by

treatment with streptozotocin, the maximal peptide transport activity increases almost twofold than in the control. In particular, diabetes increases the abundance of mRNA encoding PepT1 without altering its rate of transcription, but increasing in the stabilization of mRNA encoding the transporter. Lastly, studies show that diabetes similarly affects the protein and gene expression of the renal isoform of the transporter (Gangopadhyay *et al.*, 2002).

Bacterial infections have also been demonstrated to alter PepT1 expression level and function in the gut. For example, in rats infected with *Cryptosporidium parvum*, which causes diarrhea in children and may lead to malnutrition, PepT1 is up-regulated at transcriptional level (Barbot *et al.*, 2003). It was reported that pathogenic bacteria induce PepT1 expression in colonocytes via the transcription factor Cdx2 (Nguyen *et al.*, 2010).

PepT1 is expressed throughout the small intestine and is absent or expressed at very low levels in the human colonic mucosa under normal conditions, but there are findings that it is expressed in inflamed colonic tissues. In patients suffering from short-bowel syndrome (SBS), a devastating clinical problem characterized by diarrhea, dehydration, micronutrient depletion, and generalized malnutrition, the abundance of PepT1 mRNA in the colon is more than 5-fold that in control subjects. This up-regulation of PepT1 in the colon of SBS patients is an example of gut adaptation: the human colon can increase the luminal transport of di- and tripeptides derived from the diet or other sources during intestinal failure (Ziegler *et al.*, 2002).

Moreover, in patients with chronic ulcerative colitis and Crohn's disease, PepT1 mediates transport of the bacterial proinflammatory peptides such as formyl-methionyl-leucyl-phenylalanine (fMLP) (Merlin *et al.*, 2001), muramyl dipeptide (MDP) (Vavricka *et al.*, 2004), and L-Ala-γ-D-Glu-meso-DAP (Tri-DAP) (Dalmasso *et al.*, 2010). In particular, hPepT1-mediated transport of fMLP, potentially stimulates expression of key accessory immune molecule such as MHC-1 (Merlin *et al.*, 2001); MDP activates NF-kB and chemokine production (Vavricka *et al.*, 2004).

These data collectively indicate that, in some states of chronic inflammation, hPepT1, anomolously expressed in the colon, may play an important role in promoting colonocyte participation in host defense and pathogen clearance (Nguyen *et al.*, 2009).

There is no known pathology associated with the malfunction of the oligopeptide transporter, but a functional polymorphism in the PepT1 gene might be of relevance to inflammation and antibacterial responses in inflammatory bowel disease. In the second loop of hPepT1 transporter it was found a coding polymorphism, where the C to T nucleotide substitution corresponds to an amino acid change from serine to asparagines at residue 117 (Ser117Asn). This single nucleotide polymorphism (SNP) shows significant but reverse association with inflammatory bowel disease in patients from Sweden and Finland: the common allele C has predisposing and protective effects in the Swedish and Finnish cohorts, respectively. It was suggested that the PepT1-Asn117 variant operates a more efficient transport of MDP (Zucchelli *et al.*, 2009).

Other functional SNPs were identified: the variant Pro586Leu shows significantly reduced transport capacity (Zhang *et al.*, 2003) and also for the variant Phe28Tyr altered transport of Gly-Sar and cephalexin is observed in various transfected mammalian cells (Anderle *et al.*, 2006). PepT1 polymorphisms need additional studies, but it's evident that may have an important role in translation, degradation and membrane insertion of the transporter and may contribute to disease susceptibility.

1.4.3 Pharmacological relevance of PepT1

The structural similarity of a variety of drugs with the basic structure of di- or tri-peptides explains the transport of antibiotics, angiotensin-converting inhibitors, and antiviral agents by PepT1. Moreover, the high transport capacity of PepT1 allows fast and efficient intestinal uptake of the drugs (Daniel, 2004).

Classic and well-characterized drug substrates of PepT1 are the numerous amino beta-lactam antibiotics of the cephalosporin and penicillin classes (Ganapathy *et al.*, 1995), as well as selected angiotensin-converting enzyme inhibitors such as captopril and the ester prodrugs enalapril and fosinopril. Their interaction with PepT1 in the gut epithelium provides an oral availability generally between 40% and 90% of a dose of these drugs (Zhu *et al.*, 2000;Shu *et al.*, 2001). A variety of compounds with structures related to the cephalosporins or the ACE-ester prodrugs have also been shown to inhibit the peptide transporters, but their affinity is generally low (Daniel and Kottra, 2004). The orally active sulphonylurea compounds nateglinide and glibenclamide inhibit the peptide

transporters noncompetitively (Sawada *et al.*, 1999;Terada *et al.*, 2000). On the other hand, a series of high-affinity-type competitive could be developed on basis of lysyl-dipeptides in which the side chain amino function is blocked with a Z or $Z(NO_2)$ group especially if this modification is located in the amino-terminal position of a dipeptide (Knutter *et al.*, 2001;Theis *et al.*, 2002). Other interesting drugs shown to be PepT1-substrates include sulpiride, a selective dopamine D2 receptor antagonist (Watanabe *et al.*, 2002), and the dipeptide-mimetic bestatin that as a peptidase inhibitor also acts as an antitumor agent (Terada *et al.*, 1997). The capability of peptide transporters for the uptake of d-aminolevulinic acid (ALA) can be also used for tumor therapy (Doring *et al.*, 1998a;Neumann and Brandsch, 2003). ALA is a precursor of cellular porphyrin synthesis: laser-induced photoactivation of the accumulated porphyrins is used to submit tumor cells to necrosis (Kelty *et al.*, 2002).

In conclusion, broad substrate specificity, high transport rate and also a growing scientific interest in intestinal peptide transport in pharmacology make PepT1 a good target for efficient oral delivery of rational designed drugs.

Chapter 2.   Materials and Methods

2.1   Molecular biology

2.1.1 PepT1 cDNAs

cDNAs encoding PepT1 were cloned in pSPORT1 vector between *Sal*I and *Not*I sites (for rb PepT1-FLAG cDNA) (Mertl *et al.*, 2008) and between *Sal*I and *Hind*III sites (for sb and zb PepT1 cDNAs).

pSPORT1 (Fig.2.1) is an expression vector that presents the ampicillin resistance (AP^r) and the reported multi cloning site (MCS). At both ends of the MCS there are promotor sites for T7, T3 and M13 RNA polymerases.
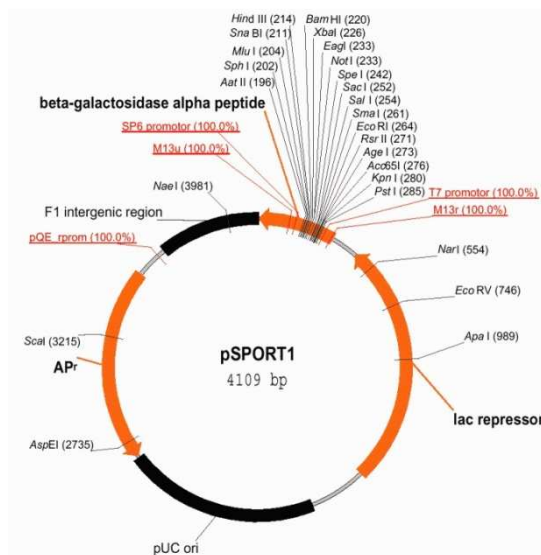
Fig.2.1 *pSPORT1 vector.*

2.1.2 Construction of point mutations

Mutations in rabbit PepT1 were obtained by site-directed mutagenesis (Quickchange Site-Directed Mutagenesis Kit, Stratagene Inc., Milano, Italy). Briefly, 20 ng of the plasmid containing the FLAG-wild-type PepT1 cDNA (Mertl *et al.*, 2008) were amplified with 2.5 units of *Pfu* DNA polymerase in the presence of overlapping primers containing in their sequence the mutated codons:

*rbPepT1 D341R: 5'-cctggtccccatcatg**cgc**gccgtggtgtatcc-3'*

*rbPepT1 H57R: 5'-ggacgacaacctgtccacggt**cgt**ctaccacacgttcgtc-3'*

*rbPepT1 R282X:5'-cgcgcagatcaagatggttacg**xxx**gtgctgttcctgtacatccc-3'*

where the original sequence *agg* was transformed in *xxx* that correspond to the following triplet for R282D **gat**, for R282A **gcg**, for R282E **gag**, for R282K **aag**, for R282Q **gac** and for R282C **tgt**. PCR amplification was performed with 25 thermal cycles of 95°C for 30 s, 55°C for 1 min, and 68°C for 14 min. Then, 10 units of *Dpn*I were added directly to the amplification reaction, and the sample was incubated for 1 h at 37 °C to digest the parental, methylated DNA. JM109 supercompetent cells were finally transformed with 1 μl of the reaction mixture and plated onto LB-ampicillin plates (see below for details). After plasmid purification, plasmid cDNAs were fully sequenced (Eurofin MWG Operon Biotech).

2.1.3 Plasmid amplification, extraction and purification

The vectors containing PepT1 cDNAs were introduced into JM109 strain of *E. Coli* by the means of the heat-shock procedure following the instructions of the bacteria supplier (Promega).

Transformed bacteria were then left to grow for about 1 h in SOC medium [tryptone 2% (w/v), yeast extract 0.5% (w/v), NaCl 10 mM, KCl 2.5 mM, glucose 20 mM], centrifuged, plated on plates containing selective medium (LB-Agar added with 50 μg/ml ampicillin) and incubated over night at 37°C. The day after, colonies were picked up and inoculated in liquid selective medium (LB added with 50 μg/ml ampicillin). Bacteria were left to grow over night at 37°C and then the plasmid DNA was extracted using Wizard® *Plus* SV Miniprep (Promega) following supplier's instruction. The extracted DNA was loaded on a 1% agarose gel in TAE 1X buffer to check the quality and to estimate the concentration.

2.1.4 In vitro transcription

In order to achieve an efficient *in vitro* transcription, the clone containing the cDNA of interest has to be linearized in 3' direction with respect to the coding region. The cDNA encoding rabbit PepT1-FLAG transporters was linearized with *Not*I and the cDNA encoding seabass and zebrafish transporters with *Hind* III. 8-10 μg of plasmid DNA were digested, then purified using the Wizard® SV Gel and PCR Clean-Up System (Promega) and eluted in 35 μl of nuclease free water. 3 μl were loaded on a 1% agarose gel in TAE 1X buffer to check the linearization. The remaining DNA was used for the *in vitro* transcription as detailed described previously (Bossi *et al.*, 2007). Briefly, the linearized DNA was incubated at 37°C for 3h in presence of 200 units of T7 RNA polymerase, 18 μl of 5X Trascription Buffer, 8 μl of 100 mM DTT, 2.5 μl of RNasin 30 U/μl, 13 μL NTPs mix (ATP, CTP, UTP 10 mM and GTP 0.5 mM), 6.5 μL of 10 mM Cap

Analog (Promega), 10 µl RNA polymerase 20 U/µl (final volume 90 µL). After 10, 20, and 40 min from the beginning of the incubation, 1 µL of 25 mM GTP was added to the reaction. After 1 h from the start of the transcription, a mix of 4 µl of 5X TB, 1 µl of 100 mM DTT, 1 µl of RNasin 30 U/µl, 5 µl of NTPs mix, 1 µl of T7 RNA polymerase 20 U/µl, 1 µl of 25 mM GTP, 4 µl of nuclease-free water was added to each sample. At the end of 3 h, the reaction was stopped by adding nuclease-free to a volume of 200 µl. All enzymes were supplied by Promega Italia, Milan, Italy.

The transcribed cRNA was extracted with phenol:chloroform:isoamyl alcohol, 25:24:1, pH 6.6, precipitated with LiCl 8 M and washed with 70% EtOH. The dried cRNA was then resuspended in a small volume of nuclease-free water and the concentration estimated using a spectrophotometer (1 A_{260nm} unit = 40 µg/ml).

Transcribed cRNAs had a modifications which mimic *in vivo* conditions: the process of 5' capping. The so called "Cap Analog" is a modified guanine ($m^7G(5')ppp(5')G$) which, although is not necessary for the protein expression, increases the translation efficiency and also protects the mRNA from degradation.

2.1.5 *Heterologous expression in oocytes*

Xenopus laevis oocytes are a powerful expression system (Fig.2.2) with numerous advantages: i) high expression rate of exogenous proteins (even after only 18 hours); ii) an efficient biosynthetic apparatus which allows all post-translational modifications necessary for the functionality and the correct targeting

of the protein; iii) high density of proteins produced upon cytoplasmic mRNA injection; iv) dimensions well adapted for microinjection and voltage clamp; v) easiness to maintain in culture for quite long period (ten or more days) with no particular sterile conditions; vi) coexpression of different proteins in various combinations by simply co-injecting the respective cRNAs; vii) low expression levels of endogenous membrane proteins (the endogenous channels have been well characterized, thus it is easy to distinguish them from the injected proteins).

Xenopus oocytes have also some disadvantages: i) the expression of exogenous protein is transient; ii) the ideal temperature for their survival (about 18°C) is usually lower than the temperature appropriate for exogenous proteins (37°C for mammalian proteins) and this can affect the folding process; iii) although quiescent cells, oocytes possess their own genetic ensemble which might interfere with the exogenous proteins.
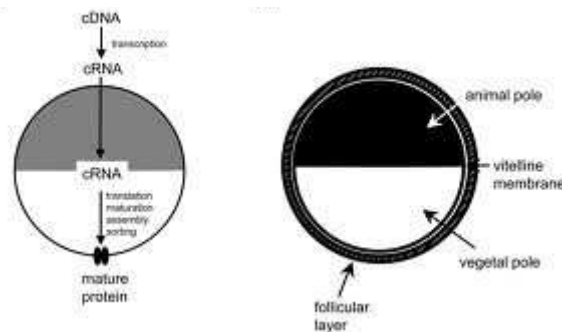
Fig.2.2 *The process of expressing exogenous proteins in Xenopus oocytes.*

Oocytes were prepared as detailed described previously (Bossi *et al.*, 2007). Oocytes were obtained from adult female *Xenopus laevis,* the frogs were anaesthetised in MS222 (tricaine methansulfonate) 0.10%(w/v) solution in tap water and portions of the

45

ovary were removed through an incision on the abdomen. The oocytes were treated with collagenase (Sigma Type IA) 1 mg/ml in ND96 Ca^+ free, for at least 1 h at 18°C. After 24 hours at 18°C in modified Barth's saline solution (MBS), the healthy looking oocytes, were injected with 12.5 ng of cRNA in 50 nl of water, using a manual microinjection system (Drummond). The oocytes were then incubated at 18°C for 3-4 days in MBS before electrophysiological studies. The experiments were carried out according to the institutional and national ethical guidelines.

2.2   Protein localization

2.2.1 Single-oocyte chemiluminescence

The expression of PepT1-FLAG isoforms at the oocyte plasma membrane was determined by the single oocyte chemiluminescence (SOC) technique (Zerangue *et al.*, 1999),(McAlear *et al.*, 2006;Rauh *et al.*, 2010), that employs enzyme amplification with a chemiluminescent substrate and sensitive linear detection with a luminometer. Oocytes expressing different FLAG-PepT1 isoforms, as well as non-transfected oocytes, were washed twice for 5 min in ice-cold ND96 pH 7.6 and then fixed with 4% paraformaldehyde in ND96 for 15 min at 4 ° C, rinsed 3×5 min with equal volumes of ND96, and then incubated for 1 hour in a 1% BSA-ND96 blocking solution (used in subsequent antibody incubation steps). Fixed and blocked oocytes were incubated for 1 h in primary mouse anti-FLAG M2 (Sigma, Milan Italy) monoclonal antibody 1 µg/ml in 1% BSA-ND96, washed 6x3min in 1% BSA-ND96, incubated for 1 hour in secondary

peroxidase-conjugated goat anti-mouse IgG 1 μg/ml, IgG-HRP (Jackson ImmunoResearch Laboratories), washed 6x3min in 1% BSA-ND96 and then 6x3min in ND96 alone. For chemiluminescence readings, each oocyte was transferred into a well of a 96 wells plate (Assay Plate White not treated flat bottom-Corning Costar) filled with 50 μl SuperSignal Femto (Pierce); the washing solution was eliminated as much as possible. Chemiluminescence was quantified with a Tecan Infinity 200 microplate reader. The plates were read not later than 5 minutes after the transfer of the first oocyte. The data were then acquired at least three times in 10 minutes and for each oocyte the mean of three readings was calculated. Results were normalized to the mean value of wild-type FLAG-PepT1 for each batch and are given in relative light units (RLU).

2.2.2 Immunohistochemistry

Oocytes in which transport activity had been confirmed electrophysiologically were fixed in 100% methanol at $-20°C$ for 2 h, then rehydrated at room temperature (RT) for 15 minutes in 50:50 (v/v) methanol/phosphate-buffered saline (PBS), followed by 2x15 minutes washes in PBS. The fixed oocytes were then embedded in Polyfreeze tissue freezing medium (Polysciences, Eppelheim, Germany) and immediately frozen in liquid nitrogen. Cryosections (7 μm) were obtained with a Leica CM 1850 cryostat. The sections were incubated in the blocking buffer [2% bovine serum albumin, BSA (w/v), 0.1% Tween in PBS] at RT for 30 min, then the primary antibody, mouse anti-FLAG M2 (SIGMA, Milan Italy, 3.8 mg/mL) 1:1000 in blocking buffer was added and incubated at RT for 1 h.

Samples were washed 3x5 min in blocking buffer at RT. The oocytes sections were then incubated in the secondary antibody [Cy^{TM} 3-conjugated AffiniPure Donkey Anti-Mouse (Jackson ImmunoResearch), 1.4 mg/mL, diluted 1:1000 in Blocking Buffer] at RT for 45 min and again washed 3x5 min with Blocking buffer. Images were observed with a fluorescence microscope Olympus BH2 through a rhodamine filter set (excitation/emission filters 550/580nm). Images were acquired with a DS-5M-L1 Nikon digital camera system.

2.3 Electrophysiology and data analysis

Membrane electrophysiology has several advantages over other techniques used in transport studies: i) the membrane voltage of the cell is under control; ii) the temporal resolution is high; iii) the results may be obtained immediately, data can be analyzed and interpreted in real-time, and consequently the protocols can be changed or adjusted during the same experimental session. These benefits may be exploited in the study of transporters, thereby adding valuable information and significantly increasing efficiency. The activity of electrogenic transporters, that translocate electrical charge, by definition, during their working cycle, is strongly influenced by the transmembrane potential. Thus, tracer flux experiments suffer from some uncertainty, because the membrane voltage is not under control, and not only the value of the electrical gradient is unknown, but it is also bound to change as a consequence of the electrogenic activity of the transporter itself. A more reliable evaluation of the activity of the transporter is obtained instead when the membrane potential is "clamped".

2.3.1 Two-Electrode Voltage-Clamp (TEVC)

The "voltage-clamp" technique was introduced by Marmont and Cole (Cole and Curtis, 1941), and by Hodgkin, Huxley and Katz (HODGKIN *et al.*, 1952) to study the ionic currents underlying the action potential in nerve axons, and it has been extended to the study of transporters soon after the cloning and expression of the first transporters in *Xenopus laevis* oocytes (Hediger *et al.*, 1987;Ikeda *et al.*, 1989;Parent *et al.*, 1992;Mager *et al.*, 1993).

The TEVC technique is based on the use of two microelectrodes, one for recording the transmembrane voltage and one for passing current (Fig.2.3). The recorded membrane voltage is compared to the desired (command) voltage and a compensating current is automatically injected into the cell by the appropriate electronic apparatus. In this technique the independent (controlled) variable is the membrane voltage, controlled by the experimenter, while the dependent (measured) variable is the membrane current.
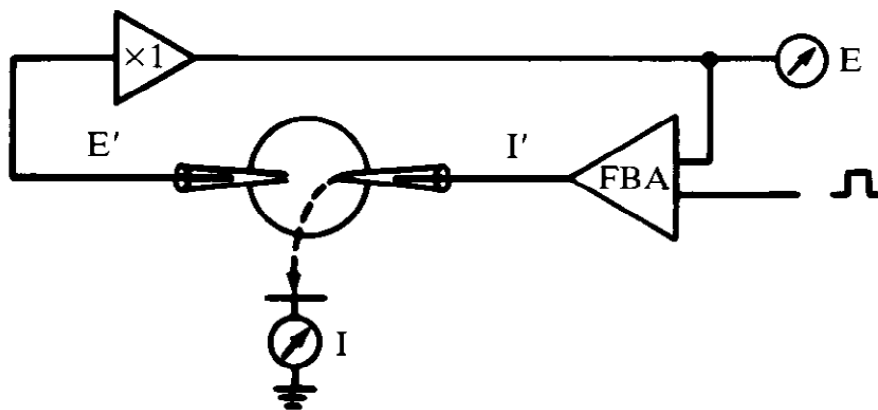
***Fig.2.3** Two-Electrode Voltage-Clamp.*
FBA is the feedback amplifier, E' is the voltage electrode and
I' is the current electrode.

When a current takes place due to the activity of the transport systems located in the membrane, a negative feedback in the circuitry injects into the oocyte a current that exactly compensates the charge flow trough the cell membrane, in order to maintain transmembrane voltage under control. In addition to keeping the membrane potential constant, membrane voltage changes of any desired form can be applied to the cell by the TEVC technique. In the case of ion-coupled transporters, the transmembrane current is an indication of the transport activity, and the possibility of accurately controlling the membrane potential is particularly crucial in voltage-dependent processes.

The *ideal* voltage clamp simply consists of a battery, a switch, a wire, the cell and an ammeter (Fig.2.4). Since the wire has zero resistance when the switch is closed, the membrane potential steps instantly to the battery voltage. This generates an impulse of current that charges the membrane capacitance ($Q = C_m V_{cmd}$), followed by a steady-state current ($I_m = V_{cmd}/R_m$) to sustain the voltage across the membrane resistance.
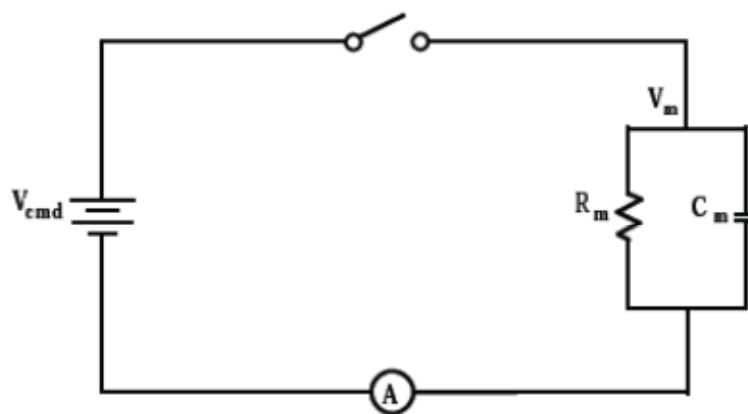
Fig.2.4 *The ideal Voltage Clamp.*

In this work some experiments were conducted in current-clamp conditions, i.e. without strict voltage control, but with the possibility of constant current injections.

2.3.2 TEVC experimental setup

A schematic view of the TEVC experimental setup used in this work.
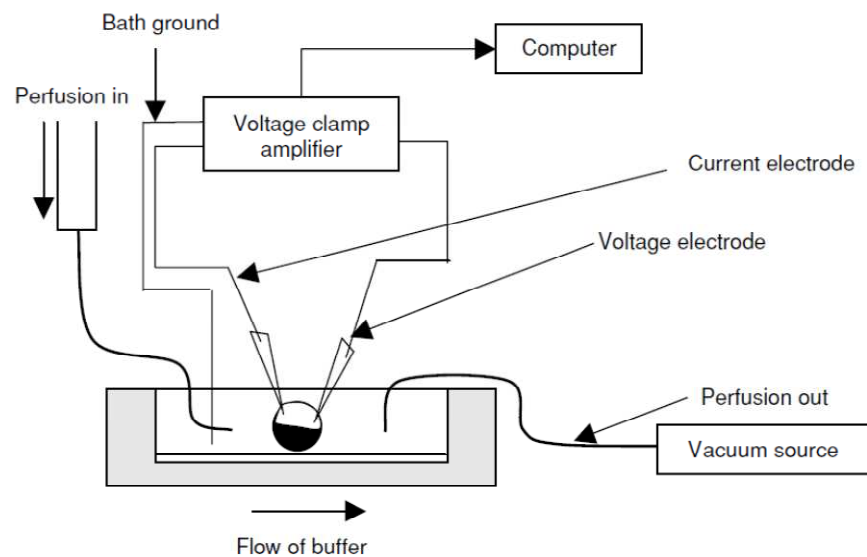
Fig.2.5 *Schematic representation of the experimental setup.*

The voltage-clamp amplifier (GeneClamp, Axon Instruments Foster City, CA, USA or Oocyte Clamp OC-725B, Warner Instruments, Hamden, CT, USA) was connected to a computer through an AD/DA (analog-digital, digital-analog) converter (DIgiData 1200, Axon Instr.). This device converts the analog signal from the amplifier to a digital signal intelligible for the computer, and vice versa. Usually, signals derived from the amplifier were also

displayed on an oscilloscope (TDS 420, TekTronix Inc., Beaverton, OR, USA).

A dissection microscope (Wild M3B, Leica Microsystems AG, Wetzlar, Germany) was used to visualize the oocyte and micromanipulators (MM-33, Märtzhäuser Wetzlar GmbH & Co. KG, Wetzlar-Steindorf, Germany) were use to move the electrodes. A perfusion system consisted of a set (16) of syringes delivers the various solutions to the unique solution inlet of the chamber (a modified version of RC-1Z, Warner Instr.). All the syringes were connected to the inlet by the use of two manifolds (MP-8, Warner Instr.) and were all positioned at the same height in order to have the same flow rate for each solution. The recording chamber has a small volume (about 200 μl, 85 *m*l/mm height) which allows a rapid solution exchange (about 8-10 seconds in our system). The solution is aspirated by a modified acquarium pump through a suction reservoir connected to the oocyte well. The oocyte was placed in the chamber and impaled with the two Ag/AgCl electrodes. Intracellular glass microelectrodes were filled with KCl 3 M and had tip resistances between 0.5 – 4 MΩ. These resistance values were usually obtained by gently breaking the tips on the bottom of the chamber. Agar bridges (3% agar in 3 M KCl) connected the bath electrodes to the experimental chamber.

All the equipments needed for the recording (the dissection microscope, the perfusion system, the oocyte chamber, micromanipulators and reference electrode) are placed inside a Faraday cage, in order to reduce the noise derived from

electromagnetic fields, and on an anti vibration table. The cage and all the instruments inside of it were grounded.

2.3.3 Protocols and data analysis

In voltage-clamp mode the holding potential (V_h) was generally -60 mV, unless otherwise indicated. The standard protocol consisted in 200 ms long pulses to test potentials from -140 to +40 mV, in 20 mV increments. Other protocols including prepulses are described in the text. The current signal was filtered at 1 kHz before sampling at 2 kHz.

Two methods were used to isolate the presteady-state currents elicited by voltage jumps (Mertl *et al.*, 2008;Sangaletti *et al.*, 2009): in the first, the slow component of a double-exponential fitting of the transient was taken to represent the presteady-state currents, while in the second, the currents remaining after subtraction of the traces in the presence from those in the absence of substrate were assumed to represent the intramembrane charge movement. The isolated traces were fitted with single exponentials to obtain the time constant of decline, and integrated to calculate the amount of displaced charge, after zeroing any residual steady-state transport current. The presence of gently decaying currents during the voltage pulse was sometimes observed in some mutants at alkaline pH. In these cases a sloping baseline was subtracted before fitting and integration. The two methods gave generally equivalent results; the subtraction method was preferred when the presteady state currents were fast, with time constants approaching that of the endogenous capacitive transients.

Data were analyzed using Clampfit 8.2 (Axon Instruments), and figures were prepared with Origin 5.0 (Microcal Software Inc., Northampton, MA, USA).

2.4 Solutions

The oocyte culture and washing solutions had the following composition (in mM), ND96: NaCl 96, KCl 2, $MgCl_2$ 1, $CaCl_2$ 1.8, Hepes 5, pH 7.6; MBS: NaCl 88, KCl 1, $NaHCO_3$ 2.4, Hepes 15, $Ca(NO_3)_2$ 0.30, $CaCl_2$ 0.41, $MgSO_4$ 0.82, sodium penicillin 10 µg/ml, streptomycin sulphate 10 µg/ml, gentamycin sulphate 100 µg/ml, nystatin 10 U/ml, pH 7.6; PBS: NaCl 138, KCl 2.7, Na_2HPO_4 8.1, KH_2PO_4 1.9, pH 7.6. The external control solution had the following composition (mM): NaCl, 98; $MgCl_2$, 1; $CaCl_2$, 1.8.

Different pH buffers were used for the various pH values: for pH 6.5, Mes 5 mM was used; Hepes 5 mM was employed for pH 7.0 and 7.5, while for pH 8.0 the buffer was Taps 5 mM. The final pH values were adjusted with HCl and NaOH. Substrates were added at the indicated concentrations to the appropriate solutions.

The non-hydrolyzable substrate Gly-Sar was used for confirmatory intracellular injection experiments. A volume of 50 nl of a concentrated solution (200 mM Gly-Sar in pH 7.5 buffer) was injected, leading to an approximate final concentration of 20 mM (assuming an oocyte volume of about 500 nl).

All substrates for electrophysiology experiments were supplied from Sigma, Milan, Italy. Irbesartan was from Sanofi-Aventis.

Experiments were performed at room temperature (20–25 °C).

Chapter 3.   Results

The identification of the structural basis of the functional mechanism of PepT1 is important because, in addition to its role in nutrient uptake, this transporter represents a major pathway for the absorption of several therapeutic drugs. Most of the above functional observations were derived from uptake data, in absence of control of the membrane voltage, or from electrophysiological measurement of steady transport currents, in presence of a dipeptide substrate. Important additional informations regarding the transport mechanism may arise from measurement of presteady-state currents, the electrophysiological signals that can be observed in absence of organic substrate, and that represent the first steps in the transport cycle (Fesce *et al.*, 2002;Peres *et al.*, 2004).

3.1   Unified modeling of PepT1

In PepT1 acidic pH appears to enhance the uptake of substrates (Fei *et al.*, 1994;Mackenzie *et al.*, 1996) due to the presence of an acidic microenvironment in the vicinity of the absorptive enterocytes generated by the activity of the Na^+/H^+ exchanger in the apical membrane (Kennedy *et al.*, 2002;Watanabe *et al.*, 2005). However, there are some apparently contradictory aspects: in fish species and in rabbits, electrophysiological measurements have indicated a substantially pH-independent maximal rate of transport (Steel *et al.*, 1997;Sangaletti *et al.*, 2009) or even a potentiating effect of alkaline pH (Kottra and Daniel, 2001;Verri *et al.*, 2003). Uptake experiments

with human PepT1 in an extended pH range have shown a bell-shaped activity–pH relationship (Fujisawa *et al.*, 2006). A similar trend has been found for the maximal transport current in the rabbit isoform (Amasheh *et al.*, 1997). From a structural point of view, the level of homology among the various transporter isoforms of mammalian and fish species is about 56% amino acidic identity and 72% similarity. However, these values can reach 72% and 90%, respectively, when considering only the human, rabbit, zebrafish, and seabass transporters, and limiting the analysis to the transmembrane domains involved in pore formation (TM 1, 3, 5, 7, 8, and 10) or to residues facing the pore (TM 2 and 4) (Meredith and Price, 2006).

Electrophysiological and biophysical analyses were used to compare the partial and complete transport cycles of the intestinal oligopeptide transporter PepT1 among three species (seabass, zebrafish, and rabbit).

3.1.1 Presteady-state currents in the different species

The PepT1s of rabbit (rbPepT1), seabass (sbPepT1), and zebrafish (zfPepT1) exhibit presteady-state currents in the absence of organic substrate. Fig.3.1 compares the currents induced in each isoform by voltage pulses in the absence and presence of saturating Gly-Gln at pH 6.5. Although experiments have been performed in a more extended range (6.0–8.0), pH 6.5 seems real physiological conditions, at least in rabbit PepT1 (based on the pH of the luminal surface of the mammalian small intestine) (Thwaites and Anderson, 2007).
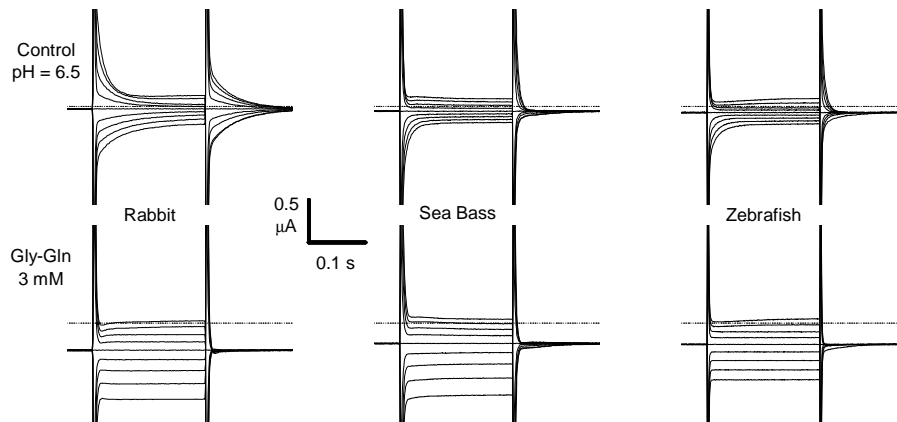
Fig.3.1 *Comparison of PepT1 presteady-state currents from three species. In the absence of organic substrate (top row), all three transporters display slowly decaying transients in response to "on" and "off" voltage steps. The bottom row shows the steady currents induced in the same oocytes by the addition of 3 mM Gly-Gln and the simultaneous disappearance of the presteady-state currents.*

Although the presteady-state currents of rbPepT1 and sbPepT1 have already been described and analyzed (Nussberger *et al.*, 1997;Sangaletti *et al.*, 2009), information on zfPepT1 is lacking. As shown in Fig.3.1 (top row), the two fish species, exhibited larger currents for hyperpolarization than for depolarizations, while the transients from rbPepT1 are approximately symmetrical around the -60 mV holding potential. Adding saturating amounts of organic substrate (3 mM Gly-Gln) elicited steady transport currents (Fig.3.1, bottom row) and, as commonly observed in most electrogenic transporters, abolished the presteady-state currents.

The presteady-state currents were separated from the fast peaks due to the endogenous oocyte capacity, using two different procedures (see Materials and Methods for details). In the first, a double exponential function has been fitted to currents recorded in the

absence of substrate. In the second, the current traces in the presence of saturating substrate have been subtracted from those in its absence and a single exponential fitted to the difference. In both cases, steady transport currents were subtracted before fitting the exponentials.

As previously observed (Mertl *et al.*, 2008;Sangaletti *et al.*, 2009), the two methods give virtually identical results. This is relevant not only to better understand the transporter mechanism, but is also important because of the intrinsic limitations of the two-exponential method. Namely, the separation of two exponentials by fitting is impossible when the two time constants are close in value. Because the time constants for charging the oocyte membrane capacity are generally around 1 ms, the two-exponential method becomes unreliable when the decay time constant of the presteady-state currents approaches this value (i.e., 2–3 ms). This is indeed the case for both fish species at the most positive potentials explored (see below). In addition, both rabbit and seabass PepT1 exhibit an acceleration of the presteady-state current decay at alkaline pH (Nussberger *et al.*, 1997;Sangaletti *et al.*, 2009). For these reasons, the subtraction method has been used to isolate these currents. Because the presteady-state currents of seabass and zebrafish are very similar to each other and the results from seabass PepT1 have previously been published (Sangaletti *et al.*, 2009), only data from zebrafish are shown here.

The voltage dependences of the decay time constant τ and the intramembrane charge movement Q obtained from the isolated presteady-state currents are shown in Fig.3.2.
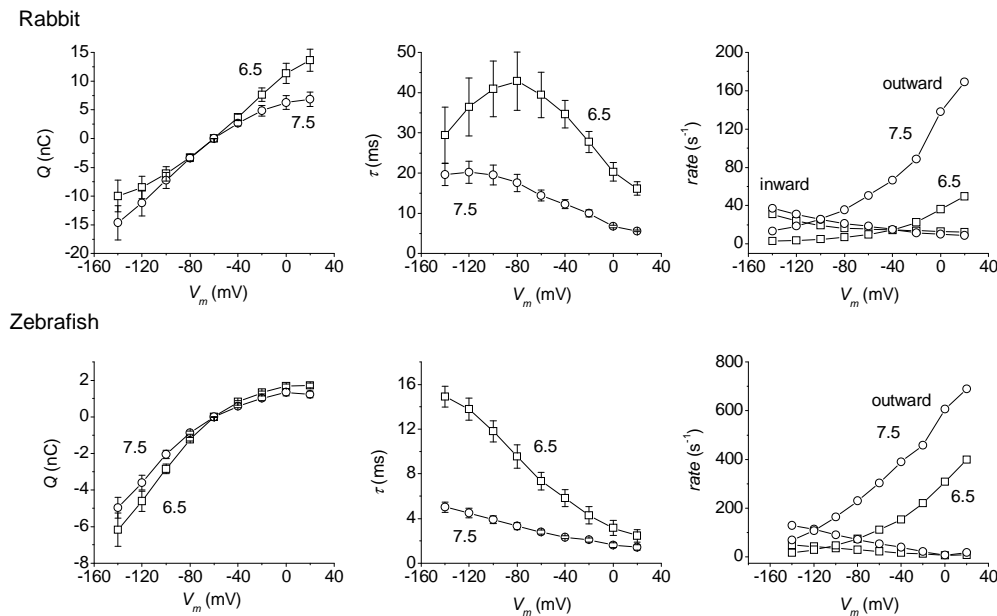
Fig.3.2 *Effects of external pH on the properties of the presteady-state currents. In all species, external alkalinization shifts the time constant vs. potential (τ/V) and the charge vs. potential (Q/V) curves toward more negative potentials. Furthermore, the time constant of decay is strongly reduced. In the rightmost column, the unidirectional rate constants of the intramembrane charge movement are shown.*

Several observations can be made when comparing the time constant vs. potential (*τ/V*) and charge vs. potential (*Q/V*) curves of the rabbit and fish PepT1. First, as already mentioned, at pH 6.5, the rbPepT1 transients are more symmetrical around the holding potential; this is confirmed by the position of the bell-shaped *τ/V* curve with a maximum at about -90 mV. For the fish transporters, only the right half of the bell-shaped curve is visible in the voltage range that can reasonably be explored; the seabass transporter appears to have a maximum at about -140 mV (Sangaletti *et al.*, 2009), whereas the maximal *τ* for the zebrafish isoform may be at even more negative voltages. Similarly, the *Q/V* curves for rbPepT1 show a clear

59

sigmoidal shape, whereas in the fish transporters only the rightmost part of a sigmoid is detectable. Therefore, the properties of the fish PepT1s are shifted to more negative potentials compared to those of the rabbit isoform.

Furthermore, from the τ/V and Q/V curves it is possible to derive (Fesce *et al.*, 2002) the unidirectional rate constants of the charge movement and their voltage dependency, according to the relations:

$$inrate = \frac{1}{\tau} \frac{Q_{in}}{Q_{max}}$$

[eqs 3.1]

$$outrate = \frac{1}{\tau} \left(1 - \frac{Q_{in}}{Q_{max}} \right)$$

The decay rates of rbPepT1 transient currents are much slower than those of both fish transporters, with sbPepT1 faster than zfPepT1 (Sangaletti *et al.*, 2009).

3.1.2 Effects of external pH on the presteady-state currents

Alkalinization of the external medium has been shown to produce negative shifts in the τ/V and the Q/V curves in rabbit and seabass PepT1 (Nussberger *et al.*, 1997;Sangaletti *et al.*, 2009). This effect was also seen in zfPepT1. Fig.3.2 compares these results between the fish and rabbit isoforms.

The equilibrium distribution of the charge moved during the presteady-state currents can be described with the Boltzmann equation:

$$Q = \frac{Q_{max}}{1 + \exp\left[\dfrac{-\left(V - V_{0.5}\right)}{\sigma}\right]},$$ [eq.3.2]

where Q_{max} is the maximal moveable charge; $V_{0.5}$ is the voltage at which half of the charge is moved (that is, the midpoint of the sigmoidal); and $\sigma = kT/q\delta$ represents a slope factor, in which q is the elementary electronic charge, k is the Boltzmann constant, T is the absolute temperature, and δ is the fraction of electrical field over which the charge movement occurs. Fitting the Q/V curves to this equation gives the parameters summarized in Tab.3.1.

	Rabbit		Seabass		Zebrafish	
pH	**6.5**	**7.5**	**6.5**	**7.5**	**6.5**	**7.5**
Q_{max} **(nC)**	33.2 ± 1.9	31.5 ± 1.2	10.2 ± 0.2	6.8 ± 0.9	11.0 ± 0.3	9.9 ± 1.1
$V_{0.5}$ **(mV)**	-41.4 ± 2.5	-100 ± 2.3	-98.7 ± 1.3	-122.0 ± 0.6	-108 ± 1.6	-119 ± 7.2
σ **(mV)**	42.9 ± 3.1	39.5 ± 1.7	23.1 ± 0.7	23 ± 2.7	31.1 ± 0.9	33.5 ± 3.3

Tab.3.1 *Boltzman equation parameters.*

The higher value of σ in the rabbit form suggests that charge movement may occur over a smaller fraction of the membrane electrical field in rabbit than in the two fish species.

The sigmoidal Q/V curve may represent the steady-state distribution of the transporter molecules between two conformations with the center of charge in two different locations of the membrane electrical field. The charge movement process may be described with the simple reaction:

$$Q_{in} \underset{inrate}{\overset{outrate}{\rightleftarrows}} Q_{out},$$
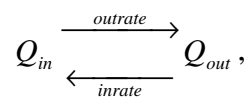
where *outrate* and *inrate* are the unidirectional rate constants, and

Q_{in} and Q_{out} are the amount of charge at an inner and outer position, respectively, in the membrane electrical field. It is easy to derive *outrate* and *inrate* from the experimental *Q/V* and *τ/V* curves, because:

$$\tau = \frac{1}{outrate + inrate} \text{ and } \frac{Q_{in}}{Q_{in} + Q_{out}} = \frac{Q_{in}}{Q_{max}} = \frac{inrate}{outrate + inrate} \text{ [eqs 3.3]}$$

where Q_{max} is the maximal moveable charge, obtained from the saturating values of the *Q/V* sigmoidal curve.

In all transporters, alkalinization sped up both the inward and outward rates, although the effect on this last parameter was much larger (Fig.3.2, bottom row). Notably, the voltages at which the in and out rates crossed showed the same shifts as the $V_{0.5}$ values.

These observations indicate that protonation of unidentified amino acids slows down the rates of the charge-moving conformational changes induced by membrane potential. Indeed, the much slower value of the decay time constant for rbPepT1 may be explained by its higher isoelectric point (Daniel *et al.*, 2006); at the same pH, it will be protonated to a higher degree than will sbPepT1 and zfPepT1. Its movements in response to voltage changes will occur less frequently for this reason.

3.1.3 Modeling PepT1 presteady-state currents

A kinetic scheme has been deviced to simulate the observed results, particularly those showing a pH-dependent increase in both unidirectional rate constants. To incorporate the slowing effects of protonation on both unidirectional rate constants, some changes were made to existing models (Mackenzie *et al.*, 1996;Nussberger *et al.*, 1997). As shown in Fig.3.3, the intramembrane charge movement

occurs between states 1 and 6, and the rearrangement of the empty transporter displaces an intrinsic net negative charge in the membrane field. This transition is bracketed by two proton-bound states (T2 and T7) effectively modulating the T1 ↔ T6 transition (see below).
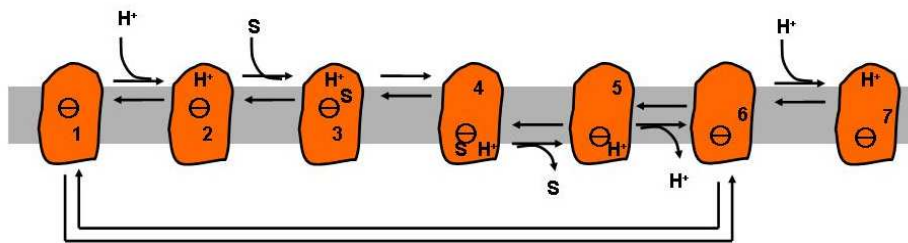
Fig.3.3 *Minimal kinetic scheme used to simulate the effect of external pH on the presteady-state currents of PepT1 transporters. Transitions T1↔T6 and T3↔ T4 are voltage-dependent. In the absence of organic substrate (S), the only possible states are T1, T2, T5, T6 and T7. External protons can bind to T1 (leading to state T2) and to T6 (leading to state T7). T2 and T7 act as traps, effectively slowing down both inward and outward charge movement.*

Extracellular oligopeptides bind to state T2, leading to state T3 and causing a partially voltage-dependent conformational rearrangement from T3 to T4, a state from which the organic substrate is released intracellularly (T5). The subsequent release of H^+ leads to the inward-facing, empty transporter (state T6).

The introduction of the protonated state T7 is justified by the need to reproduce the slowing action of external protons on the inward rate of charge movement, observed especially in the fish isoforms (i.e., the transition T6 → T1). External protons "sequester" the transporter in this state, effectively slowing down the return from the inward- to the outward-facing conformation. The transition to state T7 may represent a proton binding to an allosteric site, as has already

63

been suggested (Verri *et al.*, 2003), to account for the smaller transport current observed at acidic pH in the zebrafish PepT1.

The set of differential equations describing the complete scheme can be written as:

$$\frac{dT_1}{dt} = -(k_{12} + k_{16})T_1 + k_{21}T_2 + k_{61}T_6$$

$$\frac{dT_2}{dt} = k_{12}T_1 - (k_{21} + k_{23})T_2 + k_{32}T_3$$

$$\frac{dT_3}{dt} = k_{23}T_2 - (k_{32} + k_{34})T_3 + k_{43}T_4$$

$$\frac{dT_4}{dt} = k_{34}T_3 - (k_{43} + k_{45})T_4 + k_{54}T_5 \qquad \text{[eqs 3.4]}$$

$$\frac{dT_5}{dt} = k_{45}T_4 - (k_{54} + k_{56})T_5 + k_{65}T_6$$

$$\frac{dT_6}{dt} = k_{16}T_1 + k_{56}T_5 - (k_{61} + k_{65} + k_{67})T_6 + k_{76}T_7$$

$$\frac{dT_7}{dt} = k_{67}T_6 - k_{76}T_7$$

where T1–T7 are the probabilities that the transporter is in a given state, and the *k* values are the rate constants, either dependent or independent of concentration and voltage (see Tabs 3.2 and 3.3).

Rate	k_{12}	k_{21}	k^0_{16}	k^0_{61}	k_{56}	k_{65}	k_{67}	k_{76}	δ_{16}	δ_{61}	δ
Units	$M^{-1}s^{-1}$	s^{-1}	s^{-1}	s^{-1}	s^{-1}	$M^{-1}s^{-1}$	$M^{-1}s^{-1}$	$M^{-1}s^{-1}$			
Rabbit	9×10^9	750	152	10	1×10^5	1.5×10^7	5×10^8	400	0.45	0.26	0.71
Fish	3.5×10^9	750	1050	15	1×10^4	1.5×10^7	5×10^9	400	0.39	0.48	0.87

Tab.3.2 *Model kinetic parameters in absence of substrate.*

The unidirectional rate constants of Fig.3.2 were fitted with growing and decaying exponentials in the form

$$outrate = outrate^0 \exp\left(\delta_{out} qV / kT\right)$$

and   [eqs 3.5]

$$inrate = inrate^0 \exp\left(-\delta_{in} qV / kT\right),$$

where $outrate^0$ and $inrate^0$ are the zero-voltage rates; q, k, and T have the same meaning as in eq.3.2; and δ_{out} and δ_{in} (with $\delta_{out} + \delta_{in} = \delta$ in eq.3.2) are the asymmetric fractional dielectric distances.

Rates k_{16}, k_{61}, k_{12}, k_{21}, k_{67}, and k_{76} were determined based on the effects of voltage and external pH on the unidirectional rate constants of Fig.3.2. Assuming that the binding/unbinding of protons in transitions T1 $\leftrightarrow$ T2 and T6 $\leftrightarrow$ T7 is much faster than in T1 $\leftrightarrow$ T6, the unidirectional rate constants of charge movement *outrate* and *inrate* can be written as:

$$outrate = f_{21}k_{16}$$
$$inrate = f_{76}k_{61}$$ [eqs 3.6]

where

$$f_{21} = \frac{k_{21}}{k_{12} + k_{21}}$$

                                                                                            [eqs 3.7]

$$f_{76} = \frac{k_{76}}{k_{67} + k_{76}}$$

are modulating factors that depend on the external proton concentration (Chen *et al.*, 1996). Because k_{12} and k_{67} (but not k_{21} and k_{76}) increase with acidity, the modulating factors will reduce the values of both *outrate* and *inrate*.

The values of k_{56} and k_{65} were adjusted to account for the effects of internal pH (Nussberger *et al.*, 1997), assuming a fixed value of 7.5. Because the parameters of the two fish species were similar, they

were handled together, and a "generalized" fish transporter was modeled (Tab.3.2).

Fig.3.4 shows the results of the simulations for rabbit and the generalized fish transporter. Clearly, the simulations are in very good qualitative and, for rabbit PepT1, also quantitative agreement with the experimental results shown in Fig.3.2.
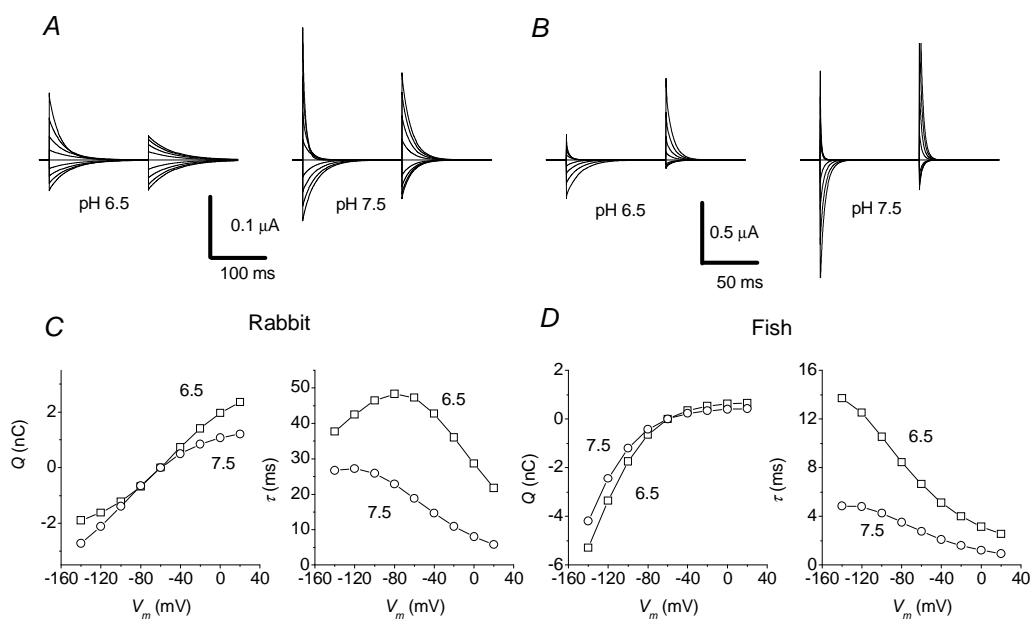
Fig.3.4 *Simulated traces of presteady-state currents at two external pH values for rabbit (A) and generalized fish (B) PepT1. The traces were analyzed following the same procedure as that used for the experimental subtracted recordings to produce the curves shown in the bottom graphs.*

3.1.4 Transport currents of PepT1

The transport currents generated by rabbit, zebrafish, and seabass PepT1 have been previously studied (Steel *et al.*, 1997;Kottra and Daniel, 2001;Verri *et al.*, 2003;Sangaletti *et al.*, 2009). These three isoforms show a similar trend: in all cases, acidic external pH increases substrate affinity, but it either decreases (Kottra and Daniel,

2001;Verri *et al.*, 2003) or does not affect (Steel *et al.*, 1997;Sangaletti *et al.*, 2009) the maximal current. These features are illustrated in Fig.3.5 for the rabbit transporter; very similar curves can be observed for the zebrafish (Verri *et al.*, 2003) and seabass isoforms (Sangaletti *et al.*, 2009). In human PepT1, on the other hand, high acidity increases both substrate affinity and I_{max} (Fei *et al.*, 1994;Mackenzie *et al.*, 1996).
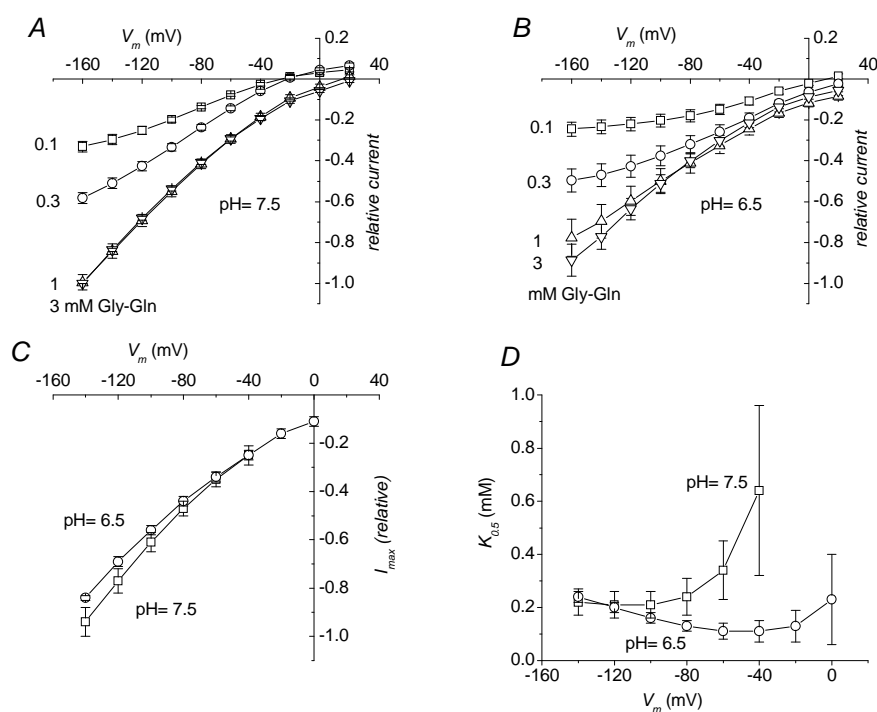
Fig.3.5 *Transport-associated current from rabbit PepT1. Top row: I/V relationships of the transport-associated currents (substrate present minus substrate absent) at pH 7.5 (A) and 6.5 (B). Bottom row: values of I_{max} (C) and K_{05} (D) obtained by fitting the concentration-current relationships from (A and B) with the Michaelis-Menten equation.*

Another interesting feature apparent in Fig.3.5 is the presence of a small outward current, especially at low substrate concentration and

alkaline pH (see below). This effect has also been reported for the zebrafish transporter (Verri *et al.*, 2003), but not for the seabass or human transporters (Mackenzie *et al.*, 1996;Sangaletti *et al.*, 2009).

The decrease in I_{max} at acidic pH in rabbit and fish transporters is unexpected given that the inwardly directed proton electrochemical gradient increases. This effect, however, might be explained by a decreased cycling rate related to the slowing of the charge movement caused by protonation. In the case of inward substrate transport, the transport cycle is circulated only in a clockwise direction, i.e., the transition of the empty transporter occurs in the T6 → T1 direction, showing large pH dependency (Fig.3.2, bottom row).

A useful index of the overall transport efficiency is given by the ratio I_{max}/K_{05}, which is the slope of the Michaelis-Menten relationship at zero substrate concentration. The largest difference in efficiency, in favor of the more acidic solution in the physiological range of membrane potential, was observed in the rabbit transporter; there was no significant difference in the zebrafish. This is in line with the acidic pH of the small intestine of rabbit but alkaline pH in zebrafish (Nalbant *et al.*, 1999).
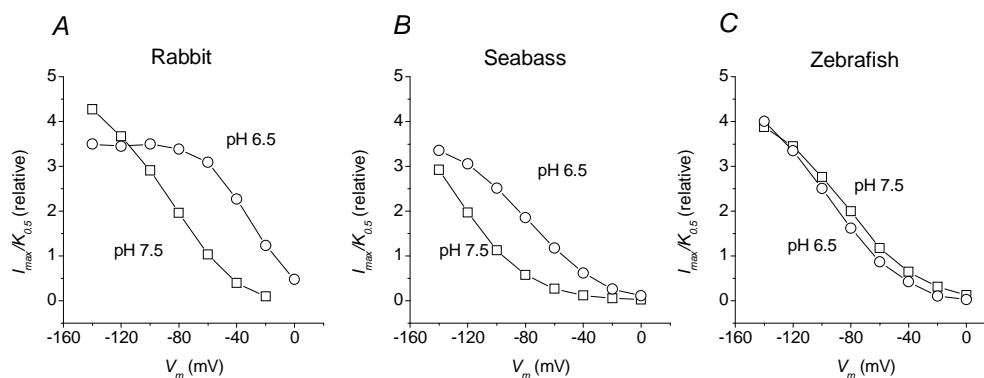
Fig.3.6 *Transport efficiency. Plots of the ratio of relative I_{max}/K_{05} for rabbit (A) seabass (B) and zebrafish (C).*

3.1.5 Transport current modeling

Kinetic models for human and rabbit PepT1 have been proposed (Mackenzie *et al.*, 1996;Irie *et al.*, 2005;Sala-Rabanal *et al.*, 2006); however, none have been tested thoroughly on rabbit or fish transporters to verify their ability to simulate the main aspects of transporter functioning. Therefore, the presteady-state current model developed above has been tested to determine its ability to simulate the characteristics of the transport-associated currents. Only the essential states necessary to complete the transport cycle were added, namely states T3 and T4, corresponding to the outward- and inward-facing conformations with bound substrate. Because the best fit of the experimentally observed charge movement required transition T1 $\leftrightarrow$ T6 to occur over 71% of the membrane electrical field for rabbit and 87% for fish (Tab.3.2), the remaining fractional voltage-dependence for protons was attributed to the T3 $\leftrightarrow$ T4 transition.

The additional kinetic parameters necessary to account for substrate binding and translocation are shown in Tab.3.3.

Rate	k_{23}	k_{32}	k^0_{34}	k^0_{43}	k_{45}	k_{54}	δ_{34}
Units	$M^{-1}s^{-1}$	s^{-1}	s^{-1}	s^{-1}	s^{-1}	$M^{-1}s^{-1}$	
Rabbit	2×10^5	20	6000	6000	5000	3.49×10^{11}	0.29
Fish	8×10^6	20	6000	6000	5000	8.89×10^{10}	0.13

Tab.3.3 *Additional parameters in presence of substrate.*

The parameters used to simulate the presteady-state currents (Tab.3.2) were not modified. In particular, k_{23} and k_{32} were chosen to give a value of K_{05} consistent with the experimental observations at pH 6.5, and k_{34} and k_{43} were set to be equal to each other at 0 voltage and were significantly faster than the other rates. Similarly k_{45} was set at a high

value, while k_{54} was derived from the other rates to satisfy the principle of detailed balance (Hille, 2001).

Fig.3.7 illustrates simulations showing the model's ability to reproduce the main findings for transport-associated currents in the different species, that is, the effects of external pH on the Michaelis-Menten parameters I_{max} and K_{05}. These parameters were obtained by applying the same procedure used for the experimental data: the I/V curves corresponding to various substrate concentrations (0.03–10 mM) were generated by numerical simulations and then I_{max} and K_{05} were obtained by fitting the dose–current curves at each potential with a Michaelis-Menten equation. The left column in Fig.3.7 simulates the rabbit transporter. At alkaline pH, I_{max} appears to remain constant (Steel *et al.*, 1997) or to slightly increase (Kottra and Daniel, 2001), while the apparent affinity decreases (higher K_{05}). Both experimental observations are reproduced by the model, although the K_{05} simulations are not completely satisfactory (Fig.3.5), possibly because "zero trans" conditions were assumed in calculations, whereas substrates can be expected to accumulate in the intracellular compartment near the membrane in real measurements. The central column of the figure represents the generalized fish transporter (Tab.3.2 and Tab.3.3). Again, the model reproduced the unique features of this transporter, namely, the increase in I_{max} at alkaline pH and the affinity decrease common to all species. To stress the versatility of the model, an opposite effect on I_{max} has been simulated, such as the increase observed with acidity in human PepT1 (Mackenzie *et al.*, 1996): this is shown in the right column of Fig.3.7, together with the usual effect on K_{05}. This last series of simulations

was obtained using the rabbit kinetic parameters with a single change: a reduction of k_{67} from $5*10^8$ to $1*10^8$ (Tab.3.2) is sufficient to produce an opposite effect of pH on I_{max}.
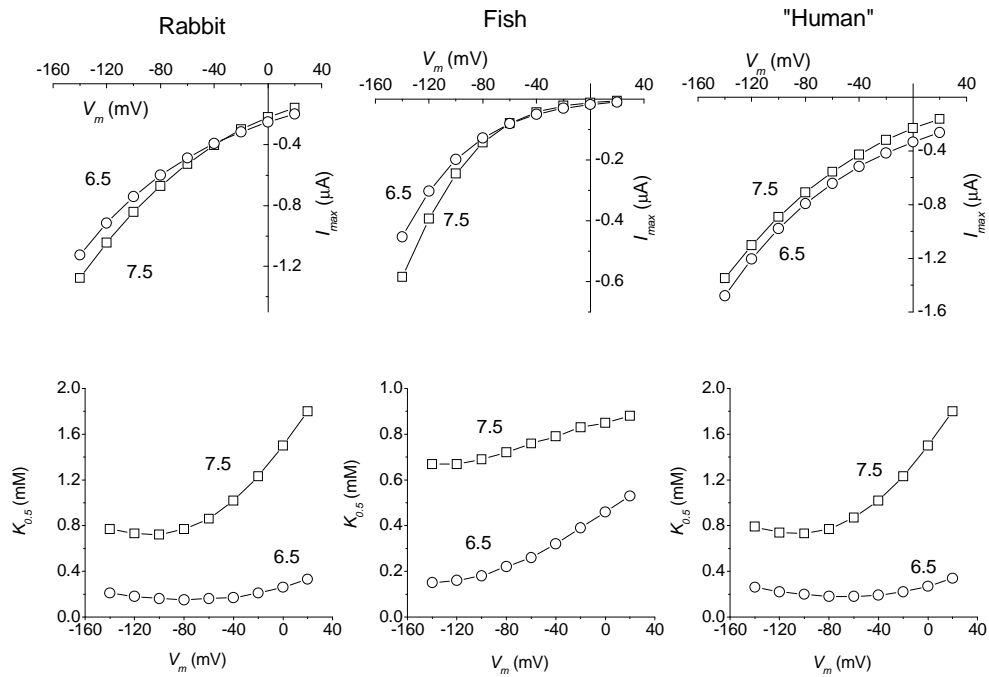
Fig.3.7 *Simulations of the Michaelis-Menten parameters. I_{max} and K_{05} were obtained by analyzing the dose-current curves generated by the model, using the rate values indicated in Tables 3.2 and 3.3 for rabbit (left column), fish (center column) and "human" (right column).*

3.2   Electrostatic gates in PepT1

Mutations of single amino acids may result in considerable changes of the transport function of nutrient transporters. In the case of PepT1, the conserved residue His 57, residing in the second transmembrane segment, as well as the corresponding residue His 87 in PepT2, were found to be essential for the functioning, whereas tyrosine residues adjacent to H57 seem to stabilize the cotransported proton when interacting with H57 (Terada *et al.*, 1996;Fei *et al.*, 1997). The nearby histidine residue His 121 (and His 142 in PepT2) is not essential, but influences the substrate binding, as H121 mutants have shown decreased affinities (Chen *et al.*, 2000). The tyrosine residue Y167 has an important function as well, since its mutation to alanine completely abolished transport via PepT1 (Yeung *et al.*, 1998). By using the cysteine scanning method Kulkarni and coworkers identified in the transmembrane segments 5 and 7 several residues important for the transport function and suggested that these segments line the putative aqueous channel (Kulkarni *et al.*, 2003b). Finally, the same authors identified two oppositely charged residues (R282 and D341) in the transmembrane segments 7 and 8, respectively, that form a salt bridge and play an important role in the substrate translocation via PepT1 (Kulkarni *et al.*, 2007). Interestingly mutation Arg282Glu appeared to convert the cotransporter in a substrate-gated, rather unspecific cation channel (Meredith, 2004;Pieri *et al.*, 2008). In addition, this mutation caused loss of sensitivity to pH.

Therefore the properties of the presteady-state currents in the wild-type and in mutants of the charge-pair residues R282 and D341

have been investigated. The properties of the transport-associated current in these mutants were studied in parallel, in the attempt of gathering a more complete picture of the roles of these residues. The position of these two residues is shown in Fig.3.8.
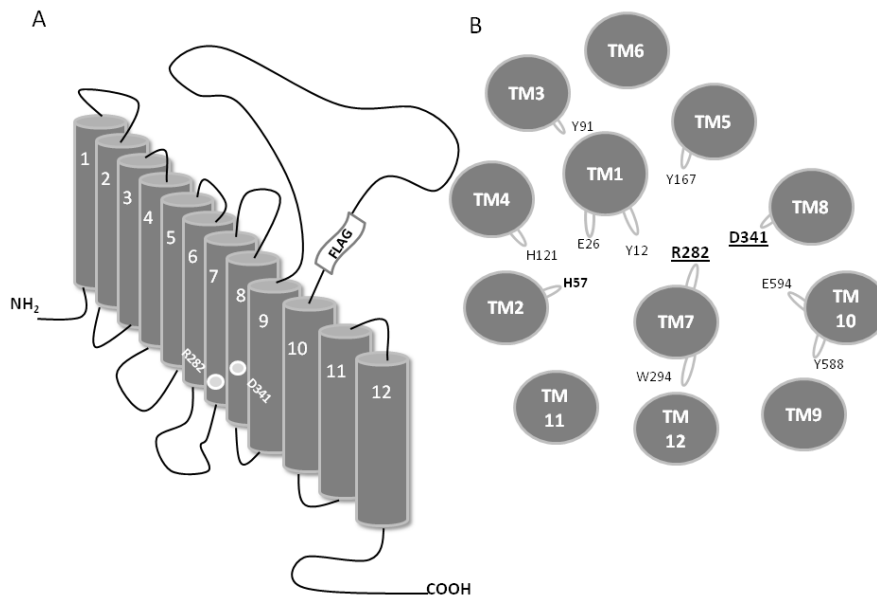
Fig.3.8 *Representation of the 12 TMDs topology of PepT1 and indication of the position of the FLAG-tag.*

3.2.1 Presteady-state currents in charge-pair mutants

Considering that the presteady-state currents of PepT1 are believed to be mostly due to the rearrangement of charges intrinsic to the transporter (Mackenzie *et al.*, 1996;Nussberger *et al.*, 1997), the behaviour of charge-reverting mutants in these positions of rbPepT1 (R282D, R282E and D341R) has been examined, as well as the conservative mutation R282K, and the substitution of arginine 282 with the non-charged non-polar alanine (R282A), or the non-charged

73

polar glutamine (R282Q). Furthermore, the essential histidine 57 (H57R) and the double mutant R282D-D341R have been tested.

Fig.3.9 shows representative traces from the various isoforms. All R282 mutants were able to generate presteady-state currents in absence of substrate, as well as transport-associated currents with amplitudes comparable to the wild-type, while the currents observed in the D341R form were smaller, and neither transporter-related nor presteady currents could be observed in the double mutant R282D-D341R and in H57R.
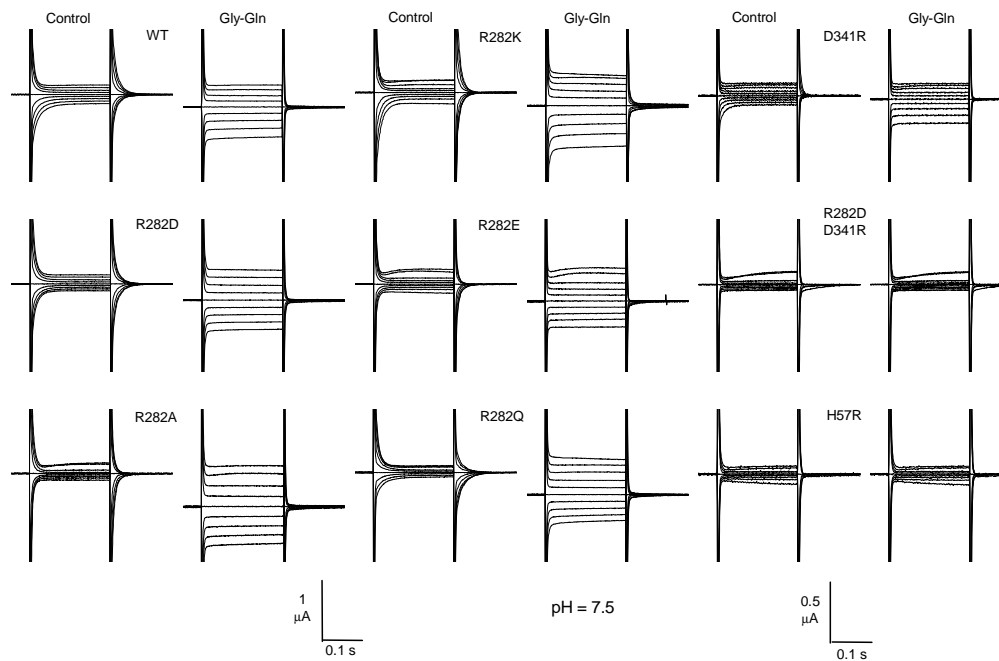
Fig.3.9 *Current responses to voltage pulses in absence and presence of substrate at pH 7.5 in the wild-type and indicated mutants of the rbPepT1.*

3.2.2 Localization and membrane expression of the FLAG protein

Immunolocalization experiments were performed to understand whether the various mutants were correctly inserted in the oocyte membrane. Representative images are shown in Fig.3.10 A. The negative controls (non-injected oocytes and oocytes expressing a wild-type transporter with no FLAG), gave no visible signal in the membrane of the oocytes. All the other isoforms were correctly localized in the membrane to a variable extent. These observations were confirmed by the single-oocyte chemiluminescence (SOC) experiments that were performed on larger numbers of oocytes from different batches (Fig.3.10 B). All functional mutants were present in the membrane at levels similar or greater than the wild-type, in agreement with previous results (Kulkarni *et al.*, 2007). Our data also confirm the correct membrane localization of the non-functional mutant H57R (Uchiyama *et al.*, 2003). However, the double mutant R282D-D341R gave only very weak signals in both the immunolocalization and in the chemiluminescence experiments, in agreement with the lack of transport-related currents (Fig.3.9).
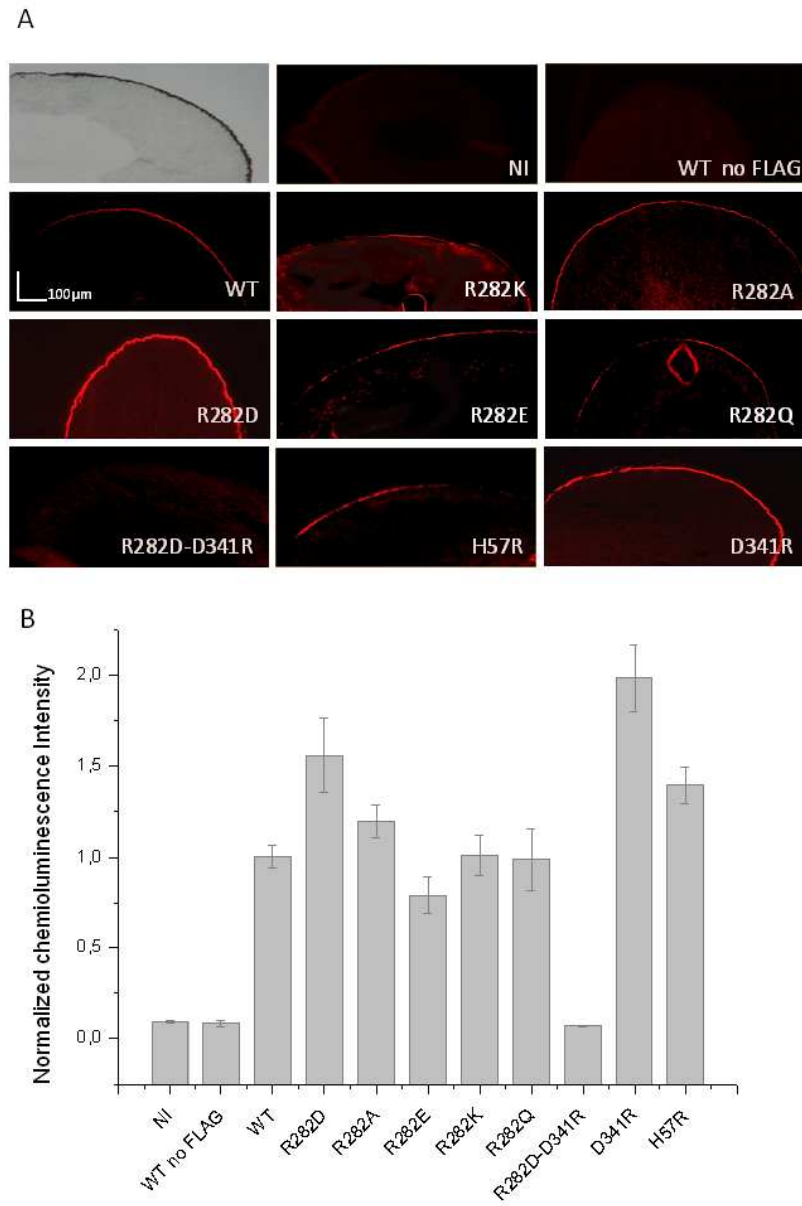
Fig.3.10 *rbPepT1wt and mutants surface expression.*
Immunohistochemistry (A) and chemiluminescence experiments (B) of
oocytes expressing FLAG-rbPepT1 WT and the indicated mutants.
.

These results are generally well correlated to the electrophysiological observations: the lack of transporter-associated currents seen in the R282D-D341R double mutant is paralleled by the weak luminescence signal in Fig.3.10 for this isoform, while the large currents displayed by the R282 mutants are in agreement with the strong signals of the localization and luminescence experiments. On the contrary the small presteady-state and transport currents recorded in the H57R and D341R forms are in contrast with the large membrane expression seen in the results reported in Fig.3.10. Based on these observations, the reduced functionality of this last mutant appears to be attributable to a defect in the molecular mechanism rather than to insufficient targeting to the membrane.

The presteady-state currents generated by the functional mutants maintained the sensitivity to external pH by showing a shift towards more negative potentials at more alkaline pH, as illustrated in Fig.3.11 for the R282D mutant. The isolated currents were analysed as explained in the Method, and the results of this analysis are plotted in the bottom row of Fig.3.11, showing the accelerating action of alkaline pH on the time constant and the shift towards more negative potentials induced by this pH on both τ/V and Q/V curves. Fitting a Boltzmann equation [eq.3.2] to the R282D data of Fig.3.11 gives $V_{0.5}=$ -45 ± 0.9 mV at pH 7.5, and 7.8 ± 6 mV at pH 6.5 in this group of oocytes. The estimated maximal moveable charge appears to remain substantially constant (41.4 ± 0.8 nC at pH 7.5 *vs* 37.6 ± 3.1 nC at pH 6.5), although these data are subject to significant errors especially at pH 7.5 because of lack of saturation at positive potentials. The comparison with the wild-type data (filled symbols in Fig.3.11) shows

that at the same pH the decay time constants of the R282D mutant are shorter and that both τ/V and Q/V curves of the mutant are shifted towards more positive potentials ($V_{0.5}$ = -59.2 ± 1.3 mV at pH 6.5 in this group). These effects were also seen, to a various degree, in all other arginine mutants.
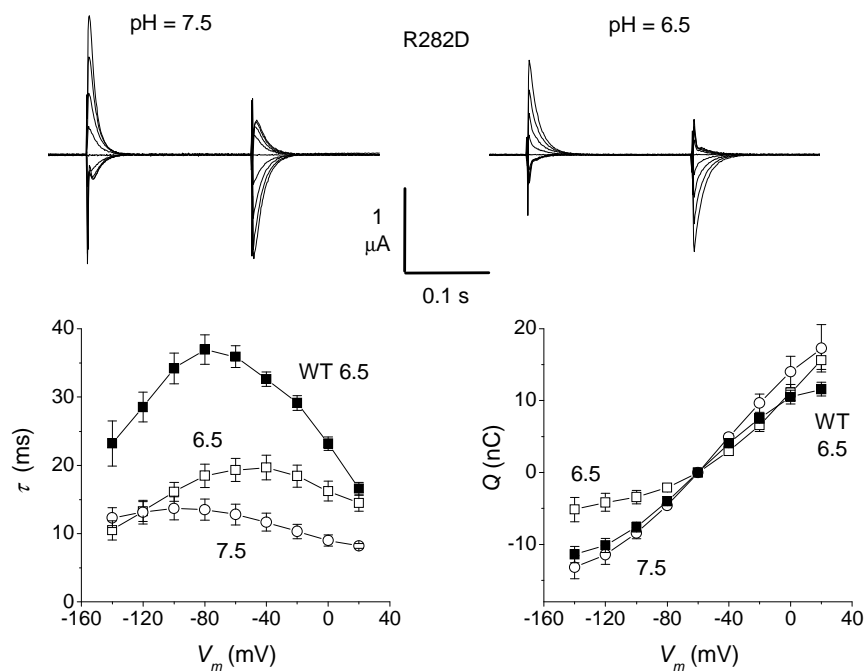
Fig.3.11 *Mutants in the charge-pair residues were pH-sensitive. Top row: traces of pre-steady-state currents isolated using the subtraction method in a representative oocyte expressing the rabbit R282D mutant at the two indicated pH values. Bottom row: values of the time constant of decay and of the amount of displaced charge in the two pH.*

3.2.3 Unidirectional rates

A more complete analysis of the charge movement properties of the different isoforms at pH 6.5 is shown in Fig.3.12. Here the Q/V curves are plotted as the amount of charge displaced in an inner position in the membrane electrical field, relative to the maximal

displaceable charge (Q_{max}), obtained from fitting Boltzmann equation [eq.3.2] to the sigmoidal curves (Fesce *et al.*, 2002). Fitting the *Q/V* curves in Fig.3.12 A to this equation gives, for the various isoforms, the parameters summarized in Tab.3.4.

	WT (11)	D341R (5)	R282K (7)	R282D (7)	R282E (7)	R282A (7)	R282Q (7)
$V_{0.5}$(mV)	-60.0 ± 1.1	-113.4 ± 2.2	-38.3 ± 4.8	-1.2 ± 1.8	+1.5 ± 7.1	+2.9 ± 4.3	-18.1 ± 6.2
σ (mV)	29.7 ± 1.4	39.3 ± 1.2	33.6 ± 2.4	34.4 ± 0.8	27.5 ± 1.1	29.2 ± 2.3	28.2 ± 1.8

Tab.3.4 *Boltzman equation parameters.*

It may be seen that in all arginine 282 mutants the *Q/V* curves are shifted towards more positive potentials compared to the wild-type, and the time constants are shorter. Conversely, replacement of the negative aspartate 341 with arginine causes a negative shift of both *τ/V* and *Q/V* curves together with an increase in the maximal time constant value (Fig.3.12 A and B).

With the partial exception of the D341R mutant, no strong changes in the slope factor *σ* can be seen in Tab.3.4, implying that the mutated residues are only marginally (if at all) involved in the charge movement underlying the presteady-state currents.

From the data in Fig.3.12 A and B, the plots of *inrate* and *outrate* for the wild-type and the six functional mutants can be obtained (Fig.3.12 C and D). These graphs show that, compared to the wild-type, the mutants of R282 exhibit faster inward and slower outward rate, while the opposite occurs in the D341R mutant.
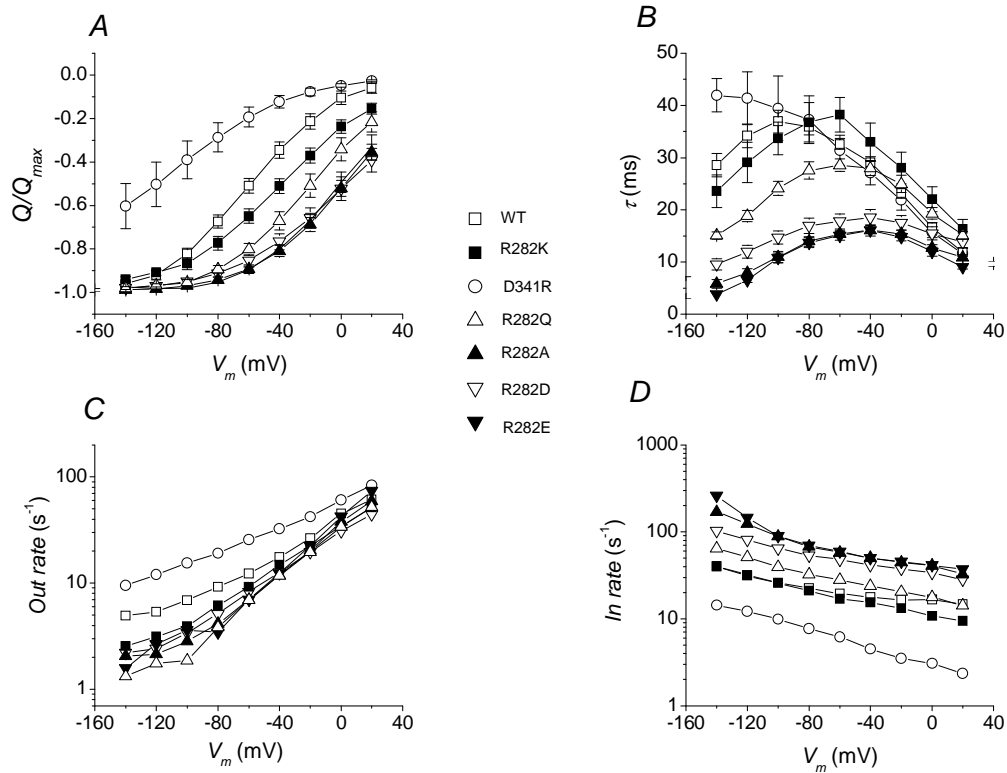
Fig.3.12 *Charge movement analysis. A and B: relative amount of moved charge and decay time constant, respectively for the indicated isoforms at pH 6.5. C and D: outward and inward rate constants.*

3.2.4 Transport currents

To complete the analysis of the electrophysiological properties of the charge-pair mutants, experiments have been performed to compare the characteristics of the transport-associated current, and their possible correlations to the presteady-state currents.

The top row of Fig.3.13 shows the records of the isolated transport currents (obtained by subtracting the currents in absence of substrate from those in presence of 1 mM Gly-Gln) in four representative oocytes expressing the WT PepT1, the R282D, the R282A, or the

D341R mutant, each tested with the usual pulse protocol at external pH 7.5. In the bottom row of Fig.3.13 the average *I/V* curves at four pH values (6.5, 7, 7.5 and 8) are plotted. The graphs are normalized to the current value at -140 mV (pH = 7.5) for a more easy comparison; however it must be remembered that the currents generated by the D341R mutant were significantly smaller in absolute value (see Fig.3.9). In all isoforms, changes in external pH caused shifts in the *I/V* curves that were in the same directions as for the presteady-state currents parameters. This observation indicates that the substrate transport activity is still pH-dependent in these three mutants. At potentials more positive than -40 mV, the shape of the relationships shows inward rectification in the wild-type and particularly in the D341R mutant, while it is much more linear in the R282D and R282A forms, that show a very clear reversal and strong outward currents. Indeed reversal of the transport current is seen also in the wild-type transporter at pH 8 (squares in Fig.3.13).

The transport current generated by the R282K mutant was qualitatively similar to that of the wild-type, while the behaviour of the R282E and R282Q mutants was comparable to R282D and R282A, respectively, with evident outward currents and clear shifts in E_{rev} induced by changes in pH and substrate concentration. For the non-conservative arginine mutants, semilog plots of E_{rev} vs. pH were linear (R > 0.98) with slopes between -38.2 (R282D) and -49.6 (R282A) mV/pH unit (Fig.3.14 A), indicating a substantial contribution of protons to the current. It may be relevant to note that the amplitude of the outward current and the position of the reversal potential are also dependent on the voltage protocol and on the level

of expression of the transporters ((Kottra *et al.*, 2002) and our observation in 3.3).
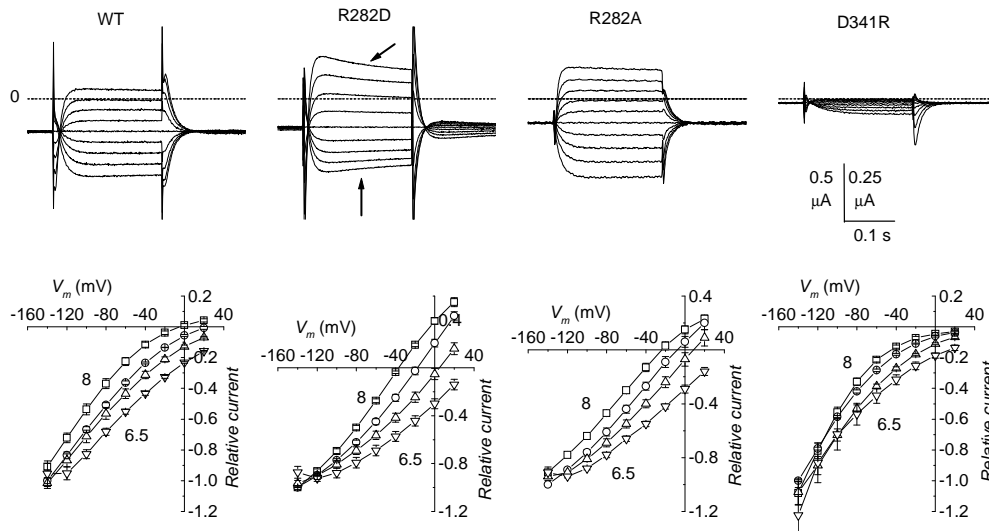
Fig.3.13 *Transport currents in the different isoforms.*
Top row: subtracted traces (1 mM Gly–Gln minus no substrate) at pH 7.5
from four representative oocytes expressing the indicated transporters. Note
the slow decay in the current traces exhibited by the R282D and R282A
mutants (arrows). Bottom row: I–V curves elicited by 1 mM Gly–Gln in the
four isoforms at different external pH values.

The estimation of the apparent affinity for external protons is made difficult by the presence of the outward currents (see below). However, limiting the analysis to the wild-type, the proton concentrations eliciting half the maximal current increase with voltage from 15 nM at -120 mV to about 770 nM at -120 mV (Fig.3.14 B), in qualitative and quantitative agreement with previous determinations (Amasheh *et al.*, 1997;Kottra *et al.*, 2002).
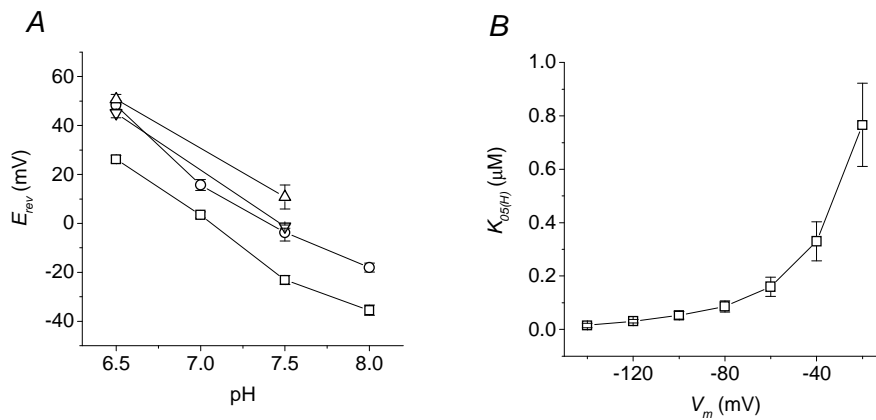
Fig.3.14 *A: pH dependence of reversal potential in the non-conservative arginine mutants. B: Apparent affinity for protons for the wild-type PepT1.*

Changing the dipeptide concentration at constant pH produces on the transport currents the effects illustrated in Fig.3.15 for the wild-type and the R282D mutant (very similar results were seen in the R282E, R282Q and R282A forms). Higher substrate concentrations applied at pH 7.5 produce an increase in current amplitude that reaches saturation at 1 mM in the wild-type, and shifts the reversal potential towards more positive values in all isoforms. Indeed, at this pH and using lower substrate concentrations, a clear reversal of the current is visible also in the wild-type, confirming previous observations (Verri *et al.*, 2003;Kottra *et al.*, 2009). The fact that changes in the concentration of a neutral substrate, such as Gly-Gln, are able to affect E_{rev} suggests that the organic substrate is translocated as a complex with the electric charge, confirming that these mutants behave as true cotransporters.
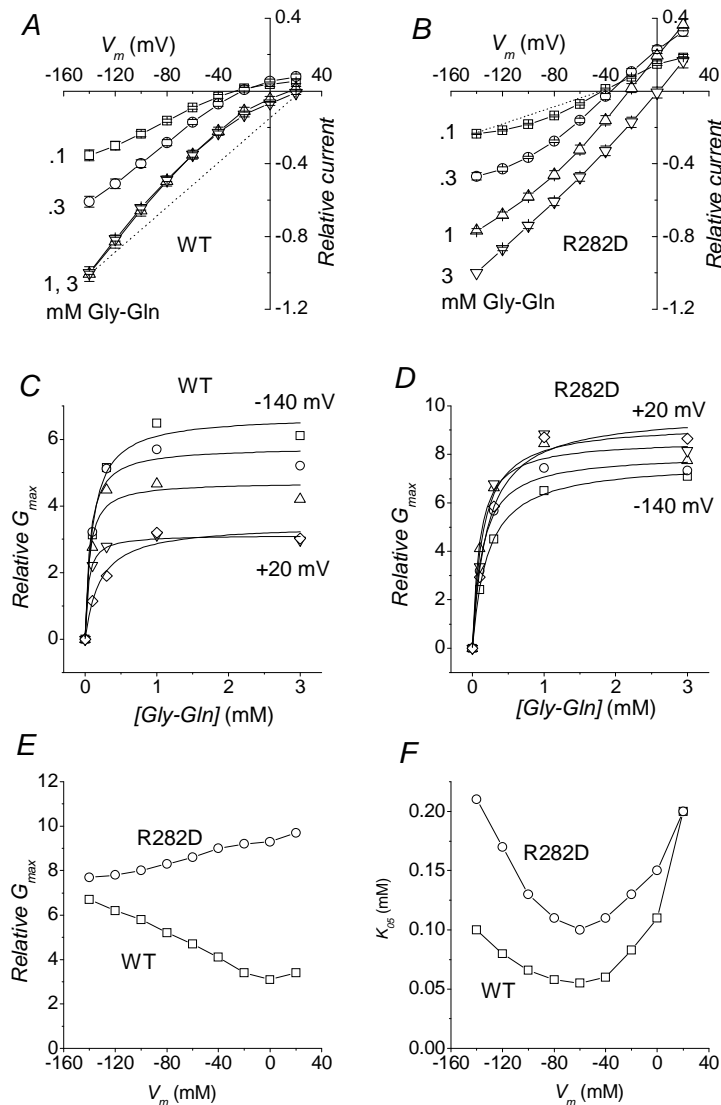
Fig.3.15 *Effects of changing the external Gly-Gln concentration on the current and the conductance at fixed pH (7.5) in the wild-type (A) and R282D (B) PepT1. Increasing [Gly–Gln]shifts E_{rev} towards more positive values. C and D: dose–conductance curves for the two isoforms. E and F: voltage dependence of the maximal conductance (G_{max}) and substrate concentration producing half G_{max} (K_{05}) obtained by fitting Michaelis–Menten equations (continuous curves) to the data in C and D (for clarity only the data at −140, −100, −60, −20 and + 20 mV are shown).*

The reversal of the current direction complicates the evaluation of the apparent affinity for the substrate from the usual current-dose plots. An alternative possibility to gain informations on the ability of the transporter to interact with the substrate is the use of the chord conductance (G) as an indicator of the level of activity. The chord conductance is defined as (Aidley, 1989):

$$G = \frac{I}{V_m - E_{rev}}$$
[eq.3.8]

This quantity is directly proportional to the transport current, but it remains always positive, being divided by the electrochemical gradient. Fig.3.15 C and D plot this quantity against the substrate concentration. Fitting these plots with a Michaelis-Menten equation gives the values of the maximal conductance (G_{max}) and of the substrate concentration producing half G_{max} (K_{05}^G). These graphs are shown in Fig.3.15 E and F. It may be noted that the different voltage-dependence of G_{max} in the two isoforms reflects the opposite curvature of the *I/V* plots in Fig. 3.15 A and B. Clearly K_{05}^G cannot be directly compared to the apparent affinity classically obtained as the substrate concentration producing the half-maximal current (Mackenzie *et al.*, 1996;Kottra and Daniel, 2001). However in the present context the aim of this analysis was to compare the properties of the mutants with those of the wild-type. Fig.3.15 F shows that K_{05}^G for the R282D mutant is greater than for the wild-type over most of the voltage range, indicating a lower affinity for the organic substrate.

3.2.5 *Charged substrates*

PepT1 transporters are known to accept as substrates several di- and tri-peptides possessing different electrical charge, provided the charged amino acid is in the amino-terminus position (Kottra *et al.*, 2002). Therefore the behaviour of the charge-pair mutants has been tested in the presence of the dipeptides. Lys-Gly, and Asp-Gly, in addition to Gly-Gln. The results are shown in Fig.3.16 for the wild-type and the mutants D341R, R282Q, R282D and R282K. As in the other experiments illustrated above, R282E and R282A behaved quite similarly to R282D and to R282Q respectively.

The inward rectifying characteristic of the wild-type, D341R and R282K transporters appears to be independent on the charge carried by the substrate. In all isoforms, Asp-Gly elicits smaller transport currents at this pH (7.5) compared to Gly-Gln. On the contrary the currents produced by Lys-Gly are larger in all cases, reaching amplitudes about twice or more that of the neutral Gly-Gln in the non-conservative arginine mutants. These results confirm previous observations on the wild-type (Amasheh *et al.*, 1997;Kottra *et al.*, 2002).
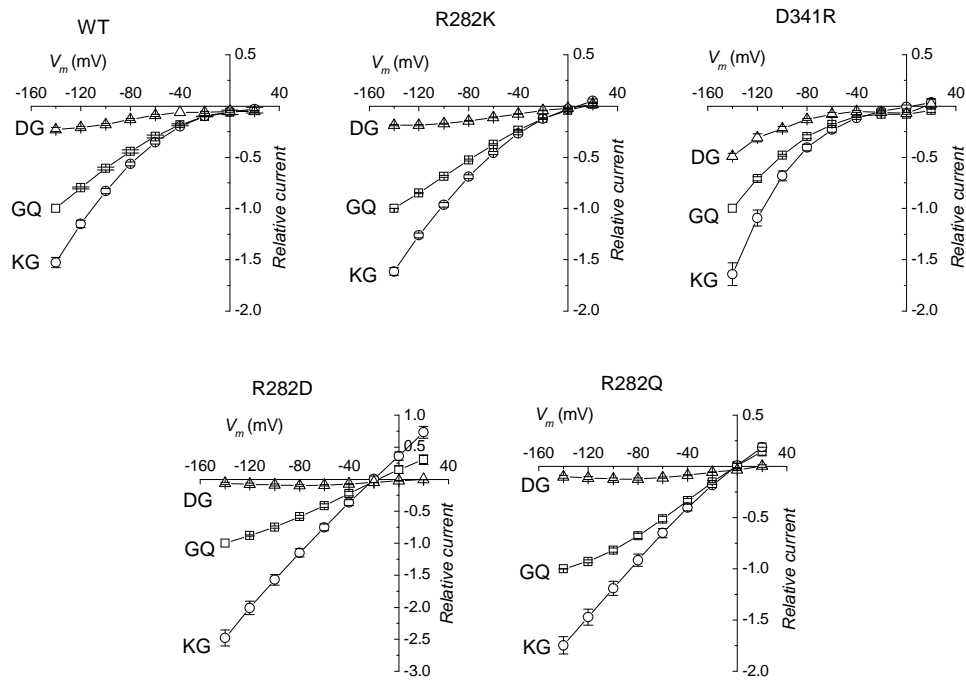
Fig.3.16 *Voltage dependence of the transport currents elicited by differently charged dipeptides (all at 1 mM) in the indicated mutants at pH 7.5.*

The potency order of the substrates remains unchanged in all functional mutants, compared to the wild-type. However, a closer look at the graphs reveals more subtle differences: the degree of reduction (compared to Gly-Gln) of the negatively charged dipeptide is greater in the non-conservative arginine mutants and smaller in the D341R form. Conversely, in these mutants Lys-Gly produces a substantially linear *I/V* relationship and significant outward currents.

3.3   *Reverse operation in PepT1*

The question of reverse operation is a relevant issue in many cotransport systems, especially in the context of neurological disorders in which leakage of neurotransmitters into the extracellular space may have profound consequences. Although the physiological role of these transporters is the reuptake, in several instances a release of neurotransmitter via the transporter has been reported. This reversed mode of operation may be either the effect or the cause of abnormal or pathological conditions. In the case of the glutamate transporters, export of glutamate may lead to the elevated extracellular levels that cause excitotoxicity (Rossi *et al.*, 2000), while in the SLC6 family reversal of the operation of the dopamine transporter is caused by amphetamines (Khoshbouei *et al.*, 2003) (Seidel *et al.*, 2005), and release of GABA through GAT1 has been hypothesized to concur in causing epileptic seizures (Richerson and Wu, 2003;Richerson and Wu, 2004).

Although the SLC15 family is distinct from the gene families of the neurotransmitter transporters cited above (SLC1 and SLC6), there is growing evidence that different families may share common structural modules (Meredith and Price, 2006;Abramson and Wright, 2009;Krishnamurthy *et al.*, 2009). It is conceivable therefore that an investigation on the structural determinants of reverse operation in PepT1 may contribute to understand the same process in the neurotransmitter transporters. Furthermore, the renal isoform of the peptide transporter, PepT2 has been identified among others in the enteric nervous system in both glia cells, and a specific subset of

neurons and could play a role in both release and reabsorption of small neuropeptides (Rühl *et al.*, 2005).

Outward currents have been observed, under certain experimaental conditions, in the zebrafish isoform of PepT1 (Verri *et al.*, 2003), and also in a mammalian isoform (Kottra *et al.*, 2009). Interestingly, in this last case it was reported that the outward currents were greatly enhanced in conditions of high intracellular substrate concentration, or following inhibition of intracellular dipeptide hydrolysis.

The two rbPepT1 mutants in arginine 282 (R282D and R282A) exhibit large outward transport currents that remain pH- and substrate concentration-dependent. An analogous mutant (R282E) of rabbit PepT1 was previously reported to exhibit characteristics similar to a substrate-gated unspecific cation channel (Meredith, 2004). Therefore the properties of reverse operation in the R282D and R282A mutants have been investigated to understand to what degree the operation of PepT1 was modified from a coupled-transport mode to a channel mode, obeying the principles of electrodiffusion.

The hypothesis of an important role of local accumulation/depletion of substrate near the intra- and extracellular sides of the transporter, previously suggested (Kottra and Daniel, 2001), was tested by employing different experimental protocols, aimed at altering the transport regime by long lasting holding potentials.

PepT1 transporters show relatively poor substrate specificity (Vig *et al.*, 2006): many di- and tri-peptides, either neutral or electrically charged, are transported, while single amino acids and

tetrapeptides are not (Herrera-Ruiz and Knipp, 2003;Daniel *et al.*, 2006). Having observed enhanced outward currents in mutants in which the positive R282 was removed, the importance of a charge in the substrate was also investigated, using both positively and negatively charge dipeptides, in addition to the zwitterionic Gly-Gln.

3.3.1 Outward transport currents of PepT1 in experimental conditions

Outward transport currents have been observed in wild-type PepT1 when depolarizing pulses of relatively short duration (50 – 250 ms) are applied with the voltage-clamp technique from negative (-40, -60 mV) holding potentials (Kottra and Daniel, 2001) (Verri *et al.*, 2003;Kottra *et al.*, 2009). Outward currents are most easily seen at alkaline pH and relatively low substrate concentrations, since increasing the concentration of either substrate or H^+ shifts the current-voltage relationships to more positive potentials, eventually bringing the reversal potential (E_{rev}) out of the experimental range (Verri *et al.*, 2003) and our unpublished observations). In addition to the results in wild-type PepT1, some mutants in arginine 282 are also capable of conducting quite large outward currents, as shown in Fig.3.17.
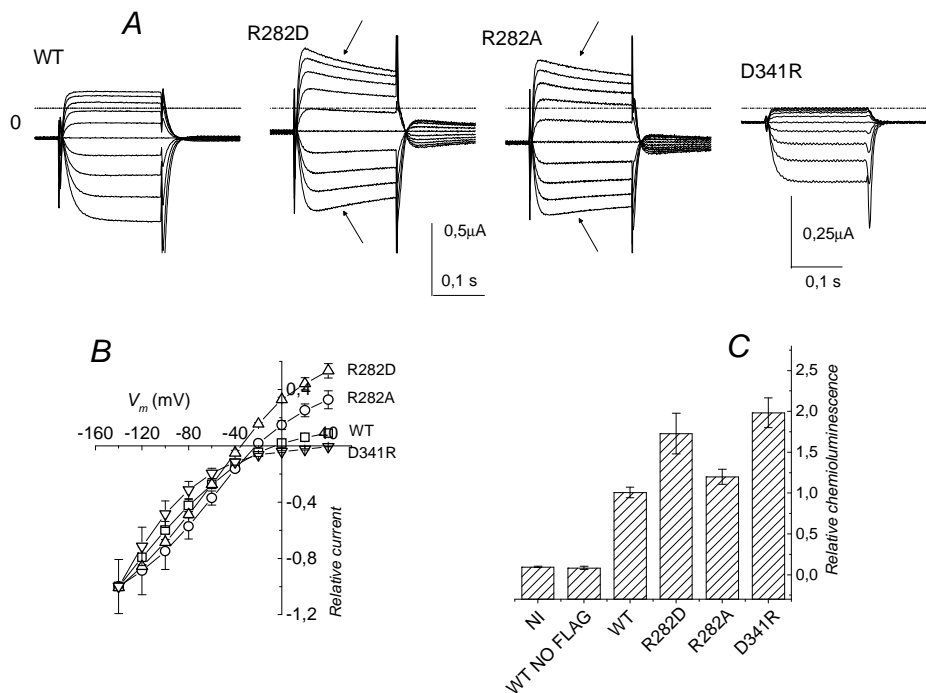
Fig.3.17 *A: Transport currents recorded in the presence of 1 mM Gly-Gln in the wild-type and indicated mutants at pH 8.0. B: I/V relationships. C: Surface expression, reported as results of the chemiluminescence experiments.*

The *I/V* relationships plotted in Fig.3.17 B show that in the same conditions of pH and substrate concentration the value of E_{rev} becomes progressively more negative as the positive charge of arginine is first neutralized to alanine and then changed in sign with aspartate. Moreover, the R282D mutant (but not R282A) generated significantly larger currents than the wild type. On the contrary, reverting the sign of the negative aspartate 341 to a positive arginine (D341R) produces a transporter which is still functional but shows reduced transport currents and no reversal in the explored voltage range. In the group of oocytes illustrated in Fig.3.17, the average

91

currents at -140 mV were: 568 ± 58 nA for wild-type, 998 ± 172 nA for R282D, 464 ± 94 nA for R282A and 184 ± 35 for D341R (mean ± SE, n = 4 – 7).

Another evident feature in the traces of the transport currents generated by the R282D and R282A mutants is the slow decline during the voltage pulse (arrows in Fig.3.17 A), a behaviour that may suggest either the existence of a deactivating process, or a progressive reduction in the driving force.

In both R282D and R282A mutants the reversal potential of the transport current is shifted by changes in either the proton concentration or the substrate concentration (Fig.3.18). This result suggests that the translocation of the two species occurs in a coupled fashion. The shifts in E_{rev} caused by the pH and substrate changes in the mutants R282D and R282A are plotted in Fig. 3.18 B and D. The slopes of the E_{rev} vs. pH curve are -42.3 and -43.7 mV/pH unit respectively; although less than the 58 mV/pH unit predicted for a pure H^+ current on the basis of the Nernst equation, these values are nevertheless consistent with a substantial contribution of H^+ to the current. Similarly, the semilog plots of E_{rev} vs [Gly-Gln] are not linear for both mutants (Fig.3.18 D) with even lower slopes compared to the pH dependence. The slope conductance (g_{slope}) of the *I/V* curves at E_{rev} has been also estimated. This parameter is plotted in Fig.3.18 as a function of pH and substrate concentration for both mutants. Interestingly, while g_{slope} increases with increasing concentrations of Gly-Gln (Fig.3.18 D), it appears to be substantially independent from the proton concentration (Fig.3.18 B). This last result is contrary to the expectations for an electrodiffusive process, that would predict instead

an increase in slope conductance when the concentration of the permeating species is raised (Hille, 2001).
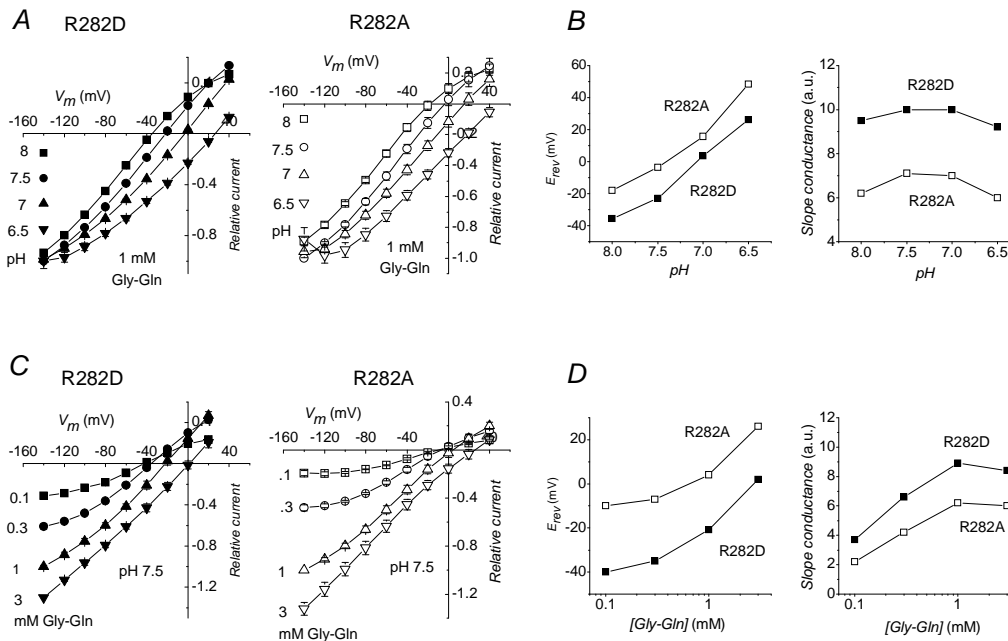
Fig.3.18 *Effects of changing pH and substrate concentration on the R282D and R282A mutants. A: External alkalinization at fixed (1 mM) Gly-Gln concentration shifts the I/V curves towards more negative potentials. The change in E_{rev} with pH is shown in B for R282D and for R282A. C: Positive shifts in the I/V curves produced by increasing the external Gly-Gln concentration at fixed pH (7.5) in the two mutants. The shifts in E_{rev} induced in this case are plotted in D, together with the slope conductance at E_{rev}; this parameter shows an increase at higher Gly-Gln concentrations.*

3.3.2 Current reversal in the wild-type and R282 mutants

The apparently anomalous effects mentioned above on the slope conductance around E_{rev}, prompted us to perform other experiments aimed at better understanding this phenomenon, both in the wild-type and in the R282D/A mutants. The necessity of further

93

controls was also suggested by the declining behaviour seen in the current traces in Fig.3.17. Long-lasting voltage- and current-clamp experiments have been performed on both wild-type and R282D mutant to investigate this point. Fig.3.19 A shows voltage-clamp experiments in which the membrane voltage was stepped twice from -40 mV to +40 mV and back: the first step was given in the absence of substrate, and the second in presence of Gly-Gln 1 mM at pH 8. In these conditions, E_{rev} should be close to -30 mV in the R282D mutant.
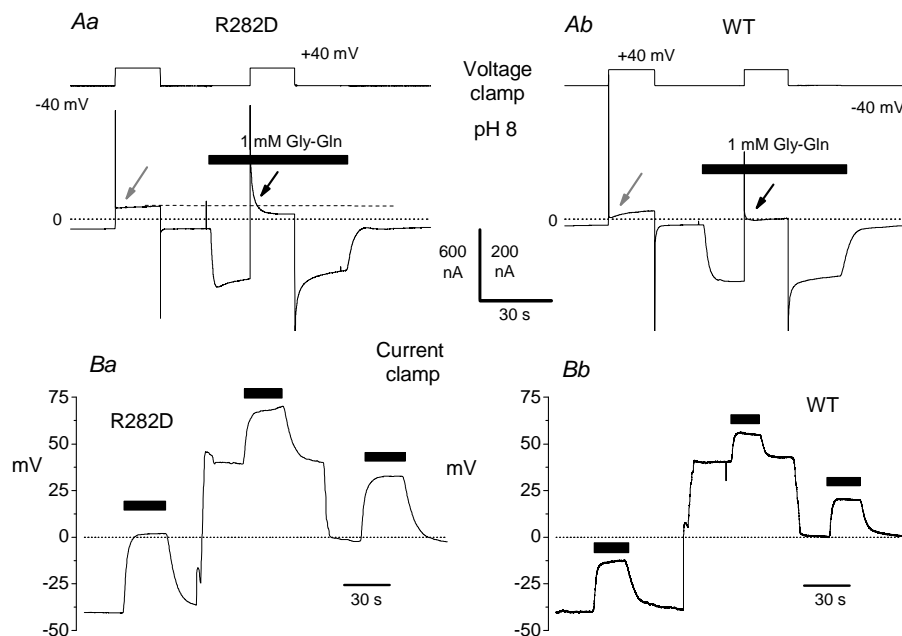
Fig.3.19 *A: Long lasting records showing the slow deactivation process following step voltage changes in R282D and WT PepT1: during the first seconds after the jump at +40 mV the current in the presence of substrate is more positive than in its absence (gray arrow); however, at later times it becomes more negative; B: Current clamp recordings at pH 8 in R282D and WT PepT1: the addition of substrate induced depolarizations, implying that an inward current was generated by the transporter.*

94

Fig.3.19 Aa shows that jumping to +40 mV when the transporter is activated by 1 mM Gly-Gln causes an instantaneous large outward current (black arrow) that declines with time constants in the order of fractions of seconds, and it is not seen in absence of the substrate (gray arrow). Initially the current is more positive than the value recorded at the same voltage in absence of substrate (dashed line), but at the end of the 20 s period at +40 mV it becomes less positive (that is, a negative current after subtraction). A qualitatively similar behaviour, although with smaller currents, was observed in the wild-type PepT1 (Fig.3.19 Ab).

Fig.3.19 B shows complementary experiments performed again on both wild-type and R282D with analogous results. The oocytes were kept in current-clamp conditions, i.e. an appropriate current was injected to keep the membrane voltage at a desired value before substrate application, but the membrane potential was let free to change as a consequence of transporter operation. The representative traces in Fig.3.19 Ba, from an oocyte expressing R282D, and in Fig.3.19 Bb, from an oocyte expressing wild-type PepT1, show that addition of 1 mM Gly-Gln at pH 8 (black bars) always induces a depolarization, irrespective of the starting value of the voltage (-40, 0 and +40 mV), indicating that the current generated by the transporter is in all cases in the inward direction.

3.3.3 The outward current is due to temporary accumulation of substrates

To discriminate whether the current decays seen in Figs 3.17 and 3.19 were due to changes in electrochemical gradient or to a

transporter-intrinsic deactivation process, a series of experiments employing different strategies was performed. Fig.3.20 illustrates the results of a representative experiment using a protocol in which three fast (200 ms) voltage ramps ranging from +40 to -100 mV (or from -140 to +40 mV) were superimposed to a long lasting voltage step to +40 (or -140) mV in conditions inducing the decay of the transport current in both directions (pH 8, 1 mM Gly-Gln).
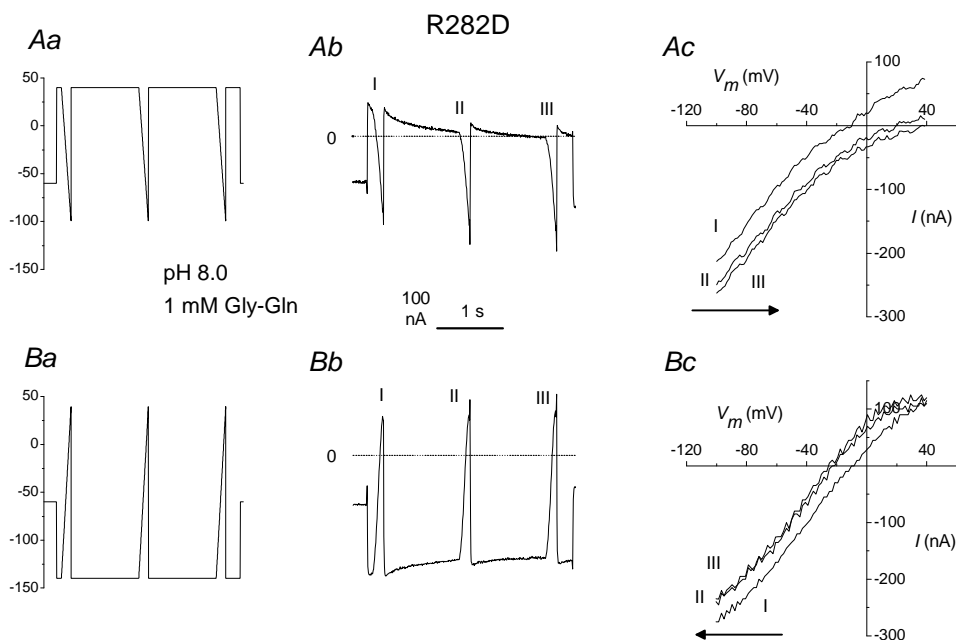
Fig.3.20 *Step and ramps protocols to investigate the basis of the transport current decline. Ab and Bb show the subtracted (substrate minus control) transport currents: both records show the slowly declining currents, which are in the outward direction in Ab and in the inward direction in Bb. Ac and Bc: I/V relationships; in Ac the reversal potential moves toward more positive values with the second and third ramp, whereas in Bc the opposite behavior is observed. I/V curves remain substantially parallel to each other.*

As shown in Fig.3.20. Ac and Bc, the *I/V* curves derived from the ramps shift along the voltage axis according to the application order and to the level of the long-lasting voltage pulse. The ramps superimposed to the depolarizing (+40 mV) pulse exhibit a progressive shift toward more positive potentials (Fig.3.20 Ac), while those applied during the pulse to -140 mV are moved with time toward more negative potentials (Fig.3.20 Bc). Interestingly, in both cases the curves remain parallel to each other, so that it may be concluded that only the reversal potential is affected, not the conductance.

These observations represent a strong indication that the decline of the transport current during either the depolarizing or the hyperpolarizing pulses is due to substrate concentration changes in the vicinity of the transporters. In fact, assuming that E_{rev} might be written as a Nernst equation for the proton-substrate complex:

$$E_{rev} = \frac{RT}{F} \ln \frac{[TC]_{out}}{[TC]_{in}} \qquad \text{[eq.3.9]}$$

where TC stands for *transported complex*, the continuous inward flow during the hyperpolarizing pulse will increase $[TC]_{in}$ (and/or decrease $[TC]_{out}$) causing E_{rev} to change with time to more negative values, as observed in Fig.3.20 Bc. On the contrary, the initial outward current seen when stepping the potential from –60 to +40 mV (Fig.3.20 Ab) will decrease $[TC]_{in}$ (and/or increase $[TC]_{out}$) shifting E_{rev} to more positive potentials (Fig.3.20 Ac).

On the whole, the results shown in Fig.3.20 indicate that the outward current seen during short depolarizations is caused by a local accumulation of the transported complex at the intracellular side of the

membrane and/or a local depletion of the complex at the extracellular side during the continuous inward transport occurring at the negative holding potential, confirming earlier suggestions (Kottra and Daniel, 2001).

In another series of experiments a prepulse lasting 2 s to +40 mV from V_h = -40 mV was applied to the membrane before moving the potential to variable 1 s long test pulses (+40 to -140 mV). Fig.3.21 shows this kind of protocol applied to an oocyte expressing the R282D mutant at pH 7.5. Upon addition of 3 mM Gly-Gln a slowly declining outward current is seen during the prepulse, while an opposite behaviour (i.e. a slowly declining inward current) is observed at the most negative test pulse potentials (Fig.3.21 A middle traces). Subtraction of the currents in the absence from those in the presence of substrate gives the isolated transport currents (Fig.3.21 A rightmost traces), in which the declining behaviour at negative potentials during the test pulses is still visible. The average *I/V* relationship obtained from the currents values at the end of the test pulses is plotted in Fig.3.21 C (open squares). It can be seen that using this protocol no outward current can be observed up to +40 mV. In contrast, a clear current reversal around +10 mV is noticeable in the same conditions of pH and Gly-Gln concentration when using the short depolarizing pulses from V_h = -60 mV (filled squares in Fig.3.21 C).

This experiment indicates that during the prepulse to +40 mV the accumulation/depletion effects are dissipated.
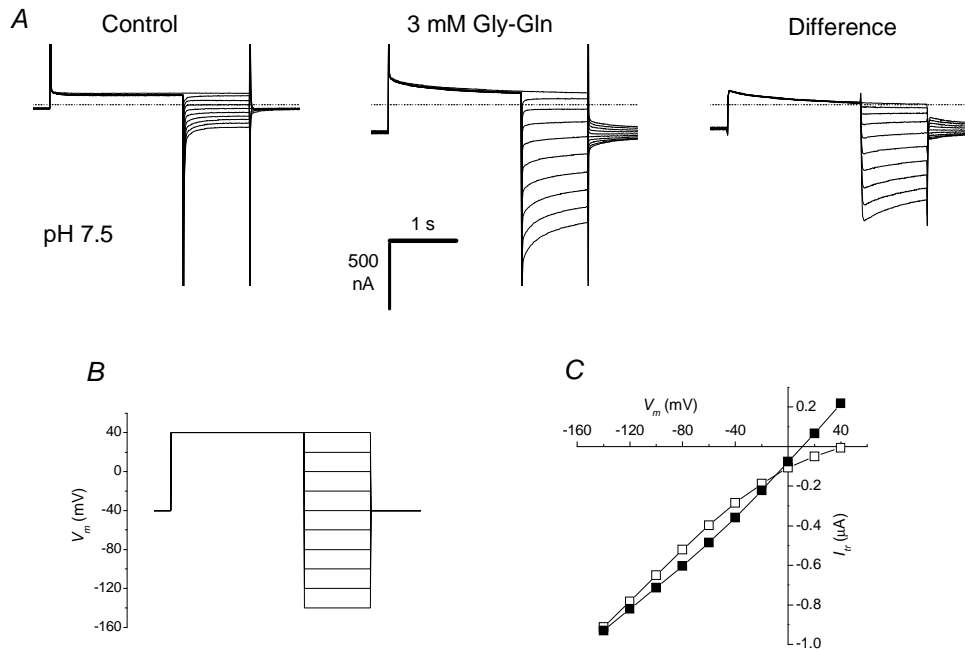
Fig.3.21 *Currents elicited by the prepulse protocol shown in B, in the absence and in the presence of 3 mM GlyGln at pH 7.5 in an oocyte expressing the R282D isoform; C: Plot of the current at the end of the test pulse in Ac (open symbols); for comparison, the filled symbols are the data obtained using the short-duration pulse protocol (from Vh -60 mV) from another oocyte in the same conditions.*

To check the physiological relevance of this phenomenon, a similar approach was applied to oocytes expressing the wild-type form of PepT1. In this case a shorter (250 ms) prepulse to +40 mV was sufficient to abolish the temporary phase of outward current (Fig.3.22). The transport-associated currents, obtained as usual by subtracting the traces in the absence from those in the presence of substrate, were always inwardly directed, even in conditions of alkaline pH and low organic substrate concentrations (Fig.3.22 A

99

rightmost traces). This correction, although modest, allows an extension of the voltage range in which the values of apparent affinity ($1/K_{05}$) and maximal current (I_{max}) can be obtained from a Michaelis-Menten analysis.
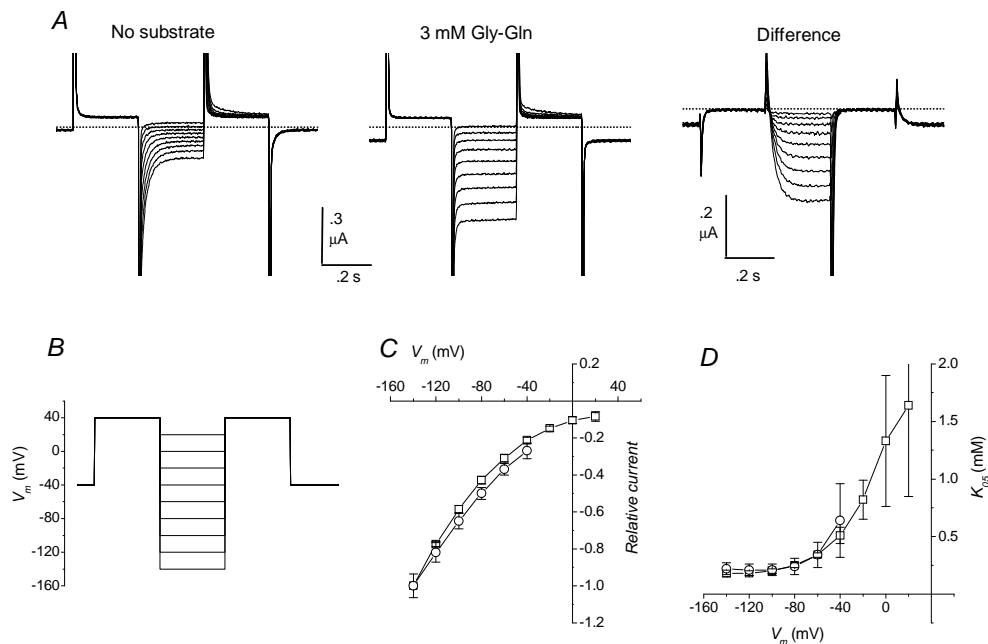
Fig.3.22 *Transport currents with the prepulse protocol. In the wild-type PepT1 a 250 ms prepulse duration was sufficient to abolish any outward current elicited by the jump from the -60 mV holding potential to positive potentials. This is demonstrated by the fact that the subtracted currents (A, rightmost traces) are all in the inward direction; C, D: I_{max} and K_{05} obtained by Michaelis-Menten analysis on dose-current curves; open circles: same parameters calculated with the usual protocol.*

The average values of K_{05} and I_{max} calculated from a group of oocytes tested with such protocol at pH 7.5 is shown in Fig.3.22 C and D (open squares), together with their counterpart obtained using the customary pulse protocol in which the test pulses were applied

100

directly from V_h = -60 mV without prepulse (open circles). It can be seen that while the data from the classical protocol are limited to -40 mV, because at more positive potentials the current at low substrate concentration becomes outwardly directed, the prepulse protocol allows an extension of the analysis up to +20 mV, although for K_{05} the statistical error becomes very large also in this case.

3.3.4 Intracellular injection of substrates

In order to find further support to the results reported above, a series of experiments has been performed injecting substrates in the cytoplasm of the oocyte. This procedure was already reported to produce significant outward transport currents in wild-type PepT1, when using hydrolysis-resistant dipeptides, or inhibiting intracellular peptidases (Kottra *et al.*, 2009). The results of our experiments on the wild-type and R282D, R282A and D341R isoforms are illustrated in Fig.3.23. In the upper part of this figure membrane voltage recordings in current-clamp condition are shown: first of all it can be noted that in all isoforms the resting membrane potential becomes significantly more negative after substrate injection (range -75 to -100 mV), compared to the initial -20 to -50 mV. This progressive hyperpolarization, already observed in the wild-type (Kottra *et al.*, 2009), develops in few minutes after injection and it is not observed in oocytes not expressing the transporters. The development of a strongly negative resting potential is clearly consistent with the activation of an outward current by the transporter as a consequence of the increased intracellular Gly-Sar concentration.
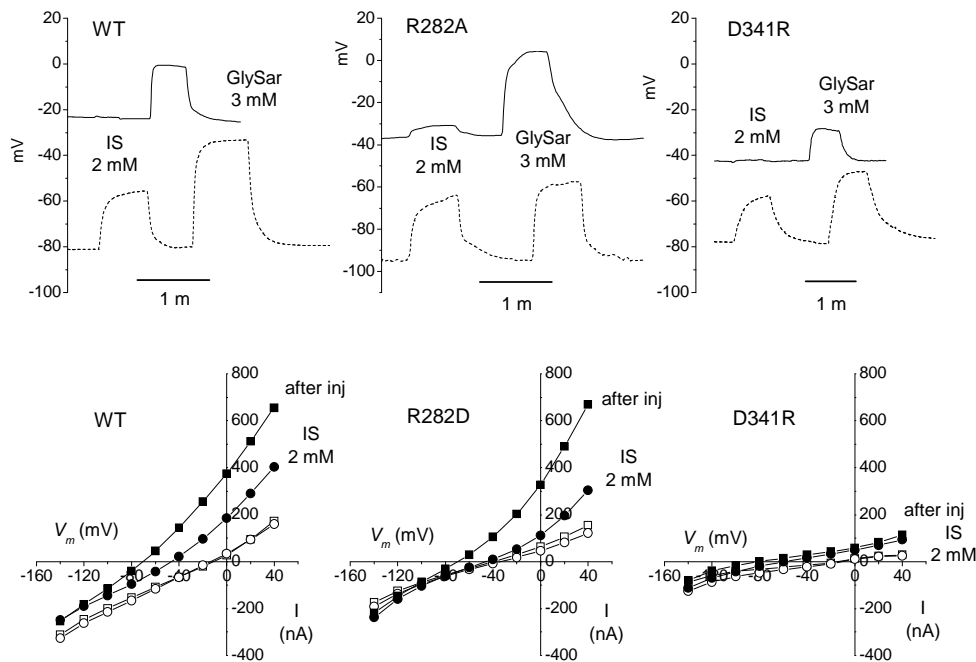
Fig.3.23 *Application of Irbesartan.*

Top row: current-clamp recordings showing the resting potential
changes induced by application of Irbesartan (IS) and Gly-Sar.
Bottom graphs: corresponding uncorrected I/V relationships before
(open symbols) and after (filled symbols) the injection of Gly-Sar.
Squares are data in the absence and circles in the presence of IS.

Additional evidence is provided by the application of the
blocker Irbesartan (IS) (Knütter *et al.*, 2009): the traces in Fig.3.23
show that while external Gly-Sar 3 mM depolarizes the membrane
when applied either before or after the intracellular injection, the
application of Irbesartan (2 mM) is effective in producing a
depolarization only after substrate injection. These last observations
indicate that, while the depolarizations induced by external Gly-Sar
are due to the development of an inward transport current, those

induced by Irbesartan are due to the inhibition of an outward current. Interestingly, the hyperpolarization of the resting membrane potential and the Irbesartan-induced depolarization are seen in all isoforms, including D341R, in spite of the much lower currents generated by this mutant. The *I/V* curves in Fig.3.23 confirm then the findings reported in the preceding figures, by showing the presence of a strong outward current following the intracellular injection of Gly-Sar, and a reduction of this current by Irbesartan.

3.3.5 Ion and substrate specificity

Previous results (Kulkarni *et al.*, 2007;Pieri *et al.*, 2008) (Meredith, 2004) have suggested that residues R282 and D341 form an ion bridge whose cyclic breaking and formation may gate the translocation process. Furthermore, it has been proposed (Meredith, 2009) that PepT1 may represent a transitional entity between transporters and channels. Then possible alterations in ion and substrate specificity in the R282D mutant have been investigated (the same results were obtained in R282A as well). The possible participation of other cations in the current elicited by the organic substrate was tested by replacing external Na^+ with K^+, Li^+ or tetramethylammonium ion (TMA^+). However these ionic substitutions did not significantly alter the shape of the *I/V* relationships in the presence of Gly-Gln at various concentrations and pH values, as shown in Fig.3.24 for pH 8 and Gly-Gln 1 mM. It can be seen that the reversal potential and the outwardly directed current are independent on the kind of cation representing the vast majority of external positive charges.
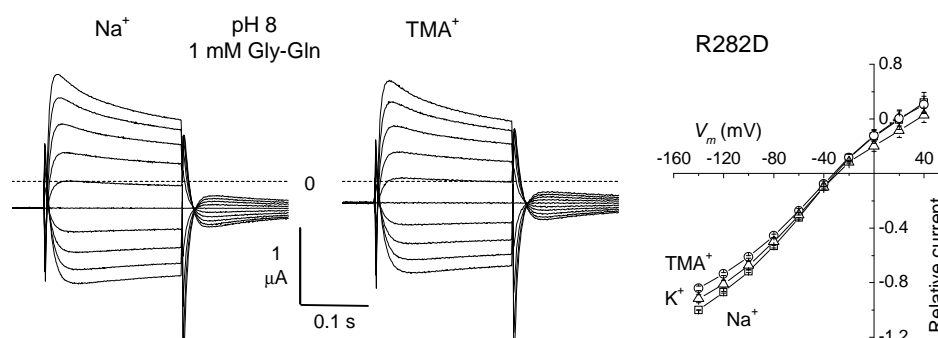
Fig.3.24 *Replacement of Na$^+$ with TMA$^+$ or K$^+$ in the external solution did not alter significantly the amplitude or the reversal potential of the transport current elicited by the organic substrate.*

This result, together with the observations of Fig.3.18 confirms therefore that the species carrying the electrical charge in both directions are indeed protons in complex with the organic substrate.

The substrate selectivity of R282D was also compared with that of the wild-type with special attention to the ability to generate reverse current. A first series of results is exemplified in Fig.3.25, where the capacity to transport di-, tri-, tetrapeptides, as well as histidine by the R282D mutant was tested. It is known (Herrera-Ruiz and Knipp, 2003;Daniel *et al.*, 2006) that PepT1 family members are able to transport several di- and tri-peptides, but not tetrapeptides. Furthermore, among the SLC15A family of transporters, the PepT subfamily is differentiated from the PHT subfamily by its inability to transport histidine. The representative records of Fig.3.25 A show that, with respect to substrate selectivity, R282D behaves in a manner similar to the wild-type transporters. The same potency order was found in the other two tested mutants, R282A and D341R (not shown). Furthermore, as illustrated in Fig.3.25 B, tripeptides (LGG)

104

are also able to generate outward current when the short pulse protocol from $V_h = -60$ mV is used.

A
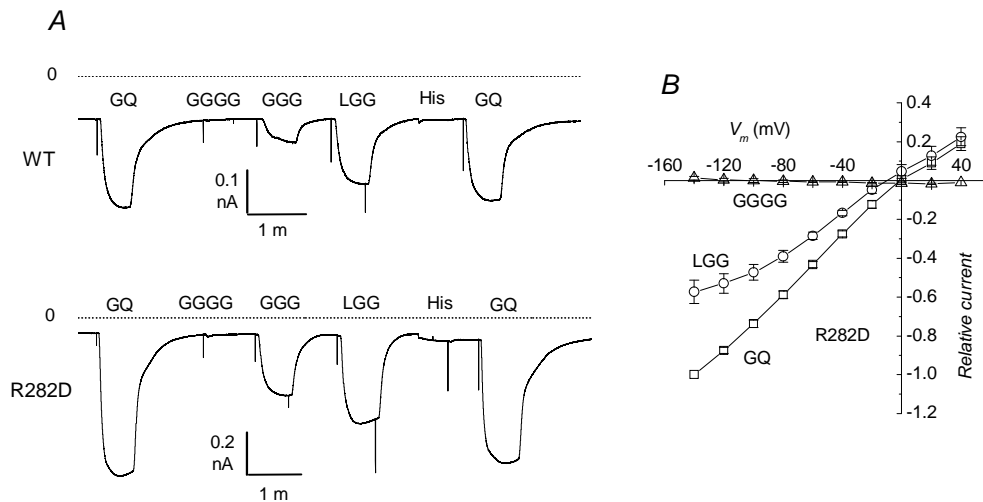
Fig.3.25 *Transport current elicited by di-, tri-, tetrapeptides and histidine in the wild-type and in the R282D mutant (GQ: gly-gln; GGGG: tetra glycine; GGG: tri glycine; LGG: leu-gly-gly; His: histidine).*

3.3.6 Charged dipeptides

In the context of the substrate selectivity analysis, it seemed particularly interesting to examine the behaviour of the mutants in the charge-pair residues when charged dipeptides were used in place of the neutral substrates employed in all previous experiments.

The relevance of introducing a negative or a positive amino acid in the substrate dipeptide, as well as its position was already studied in the wild-type PepT1 (Amasheh *et al.*, 1997) (Kottra *et al.*, 2002). An important conclusion from these studies was that the binding pocket of PepT1 can accept only neutral amino acids at the carboxy terminus, while at the amino terminus all kinds of charges can be accommodated.

105
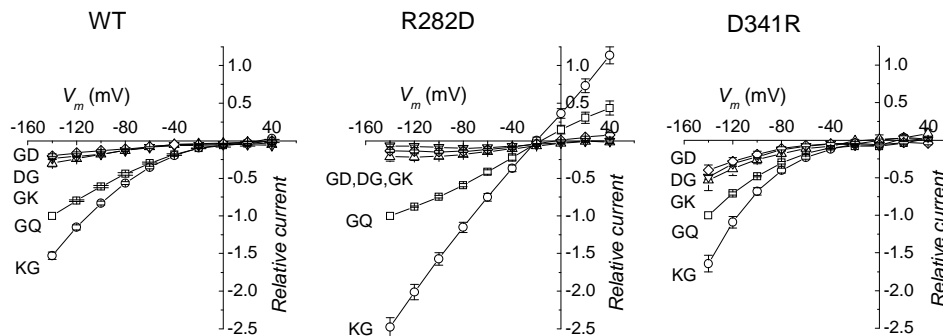
Fig.3.26 *Current-voltage relationships of the transport currents elicited by differently charged dipeptides in comparison with Gly-Gln (all at 1 mM) in the indicated isoforms at pH 7.5.*

Fig.3.26 compares the transport currents generated at the same pH (7.5) and substrate concentration (1 mM) when a positive or a negative residue is introduced in either position of the dipeptide. The transport currents were normalized to the current generated by the neutral dipeptide Gly-Gln at -140 mV in each oocyte before averaging. The previous observations on the wild-type are qualitatively confirmed in the mutants: the transport currents generated by Lys-Gly are larger compared to Gly-Gln in all isoforms, while those produced by Gly-Lys and by the two negatively charged dipeptides are smaller. However, the degree of reduction or increase is different in the two mutants: in the R282D the differences are enhanced Lys-Gly showing a much larger increase (150% vs 60% in the wild type), while the currents generated by Gly-Lys, Gly-Asp and Asp-Gly are reduced relatively more than in the wild type. In the D341R form, that produces in general smaller currents (see Fig.3.17), the Gly-Lys, Gly-Asp and Asp-Gly currents are less strongly reduced, and the Lys-Gly current increases similarly to the wild-type.

106

Furthermore, Lys-Gly can produce large outward currents in R282D, while all substrates produce strongly inward-rectifying currents in D341R.

The results for the wild-type are in line with previous observations (Amasheh *et al.*, 1997) (Kottra *et al.*, 2002), and qualitatively reflect the excess positive or negative charge of the different dipeptides at pH 7.5. The more than doubled slope of the *I/V* curves in the R282D mutant can be best explained with a nearly doubled charge/mole ratio and, in addition, with an increased turnover rate of the transporter.

On the contrary, the lack of effect in the substrate selectivity order suggests that these mutations do not interfere with the binding pocket of the transporter. This prediction has been tested by evaluating the amount of presteady-state charge movement removed by interaction with the various dipeptides. It is known that in many transporters, including PepT1 (Sala-Rabanal *et al.*, 2006;Sangaletti *et al.*, 2009) the presteady-state currents in absence of substrate are mutually exclusive with the transport currents (i.e, they are progressively reduced with corresponding increases in transport current). Fig. 3.27 shows the residual charge movement in presence of 1 mM of different dipeptides (Gly-Gln, Lys-Gly and Gly-Asp) in representative oocytes expressing the wild-type and the mutants R282D and D341R.
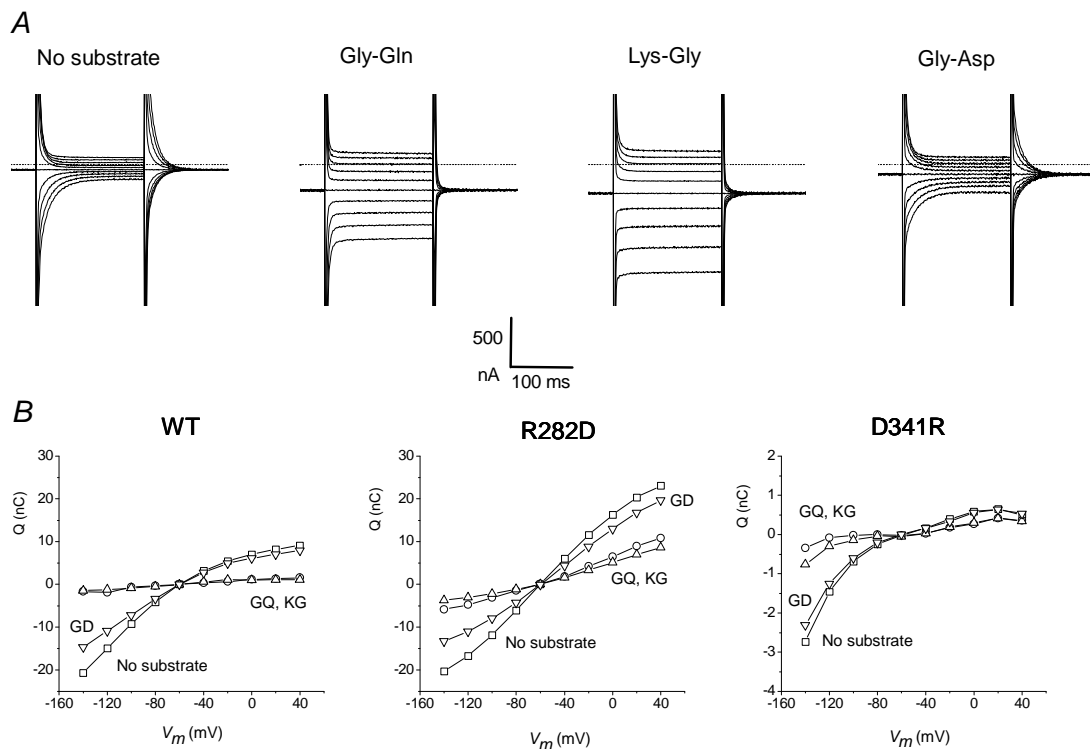
Fig. 3.27 *Residual charge movement for the wild-type and the R282D and D341R mutants in the presence of a neutral, a basic and an acidic dipeptide as indicated (all at concentration 1 mM and pH 7.5).*

As shown in the traces of Fig. 3.27, 1 mM Gly-Gln and Lys-Gly remove almost completely the presteady-state currents in the wild type, while most of this kind of current remains in presence of the same amount of Gly-Asp (the same result was observed with Asp-Gly and Gly-Lys). These observations may be quantified comparing the *Q/V* curves obtained by integrating the presteady-state current isolated using a double exponential fitting of the traces in absence of substrate (considered to represent the total charge), to the integrals of the transient currents obtained by difference of the traces in absence and in presence of substrate (residual charge) (Fesce *et al.*, 2002). These

108

data are shown in the bottom graphs of Fig. 3.27. Clearly the residual charge in the presence of 1 mM Gly-Gln and Lys-Gly is close to zero in the wild type, and for these substrates it remains a small fraction of the total charge in both mutants. In contrast, for Gly-Asp the residual charge is close to the total charge in all isoforms. Analogous results were obtained for the other, poorly functional dipeptides (not shown).

The amount of residual charge can be considered an estimate of the fraction of transporters not involved in the actual transport, i.e. transporters that do not interact with the substrate. In this view, the data of Fig. 3.27 indicate that for all isoforms Gly-Asp interacts poorly, while Gly-Gln and Lys-Gly show a comparable degree of interaction between each other, although in the mutants this level appears lower than in the wild type.

Taking together the results of Figs 3.26 and 3.27, it can be concluded that, since the level of interaction of Gly-Gln and Lys-Gly with the R282D mutant is similar, the more than twofold increase in transport current by Lys-Gly should be ascribed to the increased charge/mole ratio of the transported complex, and possibly to an increased turnover rate.

Chapter 4. Discussion

4.1 Unified modeling of PepT1

Electrophysiological results on the transport activity of PepT1 have shown differences in the various species, ranging from an acidity-induced increase in I_{max} to no change or a decrease in seabass, zebrafish, and rabbit isoforms. More consistent effects are seen in the apparent affinity for substrate, which appears to increase with acidification in all cases. Although an increase in transport-associated current with lower pH is easily understood as a consequence of a stronger protonic electrochemical gradient, an increase in current at higher pH is harder to explain. The presteady-state currents of many ion-coupled transporters in the absence of organic substrate arise from the ion–transporter interaction and are qualitatively and quantitatively related to transport activity (Peres *et al.*, 2004;Cherubino *et al.*, 2010). Therefore, the properties of such currents in three isoforms showing partially different pH dependency have been analyzed in parallel, with the aim of gathering additional information to explain the observed differences.

4.1.1 Comparison of the presteady-state currents in the different species

An analysis of the presteady-state currents with respect to the voltage dependence of the decay time constant and the amount of displaced charge showed that the two types of curves are positioned

differently (at the same external pH) on the voltage axis. The rabbit curves are positively shifted and the zebrafish curves are negatively shifted, with the seabass curves located close to the zebrafish ones. In addition, the decline in the presteady-state current following voltage jumps is faster in the zebrafish and seabass transporters than in the rabbit isoform. These results are in good agreement with the different isoelectric points of the three proteins: 7.47, 6.68, and 6.00 for rabbit, seabass, and zebrafish, respectively ((Daniel *et al.*, 2006) and our calculation). This suggests that rabbit PepT1 may be protonated more easily than the fish isoforms. If this protonation includes the residues involved in establishing states T2 and T7 in our model, it may explain the slower rates of charge movement observed at the same pH in the rabbit protein.

4.1.2 Effect of external pH on unidirectional rates

As previously reported for the rabbit and seabass transporters (Nussberger *et al.*, 1997;Sangaletti *et al.*, 2009), the charge movement characteristics of all three proteins are affected by external pH through shifts along the voltage axis and an acceleration of the decay at alkaline pH. The analysis has been extended to calculate the unidirectional rate constants of charge movement in the membrane electrical field and their dependence on external pH.

The results, shown in Fig.3.2, indicate that an increase in external protons slows down both inward and outward charge movements in all of the examined species. These observations make it unlikely that the presteady-state currents are primarily caused by the movement of external protons in the membrane electrical field, and instead suggest

that the currents are mostly due to the rearrangement of intrinsic transporter charges. These results are in agreement with models proposed for rabbit (Nussberger *et al.*, 1997) and for human PepT1 (Irie *et al.*, 2005), in which the presteady-state currents are generated largely by the movement of intrinsic transporter charges (negative, on the whole). In these models, inward and outward rates are slowed down by the binding of internal and external protons that trap the transporters in "occluded" states.

Because these models do not account for the slowing down of the inward charge movement by external protons, a modification has been introduced by adding a new state (T7 of Fig.3.3) in which the "inward facing" transporter can bind external protons. Trapping of the transporter in state T7 by external protonation may then explain the decrease in inward rate of (positive) charge movement (transition T6 → T1) caused by acidic pH. The voltage- and pH-dependence of the unidirectional rates of charge movement was best fitted with a single conformational change of the intrinsically charged transporter over 71% (rabbit) or 87% (fish) of the membrane electrical field. For this reason, a partial voltage dependence encompassing the residual fraction of the field was introduced in the transition between the outward- and inward-facing conformations of the fully loaded transporter (T3 ↔ T4).

The ability of the model to reproduce the voltage dependence of the displaced charge and the decay time constant, as well as the effects of changing external pH, was verified by simulating the presteady-state currents in the rabbit and a generalized fish PepT1 using kinetic parameters derived from experimental observations. The results in

Fig.3.4 show that the kinetic scheme of Fig.3.3 is capable of reproducing the properties of both the rabbit and fish PepT1 with only a minor adjustment of the parameters (Tab.3.2).

4.1.3 Transport currents

The model of Fig.3.3 was further tested to verify its ability to simulate the transport-associated currents. The comparison was limited to the currents generated by the neutral dipeptide Gly-Gln at pH 6.5 and 7.5, which should represent the physiological conditions of the unstirred microenvironment in which PepT1 operates, at least in mammals (Thwaites and Anderson, 2007). Because the model was constructed from observations of the presteady-state currents and the parameters were optimized to simulate the characteristics of these currents, the behavior of the transport currents cannot be completely reproduced for two main reasons. First, different substrates may present specific interactions with the transporter that are difficult to incorporate in the model. Secondly, the model does not include the effects of the variable percentage of charged vs. uncharged species of substrate at different pH. In spite of these drawbacks, Fig.3.7 shows that simulations of mammalian and fish PepT1s using the additional parameters of Tab.3.3 can reproduce the basic experimental observations. There is less agreement than that obtained for the presteady-state currents, and it is mostly limited to qualitative aspects such as changes in the relative amplitudes of I_{max} at different pH values and the common higher affinity at the more acidic pH. The general trend of the voltage dependence of affinity is mimicked, although there are significant quantitative discrepancies.

As already mentioned, the pH dependence of the maximal transport current of human PepT1 is the opposite of that of rabbit and fish (Amasheh *et al.*, 1997;Steel *et al.*, 1997;Kottra and Daniel, 2001;Verri *et al.*, 2003;Sangaletti *et al.*, 2009). In an analysis by Fujisawa and coworkers, the pH dependency of human PepT1 was bell-shaped, with maximal transport rate at pH 5.5. Although the decreasing transport at high pH values is caused by a reduced transmembrane pH gradient, the decrease at low pH results from a change in the transporter protein itself caused by protonation of a histidine residue near the substrate binding domain (Fujisawa *et al.*, 2006). The model presented here similarly predicts that I_{max} should decrease at both extreme acidic and alkaline pH. Depending on the pH at which the maximal transport rate occurs and the width of the bell-shaped I_{max} vs. pH curve (possibly related to slight structural differences in the functionally important regions), this feature can account for all observed species-specific differences in the pH dependencies, including the increase in I_{max} with acidity found in the human PepT1(Mackenzie *et al.*, 1996). The observed differences in the pH dependencies may be related to the actual pH values found in the small intestine. Although slightly acidic values are found in mammals because there is no luminal expression of the sodium-proton exchanger (NHE3), the microenvironment of zebrafish enterocytes should be alkaline, thus allowing optimal conditions for peptide transport (Verri *et al.*, 2003). Interestingly, the type-II Na^+-phosphate cotransporter cloned from the zebrafish intestine also exhibits maximal transport activation at alkaline extracellular pH (Nalbant *et al.*, 1999).

4.2   Electrostatic gates in PepT1

Different researchers studied a number of mutants in PepT1 residues R282 and D341, reporting various effects on the transport characteristics (Meredith, 2004;Kulkarni *et al.*, 2007;Pieri *et al.*, 2008;Meredith, 2009). No informations however have been published to date on the properties of the presteady-state currents generated by mutants in these residues. Then these currents have been investigated, trying also to correlate the observations regarding the initial steps of the transport cycle with those on the complete transport cycle.

4.2.1 Effects of mutations on the presteady-state currents

Single-residue mutations of arginine 282 in lysine, alanine, glutamine, glutamate or aspartate produce functional transporters displaying conspicuous presteady-state and transport currents. In contrast, both types of current are strongly reduced in the D341R mutant. Localization experiments show that all these isoforms are present in the oocyte membrane, with the mutants having in many cases significantly larger surface expression than the wild-type. While the correspondence between localization and function is very good for the wild-type, and all the arginine mutants, the lack of correlation for the D341R form suggests that its reduced activity is not due to insufficient targeting but to defects in the molecular mechanism. The other two mutations tested, the double mutant R282D-D341R, aimed to reestablish the charge pair, and H57R, did not generate presteady nor steady transport currents. However, while the latter gave a strong signal in the immunolocalization and SOC experiments, confirming

the functional nature of the defect, the double mutant R282D-D341R was not detectable in the membrane (Fig.3.10), and consequently no transporter-related currents were observed (Fig.3.9).

Changes in external pH affected the characteristics of the presteady-state currents in all functional mutants (Fig.3.11). This observation indicates that mutations deep in the structure of the transporter do not alter the ability to interact with protons even in the absence of organic substrate.

The characteristics of the presteady-state currents are changed in opposite ways by the non-conservative mutations on the two different residues: both Q/V and τ/V curves are shifted to the right along the voltage axis in the R282D, R282E, R282Q and R282A forms, and to the left in the D341R form (Fig.3.12). Boltzmann analysis of the charge vs voltage curves reveals only small changes in the slope of the sigmoidal for the arginine mutants. This observation implies the constancy of the equivalent electrical distance δ, and therefore makes it unlikely that the mutated residues could be directly involved in the charge-moving conformational rearrangement. The decrease in δ resulting from the greater slope factor for D341R (Tab.3.4) may reflect a distortion in the protein structure in this mutant, or it may simply represent an overestimate due to the lack of saturation of the Q/V curve in this mutant. However, forcing the slope parameter for D341R to the wild-type value (29.7 mV) in the Boltzmann analysis produced only negligible changes in the unidirectional rate constants.

Derivation of the unidirectional rate constants of the charge movement produces more detailed informations: the inward rate (that

is the inward rate of movement of a positive charge, or the outward rate of movement of a negative charge) is enhanced when the positive arginine 282 is neutralized to alanine or glutamine, or is replaced by a negative aspartate or glutamate; correspondingly the outward rate is diminished in these mutants with respect to the wild-type. The opposite effect occurs when the negative aspartate 341 is replaced by a positive arginine: in this case the outward rate is enhanced, while the inward rate is depressed.

This behaviour appears consistent with the idea that residues R282 and D341 participate in the generation of a local electrical field over which the voltage-dependent charge movement in absence of substrate occurs (Fig.4.1). Although only the knowledge of the atomic structure will allow making accurate calculations, it is reasonable to think that neutralization of positive arginine or reversal of its charge will generate a negative local potential that will distort the intramembrane potential profile. Conversely, the substitution of a negative aspartate with a positive arginine will alter the potential profile in the opposite (positive) way (Fig.4.1 Ba). It may be speculated that in this last case the positive electrical field generated by the arginine residue might be so strong so that very little charge movement can occur in the experimentally useful voltage range, as observed experimentally.

This explanation is analogous to that used to account for the shifting effects of divalent cations or ionic strength on voltage-dependent channels (Hille *et al.*, 1975;Hille, 2001), chapter 20).
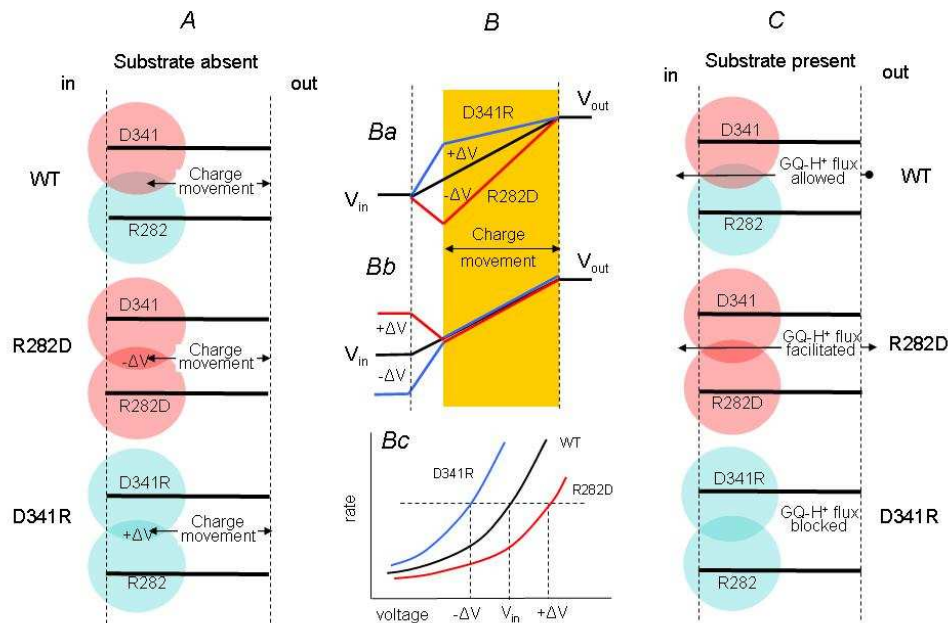
Fig.4.1 *Schematic representation of the electrostatic fields generated by the pair R282-D341 and their mutations.*

Light red and blue areas represent negative and positive electrical fields, respectively. In the absence of substrate reversal of the positive field generated by R282, causes a negative distortion to the membrane potential profile, producing an increase in the field effectively acting on the charge movement (red line in Ba). The opposite mutation D341R adds a positive component to the membrane potential profile causing a decrease in the field effectively acting on the charge movement (blue line in Ba). To reach the same level of electrical field acting on the charge movement (yellow band) the intracellular voltage (V_{in}) must compensate for these alterations and be set to $+\Delta V$ or $-\Delta V$, respectively, for the two mutants (Bb).

Referring to the potential profiles shown in Fig.4.1 Ba, the local potential increase caused by the extra arginine will reduce the electrical field acting on the charge movement by $+\Delta V$ (blue line);

118

therefore to obtain the same rate of charge movement as in the wild-type (black profile line), the intracellular potential will have to be moved more negative by ΔV (Fig.4.1 Bb, blue line). Consequently the voltage dependence of the unidirectional rates will be shifted towards more negative potentials (Fig.4.1 Bc). The same arguments in the opposite direction can be used to explain the positive shift observed in the non-conservative R282 mutants (Fig.4.1 B). Considering the exponential nature of the curves, the voltage shift will appear as a change in amplitude at a fixed potential.

The gradation of effects observed experimentally does not exactly correspond to what may be simplistically expected, i.e. that neutral substitutions (R282Q and R282A) should have less effect than charge reverting mutations (R282D and R282E). Indeed R282A appears to have effects lying midway between those of R282D and R282E, while those of R282Q are located between the wild-type and R282D. These observations suggest that the polar *vs* non-polar nature of the residues and steric factors may also be important in determining the rates of charge movement.

4.2.2 Transport currents

The amplitudes of the transport-associated currents generated by the addition of organic substrate are in good correlation with the amount of intramembrane charge movement in each isoform: while the non-conservative R282 mutants are able to generate transport currents comparable or even larger than the wild-type, D341R shows much reduced currents.

As shown in Figs 3.13, 3.14 and 3.15, in all isoforms the

transport-related currents are affected by changes in external pH and in the concentration of organic substrate. An increase in either one of these two factors cause larger currents and also shifts the curves toward more positive potentials. This effect is particularly evident in the R282 mutants that exhibit a clear reversal of the current direction. In these mutants E_{rev} shifts with the concentration of external protons with a slope between -38 and -49 mV/pH decade (depending on the isoform) that, although less than the value predicted by the Nernst equation, indicates anyway an important role of protons as charge carriers. The change in E_{rev} induced by different Gly-Gln concentration at constant pH, also observed in these mutants, can only be explained if the translocation of this neutral dipeptide occurs as a complex with an electrical charge, supporting the idea that protons bind to the carboxylic group of the substrate in the translocation process (Kulkarni *et al.*, 2007;Pieri *et al.*, 2008).

The experiments on the transport currents confirm therefore that the mutants maintain the essential characteristics of a pH-dependent cotransport system, coupling the translocation of protons and organic substrate, as in the wild-type.

The change in direction of the transport current and shift in E_{rev} with substrate concentration observed in the non-conservative arginine mutants make it difficult to estimate the apparent substrate affinity in the usual way, i.e. by fitting Michaelis –Menten equations to current *vs* concentration plots. To obtain an estimate of possible alterations in the substrate affinity in these mutants, the chord conductance of the *I/V* plots has been used (Fig.3.15) (Aidley, 1989). According to eq.3.8, this quantity is proportional to the current amplitude and it is always

positive, being divided by the electrochemical gradient ($V - E_{rev}$). As shown in Fig.3.15, the estimate of the substrate concentration producing half the maximal conductance is, in the wild-type, similar to that calculated with the usual methods (our unpublished observations, and (Mackenzie *et al.*, 1996;Kottra and Daniel, 2001)). The values of K_{05}^{G} for the R282D mutants, calculated in the same way, show a reduction of about 50% of the apparent affinity compared to the wild-type.

All functional mutants are able to transport charged dipeptides as well. The results shown in Fig.3.16 confirm previous observations (Amasheh *et al.*, 1997;Kottra *et al.*, 2002) concerning the wild-type that showed variable charge/molar ratios depending on the charge of the dipeptide and on the external pH. Therefore the small currents elicited by Asp-Gly (in contrast to the larger ones produced by Lys-Gly) can be attributed to the high percentage of the side chains bearing a negative charge at this pH (7.5). The different shape of the *I/V* curves (rectifying *vs* linear) appears to be isoform-dependent (and substrate-independent), suggesting that the translocation mechanism is determined by the structure of the transporter, and not by the nature of the substrate. The relatively stronger increase (compared to the wild-type) observed in the current generated by Lys-Gly in the non-conservative arginine mutants, indicates that in addition to the greater charge/mole ratio an increase in turnover rate may have occurred, possibly due to a faster release rate of a more strongly charged substrate complex towards the cytoplasm.

4.2.3 R282 and D341 represent the gates of the transport cycle

The idea that the transport cycle of PepT1 could be gated by these two residues was put forward by Kulkarni et al. (Kulkarni *et al.*, 2007) who proposed a cyclic breaking and reconstitution of the ionic interaction. The electrophysiological characterization of the six functional mutants, described above, gives support to this hypothesis. The shifts along the voltage axis of the charge movement parameters shown in Fig.3.12 may be explained as due to alterations in the intramembrane electrical field caused by the differently charged mutants with a likely contributions of steric effects, as mentioned above (see for example the difference between the R282A and R282Q mutants).

The different amplitude and voltage dependence of the transport current in the mutants are also relevant in this respect. With the exception of the conservative R282K mutation, all other functional mutations disrupt the charge pair, however they do so in different ways. In the non-conservative arginine mutations an excess negative charge is produced: although the details of the local conformational rearrangement of the mutated protein are unknown, it is conceivable that the passage of positively charged substrates, such as the Gly-Gln-H^+ complex might be favoured in these cases (see Fig.4.1).

As shown in the Results section, the symmetrical mutation on the other residue of the pair, that is D341R, showed much reduced presteady-state and transport currents. In contrast its expression on the plasma membrane of the oocytes was comparable with the other fully functional isoforms (Fig.3.10). The schematic representation of

Fig.4.1 suggests that in this case the presence of the positive charge of the arginine may produce an additional positive electrical field preventing protons to reach the appropriate site to form a complex with the substrate.

The experiments using charged dipeptides confirmed the efficiency order observed for the wild-type transporter at pH 7.5 (Asp-Gly < Gly-Gln < Lys-Gly) with only small relative variations in all tested mutants. This observation suggests that the mutations in the charge-pair residues affect mainly the proton interaction rather than substrate binding and translocation.

4.3   Reverse operation in PepT1

The PepT1 mutants investigated in the present work are correctly expressed in the oocyte membrane (Fig.3.17), and maintain the characteristic of true cotransporters, as it is shown by the fact that both protons and substrate concentrations affect the reversal potential of the transport current (Fig.3.18), and that the substrate selectivity is unaltered. Although qualitatively in the correct direction, the shifts in E_{rev} significantly deviate from the predictions of the Nernst equation. Further difficulties arise when examining the slope conductance of the transport current at the reversal potential: according to the theory of electrodiffusion (Hille, 2001) this parameter should increase when the concentration of the diffusing species is increased. As shown in Fig.3.18 this is verified for the dipeptide substrate Gly-Gln, but not for protons, for which no significant dependency of g_{slope} is found.

Having established that R282D and R282A can be considered as true cotransporters with some interestingly altered properties

(conspicuous outward currents), the functional and structural determinants of reverse operation in these proteins have been investigated.

4.3.1 Determinants of reverse operation in PepT1

The experiments illustrated in Fig.3.19 show that the outward currents visible in Figs 3.17 and 3.18 are only temporary and may be consequent to the active state of the transporters at negative holding potentials. These declining outward currents might be considered similar to the "tail" currents observed in voltage-activated ionic channels when stepping the voltage from a condition in which the channel is open, to other voltages where it will close (Hodgkin and Huxley, 1952;Hille, 2001). If this is the case, the *I/V* curves obtained from relatively short (<1 s) pulses may actually represent "instantaneous" *I/V* relationships of the current generated by the transporter at the level of activation of the holding potential.

The observation (Figs 3.17 and 3.20) that the transport current declines during strong voltage pulses in either depolarizing or hyperpolarizing directions suggests that this effect may arise from changes in the driving force, rather than from an intrinsic deactivation process of the transporter, because this last kind of process usually depends monotonically on voltage. The hypothesis of a reduction in driving force is demonstrated by the results of the experiments of Figs 3.20, 3.21 and 3.22, as well as from the long-lasting recordings of Fig.3.19. In fact, during a prolonged flux of the proton-substrate complex a local accumulation and/or depletion of the complex may occur in the vicinity of the transporter, and this will decrease the

concentration-dependent component of the electrochemical gradient causing a current decline.

The experiment of Fig.3.20 clearly demonstrates the occurrence of this phenomenon in both directions: in fact, during a long lasting hyperpolarization the reversal potential becomes progressively more negative in agreement with a decrease in the *out/in* ratio of the concentrations of the transported species [eq.3.9]. Vice versa, during a long lasting depolarization, the E_{rev} shift is toward more positive potentials, consistent with an increase in the *out/in* concentration ratio. However the *I/V* relationships measured at different times during the long pulses in either direction remain parallel to each other, excluding changes in the intrinsic rate of transport. Although this effect is most evident in the two arginine 282 mutants, it was shown that the hypothesis of a transport-dependent local concentration change can also explain the findings regarding the wild-type transporter (Kottra and Daniel, 2001). The experiments of Figs 3.21 and 3.22 show that using an appropriate protocol the accumulation/depletion effect can be reduced, and this leads to more accurate determinations of the kinetic properties of transport (I_{max} and K_{05}), whose values can be obtained over an extended range of membrane potentials. The ability to conduct current in the outward direction was already demonstrated in the wild-type PepT1 (Kottra *et al.*, 2009). It was shown here that not only mutants in arginine 282 but also D341R exhibit the same capacity in presence of high intracellular concentrations of a non-hydrolizable substrate. This finding indicates that the different shape of the *I/V* curves exhibited by the different isoforms (i.e. inward rectifying *vs* linear, see Figs 3.17 and 3.26),

125

obtained using a classical pulse protocol from V_h = - 60 mV is not related to an intrinsic incapacity of the wild-type and D341R forms to transport in reverse mode, but depends on the different transport rates, producing different degrees of accumulation/depletion effects. Indeed the transformation from linear to inward rectifying can be obtained using appropriate protocols (see Fig.3.21).

4.3.2 Other substrates

Of the two residues forming a putative charge-pair in the PepT1 structure, R282 and D341 (Kulkarni *et al.*, 2007;Pieri *et al.*, 2008), only mutants in arginine 282 present the outward current phenotype (Fig.3.17). Our initial results using the neutral dipeptide Gly-Gln showed that the arginine mutants facilitate the substrate flow both in terms of amplitude and direction, since the *I/V* relationships are approximately linear; while the symmetric mutation D341R has an opposite action, rendering more difficult the transport of substrates, and enhancing the inward rectification property already present in the wild-type.

The subsequent experiments in presence of different cations (Li^+, K^+ and TMA^+), and using various organic substrates, showed that the mutations do not introduce qualitative alteration in ionic selectivity, nor in substrate specificity. Protons appear to remain the charge carriers, and the potency order of substrates of different size or bearing different charge is not changed compared to the wild-type. Furthermore, the reversal of the transport current can be also observed with tripeptides, suggesting that this property is not substrate-dependent, but is intrinsic in the mutated transporter.

The selectivity order of the charged dipeptides remains substantially unaltered in the mutants compared to the wild-type at pH 7.5. The two negatively charged dipeptide produce only small currents, reflecting the high percentage of the side chains bearing a negative charge at this pH. The two positive dipeptides highlight the relevance of the position of the charge: when the lysine is at the amino terminus the transporter is able to generate larger currents, while when it is located at the carboxy terminus the currents are much reduced (Kottra *et al.*, 2002). Quantitatively, the behaviour of the charge-reverting mutants R282D and D341R is opposite in many respect: while R282D shows increased current relative to the wild-type, the current generated by D341R is much reduced (see Fig.3.17). This observation is consistent with the idea of these two residues being part of the gate controlling the flux of inward positive charges: neutralization of the positive arginine 282, or its replacement with a negative amino acid, may facilitate the approach of the positively charged transport complex, while the replacement of the negative aspartate 341 with a positive arginine may have the opposite effect. This notion is also supported by the amplified increase (relative to Gly-Gln) in the current generated by Lys-Gly in the R282D mutant compared to wild-type and D341R. This effect is mirrored by the stronger reduction in the same mutant of the current generated by Asp-Gly, compared to the wild-type. Interestingly, this last substrate produces a higher fraction of the Gly-Gln current in the D341R mutant, compared to the wild-type.

Chapter 5.   Conclusions

In this work new determinants have been identified into function and structure of PepT1 because, in addition to its role in nutrient uptake, this transporter represents a major pathway for the absorption of several therapeutic drugs.

First of all, a unified kinetic scheme has been proposed that explains the main electrophysiological properties of PepT1 in the presence and absence of organic substrate and its pH dependence. The model also can describe the behavior of different isoforms from mammalian and fish species.

Interestingly, these results suggest a dual role for protons in the operation of PepT1. In the proposed model, protons are fundamental to neutralize the transporter during the inward substrate translocation, and their release in the cytosol uncovers the net negative charge of the empty transporter, which then undergoes an energy-dissipating working stroke to return to the outward-facing conformation (transition T6 → T1 in Fig.3.3). However, protonation of the transporter in another site breaks the transport cycle and counteracts the potentiating effects of external acidity on the turnover rate. As demonstrated by the proposed model, a different balance between the two roles played by protons may generate opposite effects on the maximal transport velocity, as has been experimentally observed in human PepT1 vs. rabbit or fish transporters. The existence of two apparently contrasting actions of external protons does not negatively impact the overall efficiency of substrate uptake, because turnover rate

and affinity are generally inversely related in transport processes (Soragna *et al.*, 2005). Indeed, using the ratio of I_{max} to K_{05} as an index of the efficiency of transport, both experimental data and our model showed that PepT1 is well optimized to meet its function across species and expected physiological pH conditions.

Mutagenesis studies have shown that the oppositely charged residues Arg282 and Asp341, in the transmembrane domain 7 and 8 of PepT1, form a barrier in the absorption pathway. Substitution of Arg282 with neutral or negatively charged residues produce a shift towards more positive potentials in the characteristics of charge movement with respect to the wild-type form. Conversely replacement of Asp341 with Arg reduce both presteady-state and transport currents and produce a negative shift of the charge movement properties. In summary, residues R282 and D341 participate in the generation of a local electrical field over which the voltage-dependent charge movement in the absence of substrate occurs. Removal or reversal of the positive field generated by Arg282 cause a negative distortion to the membrane potential profile, producing an increase in the field strength effectively acting on the inward charge movement. To reach the same level of electrical field acting on the charge movement the intracellular voltage must compensate for this alteration and be set to less negative values. In contrast, the mutation Asp341Arg adds a positive component to the membrane potential profile and must be compensate by an increased membrane negativity. Thus, the shown results support the idea that Arg282 and Asp341 play the role of electrostatic gates in the PepT1 transport cycle.

Finally, mutants in the putative charge pair residues Arg282 and Asp341 of rabbit PepT1 have been shown exhibit properties useful to better understand the possibility of reverse transport. In fact, wild-type and Arg282 mutants, while retaining the essential characteristics of proton-coupled cotransporters, exhibit outward currents in the presence of Gly-Gln. Long-lasting voltage- and current-clamp experiments have shown that these currents are only temporary, and reflect accumulation and/or depletion effects near the membrane. The reversal potential of the outward currents is affected by both pH and substrate concentration, confirming coupled transport in the wild-type and in the mutants as well. Removal of arginine 282 appears to facilitate the flow of the transported complex in both directions, while replacement of aspartate 341 with a positive residue limits the transport rate and strengthens the inwardly-rectifying characteristics of the wild-type transporter. This observation is consistent with the idea of these two residues being part of the gate controlling the flux of inward positive charges.

This work has contributed to better understand the mode of transport by which PepT1 binds and transports its substrates that it's of great interest to researchers; moreover these detailed functional information can be also used to make PepT1 a good drug delivery system.

Bibliography

Abramson,J., Smirnova,I., Kasho,V., Verner,G., Kaback,H.R., Iwata,S. (2003). Structure and mechanism of the lactose permease of Escherichia coli. Science *301*, 610-615.

Abramson,J., Wright,E.M. (2009). Structure and function of Na+-symporters with inverted repeats. Curr.Opin.Struct.Biol. *19*, 425-432.

Aidley,D.J. (1989). The Physiology of Excitable Cells. Cambridge: Cambridge University Press.

Amasheh,S., Wenzel,U., Boll,M., Dorn,D., Weber,W.-M., Clauss,W., Daniel,H. (1997). Transport of Charged Dipeptides by the Intestinal H+/Peptide Symporter PepT1 Expressed in Xenopus laevis Oocytes. J.Membr.Biol. *155*, 247-256.

Anderle,P., Nielsen,C.U., Pinsonneault,J., Krog,P.L., Brodin,B., Sadee,W. (2006). Genetic variants of the human dipeptide transporter PEPT1. J.Pharmacol.Exp.Ther. *316*, 636-646.

Armstrong,C.M., Bezanilla,F. (1974). Charge movement associated with the opening and closing of the activation gates of the Na channels. J.Gen.Physiol *63*, 533-552.

Ashida,K., Katsura,T., Motohashi,H., Saito,H., Inui,K. (2002). Thyroid hormone regulates the activity and expression of the peptide transporter PEPT1 in Caco-2 cells. Am.J.Physiol Gastrointest.Liver Physiol *282*, G617-G623.

Avissar,N.E., Ziegler,T.R., Wang,H.T., Gu,L.H., Miller,J.H., Iannoli,P., Leibach,F.H., Ganapathy,V., Sax,H.C. (2001). Growth factors regulation of rabbit sodium-dependent neutral amino acid transporter ATB0 and oligopeptide transporter 1 mRNAs expression after enteretomy. JPEN J.Parenter.Enteral Nutr. *25*, 65-72.

Bailey,P.D., Boyd,C.A., Bronk,J.R., Collier,I.D., Meredith,D., Morgan,K.M., Temple,C.S. (2000). How to Make Drugs Orally Active: A Substrate Template for Peptide Transporter PepT1. Angew.Chem.Int.Ed Engl. *39*, 505-508.

Barbot,L., Windsor,E., Rome,S., Tricottet,V., Reynes,M., Topouchian,A., Huneau,J.F., Gobert,J.G., Tome,D., Kapel,N. (2003). Intestinal peptide transporter PepT1 is over-expressed during acute cryptosporidiosis in suckling rats as a result of both malnutrition and experimental parasite infection. Parasitol.Res. *89*, 364-370.

Berlioz,F., Julien,S., Tsocas,A., Chariot,J., Carbon,C., Farinotti,R., Roze,C. (1999). Neural modulation of cephalexin intestinal absorption through the di- and tripeptide brush border transporter of rat jejunum in vivo. J.Pharmacol.Exp.Ther. *288*, 1037-1044.

Berlioz,F., Maoret,J.J., Paris,H., Laburthe,M., Farinotti,R., Roze,C. (2000). alpha(2)-adrenergic receptors stimulate oligopeptide transport in a human intestinal cell line. J.Pharmacol.Exp.Ther. *294*, 466-472.

Bolger,M.B., Haworth,I.S., Yeung,A.K., Ann,D., von Grafenstein,H., Hamm-Alvarez,S., Okamoto,C.T., Kim,K.J., Basu,S.K., Wu,S., Lee,V.H. (1998). Structure, function, and molecular modeling approaches to the study of the intestinal dipeptide transporter PepT1. J.Pharm.Sci. *87*, 1286-1291.

Bossi,E., Centinaio,E., Castagna,M., Giovannardi,S., Vincenti,S., Sacchi,V.F., Peres,A. (1999). Ion binding and permeation through the lepidopteran amino acid transporter KAAT1 expressed in Xenopus oocytes. J.Physiol *515 (Pt 3)*, 729-742.

Bossi,E., Fabbrini,M.S., Ceriotti,A. (2007). Exogenous Protein Expression in Xenopus Laevis Oocyte, Basic Procedure. In: *In Vitro Transcription and Translation Protocols*, ed. G.GrandiTotowa NJ: Humana Press, 107-131.

Brandsch,M., Thunecke,F., Kullertz,G., Schutkowski,M., Fischer,G., Neubert,K. (1998). Evidence for the absolute conformational specificity of the intestinal H+/peptide symporter, PEPT1. J.Biol.Chem. *273*, 3861-3864.

Buyse,M., Berlioz,F., Guilmeau,S., Tsocas,A., Voisin,T., Peranzi,G., Merlin,D., Laburthe,M., Lewin,M.J., Roze,C., Bado,A. (2001). PepT1-mediated epithelial transport of dipeptides and cephalexin is enhanced by luminal leptin in the small intestine. J.Clin.Invest *108*, 1483-1494.

Catterall,W.A. (1993). Structure and function of voltage-gated ion channels. Trends Neurosci. *16*, 500-506.

Chen,X.-Z., Coady,M.J., Lapointe,J.-Y. (1996). Fast voltage clamp discloses a new component of presteady-state currents from the Na^+-glucose cotransporter. Biophys.J. *71*, 2544-2552.

Chen,H., Pan,Y., Wong,E.A., Bloomquist,J.R., Webb,K.E., Jr. (2002). Molecular cloning and functional expression of a chicken intestinal peptide transporter (cPepT1) in Xenopus oocytes and Chinese hamster ovary cells. J.Nutr. *132*, 387-393.

Chen,X.Z., Steel,A., Hediger,M.A. (2000). Functional roles of histidine and tyrosine residues in the H(+)-peptide transporter PepT1. Biochem.Biophys.Res.Commun. *272*, 726-730.

Chen,H., Wong,E.A., Webb,K.E., Jr. (1999). Tissue distribution of a peptide transporter mRNA in sheep, dairy cows, pigs, and chickens. J.Anim Sci. *77*, 1277-1283.

Cherubino,F., Bossi,E., Miszner,A., Ghezzi,C., Peres,A. (2010). Transient currents in the glycine neuronal cotransporter GlyT1. J.Mol.Neurosci. *41*, 243-251.

Cole,K.S., Curtis,H.J. (1941). MEMBRANE POTENTIAL OF THE SQUID GIANT AXON DURING CURRENT FLOW. J.Gen.Physiol *24*, 551-563.

Covitz,K.M., Amidon,G.L., Sadee,W. (1998). Membrane topology of the human dipeptide transporter, hPEPT1, determined by epitope insertions. Biochemistry *37*, 15214-15221.

Dalmasso,G., Nguyen,H.T., Charrier-Hisamuddin,L., Yan,Y., Laroui,H., Demoulin,B., Sitaraman,S.V., Merlin,D. (2010). PepT1 mediates transport of the pro-inflammatory bacterial tripeptide L-Ala-{gamma}-D-Glu-meso-DAP in intestinal epithelial cells. Am.J.Physiol Gastrointest.Liver Physiol.

Dalmasso,G., Nguyen,H.T., Yan,Y., Laroui,H., Charania,M.A., Obertone,T.S., Sitaraman,S.V., Merlin,D. (2011). MicroRNA-92b regulates expression of the oligopeptide transporter PepT1 in intestinal epithelial cells. Am.J.Physiol Gastrointest.Liver Physiol *300*, G52-G59.

Daniel,H. (2004). Molecular and integrative physiology of intestinal peptide transport. Annu.Rev.Physiol *66*, 361-384.

Daniel,H., Kottra,G. (2004). The proton oligopeptide cotransporter family SLC15 in physiology and pharmacology. Pflugers Arch. *447*, 610-618.

Daniel,H., Spanier,B., Kottra,G., Weitz,D. (2006). From Bacteria to Man: Archaic Proton-Dependent Peptide Transporters at Work. Physiology *21*, 93-102.

de Sanctis,L., Bonetti,G., Bruno,M., De Luca,F., Bisceglia,L., Palacin,M., Dianzani,I., Ponzone,A. (2001). Cystinuria phenotyping by oral lysine and arginine loading. Clin.Nephrol. *56*, 467-474.

Doring,F., Walter,J., Will,J., Focking,M., Boll,M., Amasheh,S., Clauss,W., Daniel,H. (1998a). Delta-aminolevulinic acid transport by intestinal and renal peptide transporters and its physiological and clinical implications. J.Clin.Invest *101*, 2761-2767.

Doring,F., Will,J., Amasheh,S., Clauss,W., Ahlbrecht,H., Daniel,H. (1998b). Minimal molecular determinants of substrates for recognition by the intestinal peptide transporter. J.Biol.Chem. *273*, 23211-23218.

Erickson,R.H., Kim,Y.S. (1990). Digestion and absorption of dietary protein. Annu.Rev.Med. *41*, 133-139.

Fei,Y.J., Fujita,T., Lapp,D.F., Ganapathy,V., Leibach,F.H. (1998). Two oligopeptide transporters from Caenorhabditis elegans: molecular cloning and functional expression. Biochem.J. *332 (Pt 2)*, 565-572.

Fei,Y.J., Kanai,Y., Nussberger,S., Ganapathy,V., Leibach,F.H., Romero,M.F., Singh,S.K., Boron,W.F., Hediger,M.A. (1994).

Expression cloning of a mammalian proton-coupled oligopeptide transporter. Nature *368*, 563-566.

Fei,Y.J., Liu,W., Prasad,P.D., Kekuda,R., Oblak,T.G., Ganapathy,V., Leibach,F.H. (1997). Identification of the histidyl residue obligatory for the catalytic activity of the human H+/peptide cotransporters PEPT1 and PEPT2. Biochemistry *36*, 452-460.

Fei,Y.J., Sugawara,M., Liu,J.C., Li,H.W., Ganapathy,V., Ganapathy,M.E., Leibach,F.H. (2000). cDNA structure, genomic organization, and promoter analysis of the mouse intestinal peptide transporter PEPT1. Biochim.Biophys.Acta *1492*, 145-154.

Fesce,R., Giovannardi,S., Binda,F., Bossi,E., Peres,A. (2002). The relation between charge movement and transport-associated currents in the GABA cotransporter rGAT1. Journal of Physiology *545*, 739-750.

Forlani,G., Bossi,E., Perego,C., Giovannardi,S., Peres,A. (2001). Three kinds of currents in the canine betaine-GABA transporter BGT-1 expressed in Xenopus laevis oocytes. Biochim.Biophys.Acta *1538*, 172-180.

Fujisawa,Y., Tateoka,R., Nara,T., Kamo,N., Taira,T., Miyauchi,S. (2006). The Extracellular pH Dependency of Transport Activity by Human Oligopeptide Transporter 1 (hPEPT1) Expressed Stably in Chinese Hamster Ovary (CHO) Cells: A Reason for the Bell-Shaped Activity *versus* pH. Biol.Pharm.Bull. *29*, 997-1005.

Ganapathy,M.E., Brandsch,M., Prasad,P.D., Ganapathy,V., Leibach,F.H. (1995). Differential recognition of beta -lactam antibiotics by intestinal and renal peptide transporters, PEPT 1 and PEPT 2. J.Biol.Chem. *270*, 25672-25677.

Ganapathy,V., Burckhardt,G., Leibach,F.H. (1984). Characteristics of glycylsarcosine transport in rabbit intestinal brush-border membrane vesicles. J.Biol.Chem. *259*, 8954-8959.

Ganapathy,V., Burckhardt,G., Leibach,F.H. (1985). Peptide transport in rabbit intestinal brush-border membrane vesicles studied with a potential-sensitive dye. Biochim.Biophys.Acta *816*, 234-240.

Ganapathy, Leibach,F.H. (1985). Is intestinal peptide transport energized by a proton gradient? Am.J.Physiol *249*, G153-G160.

Gangopadhyay,A., Thamotharan,M., Adibi,S.A. (2002). Regulation of oligopeptide transporter (Pept-1) in experimental diabetes. Am.J.Physiol Gastrointest.Liver Physiol *283*, G133-G138.

Guerrini,L., Gong,S.S., Mangasarian,K., Basilico,C. (1993). Cis- and trans-acting elements involved in amino acid regulation of asparagine synthetase gene expression. Mol.Cell Biol. *13*, 3202-3212.

Hauser,M., Kauffman,S., Naider,F., Becker,J.M. (2005). Substrate preference is altered by mutations in the fifth transmembrane domain of Ptr2p, the di/tri-peptide transporter of Saccharomyces cerevisiae. Mol.Membr.Biol. *22*, 215-227.

Hediger,M.A., Coady,M.J., Ikeda,T.S., Wright,E.M. (1987). Expression cloning and cDNA sequencing of the Na+/glucose co-transporter. Nature *330*, 379-381.

Hediger,M.A., Romero,M.F., Peng,J.B., Rolfs,A., Takanaga,H., Bruford,E.A. (2004). The ABCs of solute carriers: physiological, pathological and therapeutic implications of human membrane transport proteinsIntroduction. Pflugers Arch. *447*, 465-468.

Hellier,M.D., Perrett,D., Holdsworth,C.D., Thirumalai,C. (1971). Absorption of dipeptides in normal and cystinuric subjects. Gut *12*, 496-497.

Herrera-Ruiz,D., Knipp,G.T. (2003). Current Perspectives on Established and Putative Mammalian Oligopeptide Transporters. J.Pharmacol.Sci. *92*, 691-714.

Hille, B. Ionic channels of excitable membranes. 3. 2001. Sunderland, MA, USA, Sinauer Ass.
Ref Type: Serial (Book,Monograph)

Hille,B., Woodhull,A.M., Shapiro,B.I. (1975). Negative surface charge near sodium channels of nerve: divalent ions, monovalent ions and pH. Philosophical Transactions of the Royal Society B *270*, 301-318.

Hodgkin,A.L., Huxley,A.F. (1952). The components of membrane conductance in the giant axon of Loligo. J.Physiol. *116*, 473-496.

HODGKIN,A.L., HUXLEY,A.F., KATZ,B. (1952). Measurement of current-voltage relations in the membrane of the giant axon of Loligo. J.Physiol *116*, 424-448.

Huang,Y., Lemieux,M.J., Song,J., Auer,M., Wang,D.N. (2003). Structure and mechanism of the glycerol-3-phosphate transporter from Escherichia coli. Science *301*, 616-620.

Ihara,T., Tsujikawa,T., Fujiyama,Y., Bamba,T. (2000). Regulation of PepT1 peptide transporter expression in the rat small intestine under malnourished conditions. Digestion *61*, 59-67.

Ikeda,T.S., Hwang,E.S., Coady,M.J., Hirayama,B.A., Hediger,M.A., Wright,E.M. (1989). Characterization of a Na+/glucose cotransporter cloned from rabbit small intestine. J.Membr.Biol. *110*, 87-95.

Irie,M., Terada,T., Katsura,T., Matsuoka,S., Inui,K. (2005). Computational modeling of H+-coupled peptide transport via human PEPT1. J.Physiol. *565*, 429-439.

Kelty,C.J., Brown,N.J., Reed,M.W., Ackroyd,R. (2002). The use of 5-aminolaevulinic acid as a photosensitiser in photodynamic therapy and photodiagnosis. Photochem.Photobiol.Sci. *1*, 158-168.

Kennedy,D.J., Leibach,F.H., Ganapathy,V., Thwaites,D.T. (2002). Optimal absorptive transport of the dipeptide glycylsarcosine is dependent on functional Na$^+$/H$^+$ exchange activity. Pflug.Arch. *445*, 139-146.

Khoshbouei,H., Wang,H., Lechleiter,J.D., Javitch,J.A., Galli,A. (2003). Amphetamine-induced Dopamine efflux. A voltage-sensitive and intracellular Na-dependent mechanism. J.Biol.Chem. *278*, 12070-12077.

Knutter,I., Theis,S., Hartrodt,B., Born,I., Brandsch,M., Daniel,H., Neubert,K. (2001). A novel inhibitor of the mammalian peptide transporter PEPT1. Biochemistry *40*, 4454-4458.

Kottra,G., Daniel,H. (2001). Bidirectional electrogenic transport of peptides by the proton-coupled carrier PEPT1 in *Xenopus laevis* oocytes: its asymmetry and symmetry. J.Physiol. *536*, 495-503.

Kottra,G., Frey,I., Daniel,H. (2009). Inhibition of intracellular dipeptide hydrolysis uncovers large outward transport currents of the peptide transporter PEPT1 in Xenopus oocytes. Pflug.Arch. *457*, 809-820.

Kottra,G., Stamfort,A., Daniel,H. (2002). PEPT1 as a Paradigm for Membrane Carriers That Mediate Electrogenic Bidirectional Transport of Anionic, Cationic, and Neutral Substrates. J.Biol.Chem. *277*, 32683-32691.

Krishnamurthy,H., Piscitelli,C.L., Gouaux,E. (2009). Unlocking the molecular secrets of sodium-coupled transporters. Nature *459*, 347-355.

Kulkarni,A.A., Davies,D.L., Links,J.S., Patel,L.N., Lee,V.H., Haworth,I.S. (2007). A charge pair interaction between Arg282 in transmembrane segment 7 and Asp341 in transmembrane segment 8 of hPepT1. Pharm.Res. *24*, 66-72.

Kulkarni,A.A., Haworth,I.S., Lee,V.H. (2003a). Transmembrane segment 5 of the dipeptide transporter hPepT1 forms a part of the substrate translocation pathway. Biochem.Biophys.Res.Commun. *306*, 177-185.

Kulkarni,A.A., Haworth,I.S., Uchiyama,T., Lee,V.H. (2003b). Analysis of transmembrane segment 7 of the dipeptide transporter hPepT1 by cysteine-scanning mutagenesis. J.Biol.Chem. *278*, 51833-51840.

Lee,V.H., Chu,C., Mahlin,E.D., Basu,S.K., Ann,D.K., Bolger,M.B., Haworth,I.S., Yeung,A.K., Wu,S.K., Hamm-Alvarez,S., Okamoto,C.T. (1999). Biopharmaceutics of transmucosal peptide and protein drug administration: role of transport mechanisms with a focus on the involvement of PepT1. J.Control Release *62*, 129-140.

Lester,H.A., Cao,Y., Mager,S. (1996). Listening to neurotransmitter transporters. Neuron *17*, 807-810.

Liang,R., Fei,Y.J., Prasad,P.D., Ramamoorthy,S., Han,H., Yang-Feng,T.L., Hediger,M.A., Ganapathy,V., Leibach,F.H. (1995). Human intestinal H+/peptide cotransporter. Cloning, functional expression, and chromosomal localization. J.Biol.Chem. *270*, 6456-6463.

Loo,D.D., Hirayama,B.A., Gallardo,E.M., Lam,J.T., Turk,E., Wright,E.M. (1998). Conformational changes couple Na+ and glucose transport. Proc.Natl.Acad.Sci.U.S.A *95*, 7789-7794.

Mackenzie,B., Loo,D.D., Fei,Y., Liu,W.J., Ganapathy,V., Leibach,F.H., Wright,E.M. (1996). Mechanisms of the human intestinal H+-coupled oligopeptide transporter hPEPT1. J.Biol.Chem. *271*, 5430-5437.

Mager,S., Kleinberger-Doron,N., Keshet,G.I., Davidson,N., Kanner,B.I., Lester,H.A. (1996). Ion binding and permeation at the GABA transporter GAT1. J.Neurosci. *16*, 5405-5414.

Mager,S., Naeve,J., Quick,M., Labarca,C., Davidson,N., Lester,H.A. (1993). Steady states, charge movements, and rates for a cloned GABA transporter expressed in Xenopus oocytes. Neuron *10*, 177-188.

McAlear,S.D., Liu,X., Williams,J.B., McNicholas-Bevensee,C.M., Bevensee,M.O. (2006). Electrogenic Na/HCO3 cotransporter (NBCe1) variants expressed in Xenopus oocytes: functional comparison and roles of the amino and carboxy termini. J.Gen.Physiol. *127*, 639-658.

McGuffin,L.J., Bryson,K., Jones,D.T. (2000). The PSIPRED protein structure prediction server. Bioinformatics. *16*, 404-405.

Meredith,D. (2004). Site-directed Mutation of Arginine 282 to Glutamate Uncouples the Movement of Peptides and Protons by the Rabbit Proton-peptide Cotransporter PepT1. J.Biol.Chem. *279*, 15795-15798.

Meredith,D. (2009). Review. The mammalian proton-coupled peptide cotransporter PepT1: sitting on the transporter-channel fence? Philos.Trans.R.Soc.Lond B Biol.Sci. *364*, 203-207.

Meredith,D., Price,R.A. (2006). Molecular Modeling of PepT1 — Towards a Structure. J.Membr.Biol. *213*, 79-88.

Merlin,D., Si-Tahar,M., Sitaraman,S.V., Eastburn,K., Williams,I., Liu,X., Hediger,M.A., Madara,J.L. (2001). Colonic epithelial hPepT1 expression occurs in inflammatory bowel disease: transport of bacterial peptides influences expression of MHC class 1 molecules. Gastroenterology *120*, 1666-1679.

Mertl,M., Daniel,H., Kottra,G. (2008). Substrate-induced changes in the density of peptide transporter PEPT1 expressed in Xenopus oocytes. Am.J.Physiol Cell Physiol *295*, C1332-C1343.

Muller,U., Brandsch,M., Prasad,P.D., Fei,Y.J., Ganapathy,V., Leibach,F.H. (1996). Inhibition of the H+/peptide cotransporter in the human intestinal cell line Caco-2 by cyclic AMP. Biochem.Biophys.Res.Commun. *218*, 461-465.

Nalbant,P., Boehmer,C., Dehmelt,L., Wehner,F., Werner,A. (1999). Functional characterization of a Na^+-phosphate cotransporter (NaP_i-II) from zebrafish and identification of related transcripts. J.Physiol. *520*, 79-89.

Neumann,J., Brandsch,M. (2003). Delta-aminolevulinic acid transport in cancer cells of the human extrahepatic biliary duct. J.Pharmacol.Exp.Ther. *305*, 219-224.

NEWEY,H., SMYTH,D.H. (1960). Intracellular hydrolysis of dipeptides during intestinal absorption. J.Physiol *152*, 367-380.

Newstead,S., Drew,D., Cameron,A.D., Postis,V.L., Xia,X., Fowler,P.W., Ingram,J.C., Carpenter,E.P., Sansom,M.S., McPherson,M.J., Baldwin,S.A., Iwata,S. (2011). Crystal structure of a prokaryotic homologue of the mammalian oligopeptide-proton symporters, PepT1 and PepT2. EMBO J. *30*, 417-426.

Nguyen,H.T., Dalmasso,G., Powell,K.R., Yan,Y., Bhatt,S., Kalman,D., Sitaraman,S.V., Merlin,D. (2009). Pathogenic bacteria induce colonic PepT1 expression: an implication in host defense response. Gastroenterology *137*, 1435-1447.

Nguyen,H.T., Dalmasso,G., Yan,Y., Laroui,H., Dahan,S., Mayer,L., Sitaraman,S.V., Merlin,D. (2010). MicroRNA-7

modulates CD98 expression during intestinal epithelial cell differentiation. J.Biol.Chem. *285*, 1479-1489.

Nussberger,S., Steel,A., Trotti,D., Romero,M.F., Boron,W.F., Hediger,M.A. (1997). Symmetry of H+ binding to the intra- and extracellular side of the H+-coupled oligopeptide cotransporter PepT1. J.Biol.Chem. *272*, 7777-7785.

Pan,X., Terada,T., Irie,M., Saito,H., Inui,K. (2002). Diurnal rhythm of H+-peptide cotransporter in rat small intestine. Am.J.Physiol Gastrointest.Liver Physiol *283*, G57-G64.

Panitsas,K.E., Boyd,C.A., Meredith,D. (2006). Evidence that the rabbit proton-peptide co-transporter PepT1 is a multimer when expressed in Xenopus laevis oocytes. Pflugers Arch. *452*, 53-63.

Parent,L., Supplisson,S., Loo,D.D., Wright,E.M. (1992). Electrogenic properties of the cloned Na+/glucose cotransporter: I. Voltage-clamp studies. J.Membr.Biol. *125*, 49-62.

Peres,A., Giovannardi,S., Bossi,E., Fesce,R. (2004). Electrophysiological insights into the mechanism of ion-coupled cotransporters. News Physiol Sci. *19*, 80-84.

Pieri,M., Gan,C., Bailey,P., Meredith,D. (2009). The transmembrane tyrosines Y56, Y91 and Y167 play important roles in determining the affinity and transport rate of the rabbit proton-coupled peptide transporter PepT1. Int.J.Biochem.Cell Biol. *41*, 2204-2213.

Pieri,M., Hall,D., Price,R., Bailey,P., Meredith,D. (2008). Site-directed mutagenesis of Arginine282 suggests how protons and peptides are co-transported by rabbit PepT1. Int.J.Biochem.Cell Biol. *40*, 721-730.

Pohjanpelto,P., Holtta,E. (1990). Deprivation of a single amino acid induces protein synthesis-dependent increases in c-jun, c-myc, and ornithine decarboxylase mRNAs in Chinese hamster ovary cells. Mol.Cell Biol. *10*, 5814-5821.

Rauh,R., Diakov,A., Tzschoppe,A., Korbmacher,J., Azad,A.K., Cuppens,H., Cassiman,J.-J., Dötsch,J., Sticht,H., Korbmacher,C. (2010). A mutation of the epithelial sodium channel associated

with atypical cystic fibrosis increases channel open probability and reduces Na+ self inhibition. J.Physiol. *588*, 1211-1225.

Richerson,G.B., Wu,Y. (2003). Dynamic equilibrium of neurotransmitter transporters: not just for reuptake anymore. J.Neurophys. *90*, 1363-1374.

Richerson,G.B., Wu,Y. (2004). Role of the GABA Transporter in Epilepsy. In: Recent Advances in Epilepsy Research, ed. D.K.Binder, H.E.Scharfman Kluwer Academic/Plenum, 76-91.

Rossi,D.J., Oshima,T., Attwell,D. (2000). Glutamate release in severe brain ischaemia is mainly by reversed uptake. Nature *403*, 316-321.

Rühl,A., Hoppel,S., Frey,I., Daniel,H., Schemann,M. (2005). Functional expression of the peptide transporter PEPT2 in the mammalian enteric nervous system. J.Comp.Neurol. *490*, 1-11.

Saito,H., Motohashi,H., Mukai,M., Inui,K. (1997). Cloning and characterization of a pH-sensing regulatory factor that modulates transport activity of the human H+/peptide cotransporter, PEPT1. Biochem.Biophys.Res.Commun. *237*, 577-582.

Saito,H., Okuda,M., Terada,T., Sasaki,S., Inui,K. (1995). Cloning and characterization of a rat H+/peptide cotransporter mediating absorption of beta-lactam antibiotics in the intestine and kidney. J.Pharmacol.Exp.Ther. *275*, 1631-1637.

Sala-Rabanal,M., Loo,D.D.F., Hirayama,B.A., Turk,E., Wright,E.M. (2006). Molecular interactions between dipeptides, drugs and the human intestinal H+/oligopeptide cotransporter, hPEPT1. J.Physiol. *574*, 149-166.

Sangaletti,R., Terova,G., Peres,A., Bossi,E., Corà,S., Saroglia,M. (2009). Functional expression of the oligopeptide transporter PepT1 from the sea bass *Dicentrachus labrax*. Pflugers Archiv European Journal of Physiology *459*, 47-54.

Sawada,K., Terada,T., Saito,H., Hashimoto,Y., Inui,K. (1999). Effects of glibenclamide on glycylsarcosine transport by the rat peptide transporters PEPT1 and PEPT2. Br.J.Pharmacol. *128*, 1159-1164.

Seidel,S., Singer,E.A., Just,H., Farhan,H., Scholze,P., Kudlacek,O., Holy,M., Koppatz,K., Krivanek,P., Freissmuth,M., Sitte,H.H. (2005). Amphetamines take two to tango: an oligomer-based counter-transport model of neurotransmitter transport explores the amphetamine action. Mol.Pharmacol. *67*, 140-151.

Shu,C., Shen,H., Hopfer,U., Smith,D.E. (2001). Mechanism of intestinal absorption and renal reabsorption of an orally active ace inhibitor: uptake and transport of fosinopril in cell cultures. Drug Metab Dispos. *29*, 1307-1315.

Soragna,A., Bossi,E., Giovannardi,S., Pisani,R., Peres,A. (2005). Relations between substrate affinities and charge equilibration rates in the GABA cotransporter rGAT1. J.Physiol. *562*, 333-345.

Steel,A., Nussberger,S., Romero,M.F., Boron,W.F., Boyd,C.A., Hediger,M.A. (1997). Stoichiometry and pH dependence of the rabbit proton-dependent oligopeptide transporter PepT1. J.Physiol. *498*, 563-569.

Steiner,H.Y., Naider,F., Becker,J.M. (1995). The PTR family: a new group of peptide transporters. Mol.Microbiol. *16*, 825-834.

Sterchi,E.E., Woodley,J.F. (1980). Peptide hydrolases of the human small intestinal mucosa: distribution of activities between brush border membranes and cytosol. Clin.Chim.Acta *102*, 49-56.

Stevens,B.R., Kaunitz,J.D., Wright,E.M. (1984). Intestinal transport of amino acids and sugars: advances using membrane vesicles. Annu.Rev.Physiol *46*, 417-433.

Sun,B.W., Zhao,X.C., Wang,G.J., Li,N., Li,J.S. (2003). Hormonal regulation of dipeptide transporter (PepT1) in Caco-2 cells with normal and anoxia/reoxygenation management. World J.Gastroenterol. *9*, 808-812.

Tame,J.R., Sleigh,S.H., Wilkinson,A.J., Ladbury,J.E. (1996). The role of water in sequence-independent ligand binding by an oligopeptide transporter protein. Nat.Struct.Biol. *3*, 998-1001.

Tanaka,H., Miyamoto,K.I., Morita,K., Haga,H., Segawa,H., Shiraga,T., Fujioka,A., Kouda,T., Taketani,Y., Hisano,S., Fukui,Y., Kitagawa,K., Takeda,E. (1998). Regulation of the PepT1

peptide transporter in the rat small intestine in response to 5-fluorouracil-induced injury. Gastroenterology *114*, 714-723.

Terada,T., Saito,H., Mukai,M., Inui,K. (1996). Identification of the histidine residues involved in substrate recognition by a rat H$^+$/peptide cotransporter, PEPT1. FEBS Lett. *394*, 196-200.

Terada,T., Saito,H., Mukai,M., Inui,K. (1997). Characterization of stably transfected kidney epithelial cell line expressing rat H+/peptide cotransporter PEPT1: localization of PEPT1 and transport of beta-lactam antibiotics. J.Pharmacol.Exp.Ther. *281*, 1415-1421.

Terada,T., Sawada,K., Saito,H., Hashimoto,Y., Inui,K. (2000). Inhibitory effect of novel oral hypoglycemic agent nateglinide (AY4166) on peptide transporters PEPT1 and PEPT2. Eur.J.Pharmacol. *392*, 11-17.

Thamotharan,M., Bawani,S.Z., Zhou,X., Adibi,S.A. (1998). Mechanism of dipeptide stimulation of its own transport in a human intestinal cell line. Proc.Assoc.Am.Physicians *110*, 361-368.

Thamotharan,M., Bawani,S.Z., Zhou,X., Adibi,S.A. (1999a). Functional and molecular expression of intestinal oligopeptide transporter (Pept-1) after a brief fast. Metabolism *48*, 681-684.

Thamotharan,M., Bawani,S.Z., Zhou,X., Adibi,S.A. (1999b). Hormonal regulation of oligopeptide transporter pept-1 in a human intestinal cell line. Am.J.Physiol *276*, C821-C826.

Theis,S., Knutter,I., Hartrodt,B., Brandsch,M., Kottra,G., Neubert,K., Daniel,H. (2002). Synthesis and characterization of high affinity inhibitors of the H+/peptide transporter PEPT2. J.Biol.Chem. *277*, 7287-7292.

Thwaites,D.T., Anderson,C.M.H. (2007). H+-coupled nutrient, micronutrient and drug transporters in the mammalian small intestine. Exp.Physiol. *92*, 603-619.

Thwaites,D.T., Kennedy,D.J., Raldua,D., Anderson,C.M., Mendoza,M.E., Bladen,C.L., Simmons,N.L. (2002). H/dipeptide absorption across the human intestinal epithelium is controlled

indirectly via a functional Na/H exchanger. Gastroenterology *122*, 1322-1333.

Uchiyama,T., Kulkarni,A.A., Davies,D.L., Lee,V.H. (2003). Biophysical evidence for His57 as a proton-binding site in the mammalian intestinal transporter hPepT1. Pharm.Res. *20*, 1911-1916.

Urtti,A., Johns,S.J., Sadee,W. (2001). Genomic structure of proton-coupled oligopeptide transporter hPEPT1 and pH-sensing regulatory splice variant. AAPS.PharmSci. *3*, E6.

Vavricka,S.R., Musch,M.W., Chang,J.E., Nakagawa,Y., Phanvijhitsiri,K., Waypa,T.S., Merlin,D., Schneewind,O., Chang,E.B. (2004). hPepT1 transports muramyl dipeptide, activating NF-kappaB and stimulating IL-8 secretion in human colonic Caco2/bbe cells. Gastroenterology *127*, 1401-1409.

Verri,T., Kottra,G., Romano,A., Tiso,N., Peric,M., Maffia,M., Boll,M., Argenton,F., Daniel,H., Storelli,C. (2003). Molecular and functional characterisation of the zebrafish (Danio rerio) PEPT1-type peptide transporter. FEBS Lett. *549*, 115-122.

Vig,B.S., Stouch,T.R., Timoszyk,J.K., Quan,Y., Wall,D.A., Smith,R.L., Faria,T.N. (2006). Human PEPT1 Pharmacophore Distinguishes between Dipeptide Transport and Binding. J.Med.Chem. *49*, 3636-3644.

Watanabe,C., Kato,Y., Ito,S., Kubo,Y., Sai,Y., Tsuji,A. (2005). Na^+/H^+ exchanger 3 affects transport property of H^+/oligopeptide transporter 1. Drug Metab.Pharmacokinet. *20*, 443-451.

Watanabe,K., Sawano,T., Terada,K., Endo,T., Sakata,M., Sato,J. (2002). Studies on intestinal absorption of sulpiride (1): carrier-mediated uptake of sulpiride in the human intestinal cell line Caco-2. Biol.Pharm.Bull. *25*, 885-890.

Wenzel,U., Kuntz,S., Diestel,S., Daniel,H. (2002). PEPT1-mediated cefixime uptake into human intestinal epithelial cells is increased by Ca2+ channel blockers. Antimicrob.Agents Chemother. *46*, 1375-1380.

Xu,L., Haworth,I.S., Kulkarni,A.A., Bolger,M.B., Davies,D.L. (2009). Mutagenesis and cysteine scanning of transmembrane domain 10 of the human dipeptide transporter. Pharm.Res. *26*, 2358-2366.

Yeung,A.K., Basu,S.K., Wu,S.K., Chu,C., Okamoto,C.T., Hamm-Alvarez,S.F., Von Grafenstein,H., Shen,W.C., Kim,J.K., Bolger,M.B., Haworth,I.S., Ann,D.K., Lee,V.H.L. (1998). Molecular identification of a role for tyrosine 167 in the function of the human intestinal proton-coupled dipeptide transporter (hPepT1). Biochem.Biophys.Res.Comm. *250*, 103-107.

Yin,Y., He,X., Szewczyk,P., Nguyen,T., Chang,G. (2006). Structure of the multidrug transporter EmrD from Escherichia coli. Science *312*, 741-744.

Zerangue,N., Schwappach,B., Jan,Y.N., Jan,L.Y. (1999). A new ER trafficking signal regulates the subunit stoichiometry of plasma membrane K(ATP) channels. Neuron *22*, 537-548.

Zhang,E.Y., Emerick,R.M., Pak,Y.A., Wrighton,S.A., Hillgren,K.M. (2004). Comparison of human and monkey peptide transporters: PEPT1 and PEPT2. Mol.Pharm. *1*, 201-210.

Zhang,M., Zhang,L., Cheung,P.C., Dong,J. (2003). Fractionation and characterization of a Polysaccharide from the sclerotia of Pleurotus tuber-regium by preparative size-exclusion chromatography. J.Biochem.Biophys.Methods *56*, 281-289.

Zhu,T., Chen,X.Z., Steel,A., Hediger,M.A., Smith,D.E. (2000). Differential recognition of ACE inhibitors in Xenopus laevis oocytes expressing rat PEPT1 and PEPT2. Pharm.Res. *17*, 526-532.

Ziegler,T.R., Fernandez-Estivariz,C., Gu,L.H., Bazargan,N., Umeakunne,K., Wallace,T.M., Diaz,E.E., Rosado,K.E., Pascal,R.R., Galloway,J.R., Wilcox,J.N., Leader,L.M. (2002). Distribution of the H+/peptide transporter PepT1 in human intestine: up-regulated expression in the colonic mucosa of patients with short-bowel syndrome. Am.J.Clin.Nutr. *75*, 922-930.

Zucchelli,M., Torkvist,L., Bresso,F., Halfvarson,J., Hellquist,A., Anedda,F., Assadi,G., Lindgren,G.B., Svanfeldt,M., Janson,M.,

Noble,C.L., Pettersson,S., Lappalainen,M., Paavola-Sakki,P., Halme,L., Farkkila,M., Turunen,U., Satsangi,J., Kontula,K., Lofberg,R., Kere,J., D'Amato,M. (2009). PepT1 oligopeptide transporter (SLC15A1) gene polymorphism in inflammatory bowel disease. Inflamm.Bowel.Dis. *15*, 1562-1569.